AN ABSTRACT OF THE THESIS OF

Matthew Jose Rodrigues for the degree of Master of Science in Mechanical Engineering presented on June 5, 2014.

Title: Heat Transfer During the Piston-Cylinder Expansion of a Gas

Abstract approved: _____

James A. Liburdy

The expansion of a gas within a piston-cylinder arrangement is studied in order to obtain a better understanding of the heat transfer which occurs during this process. While the situation of heat transfer during the expansion of a gas has received considerable attention, the process is still not very well understood. In particular, the time dependence of heat transfer has not been well studied, with many researchers instead focused on average heat transfer rates. Additionally, many of the proposed models are not in agreement with each other and are usually dependent on experimentally determined coefficients which have been found to vary widely between test geometries and operating conditions. Therefore, the expansion process is analyzed in order to determine a model for the time dependence of heat transfer during the expansion. A model is developed for the transient heat transfer by assuming that the expansion behaves in a polytropic manner. This leads to a heat transfer model written in terms of an unknown polytropic exponent, *n*. By examining the physical significance of this parameter, it is proposed that the polytropic exponent can be related to a ratio of the time scales associated with the expansion process, such as a characteristic Peclet number.

Experiments are conducted to test the proposed heat transfer model and to establish a relationship for the polytropic exponent. The tests are performed using an apparatus that consists of a single piston-cylinder, which allows for pressure-volume data to be collected during the expansion of a hot gas. These experiments justify the polytropic expansion assumption, and from these results models are developed for the polytropic exponent. Heat transfer data are also collected from these experiments through applying an energy balance on the gas during expansion. These heat transfer data are used to compare the Nusselt number predicted by the proposed model with the experimentally determined Nusselt number. It is found that the proposed model agrees very well with the experimental data, and accurately captures the time dependence of the heat transfer characteristics. The proposed model also accurately handles variations in the heat transfer characteristics due to the different test conditions studied. By capturing the transient effects of heat transfer during the expansion process, the proposed model should be a more accurate tool in determining heat loss during the expansion of a gas than previously developed models.

Heat Transfer During the Piston-Cylinder Expansion of a Gas

by
Matthew Jose Rodrigues

A THESIS

submitted to

Oregon State University

in partial fulfillment of
the requirements for the
degree of

Master of Science

Presented June 5, 2014
Commencement June 2014

Master of Science thesis of Matthew Jose Rodrigues presented on June 5, 2014

APPROVED:

Major Professor, representing Mechanical Engineering

Head of the School of Mechanical, Industrial, and Manufacturing Engineering

Dean of the Graduate School

I understand that my thesis will become part of the permanent collection of Oregon State University libraries. My signature below authorizes release of my thesis to any reader upon request.

Matthew Jose Rodrigues, Author

ACKNOWLEDGEMENTS

There have been many people involved in the preparation of this thesis, both directly and indirectly, to whom I am extremely grateful. Dr. Liburdy, thank you for your guidance; allowing me to explore, get confused, and ultimately learn, while keeping me on track and teaching me both in and out of the classroom. Without your investment of patience, knowledge, time, and energy none of this research would have been completed. Bill Snell, I am extremely grateful for the time and energy you have invested into me, both personally and professionally, and for providing the opportunity for me to combine the worlds of academia and industry. Sean Kirkpatrick, you have been a continual resource and source of advice in the preparation of this thesis, and I am thankful to have you as a lab-mate and friend. Dr. Evans, Dr. Kanury, and Dr. Skyllingstad, thank you for being willing to serve as members of my committee, and for your valuable input to this work. I am also thankful to Long Haul Power, LLC, for their financial support and for use of the test equipment in this research.

Finally, I would like to thank my parents, Northon and Doris, for giving me such a strong educational foundation; my siblings, Nathaniel and Jennifer, for their constant encouragement; and my wife Natalie, who is my greatest encourager, supporter, adviser, and friend.

TABLE OF CONTENTS

Page

1 Introduction 1

1.1 General Problem Statement 2

1.2 Literature Review 5

1.2.1 Pseudo-Steady State Models 7
1.2.2 Transient Models 12

1.3 Specific Problem Statement 16

2 Analysis 18

2.1 Model Development 18

2.2 Alternate Expressions 24

2.3 Model Discussion 26

2.4 Flow Considerations 30

2.5 Polytropic Exponent 32

3 Experimental Methodology 37

3.1 Experimental Setup 38

3.2 Data Reduction 41

3.3 Test Conditions 47

3.4 Uncertainty Analysis 50

TABLE OF CONTENTS (Continued)

Page

4 Results & Discussion 56

4.1 Experimental Results 57

4.2 Expansion Characteristics 63

4.3 Heat Transfer Characteristics 72

4.4 Alternative Length Scales 76

4.5 Model for the Polytropic Exponent 82

4.5.1 Model Based on the Characteristic Peclet Number 83
4.5.2 Model Based on the Mean Piston Speed 89

4.6 Heat Transfer Model Validation 93

4.7 Model Comparison 99

5 Conclusions 107

5.1 Transient Predictive Capability 108

5.2 Universality 110

5.3 Recommendations 112

BIBLIOGRAPHY 115

APPENDIX 118

LIST OF FIGURES

Figure		Page
1.1	Schematic of heat transfer during a piston-cylinder expansion process as currently studied	2
2.1	Schematic showing control volume used for the analysis of the expansion process.	19
3.1	Schematic of experimental apparatus used to conduct tests.	39
4.1	Bomb data for Test Case D, used to determine combustion time.	58
4.2	Pressure and volume versus time for a combustion and expansion event, showing that combustion is complete by the time expansion begins. Data shown is from Test Case D	59
4.3	Measured cylinder volume versus time during expansion for Test Case D.	60
4.4	Measured cylinder pressure versus time during expansion for Test Case D.	61
4.5	Measured cylinder pressure versus volume during expansion for Test Case D.	61
4.6	Measured cylinder pressure versus volume during expansion for Test Case D, logarithmic scale.	63
4.7	Measured gas pressure during expansion versus dimensionless distance from piston to cylinder head for each test case.	65
4.8	Bulk gas temperature during expansion versus dimensionless distance from piston to cylinder head for each test case.	65
4.9	Gas density during expansion versus dimensionless distance from piston to cylinder head for each test case.	67
4.10	Piston velocity during expansion versus dimensionless distance from piston to cylinder head for each test case.	67
4.11	Instantaneous Reynolds number during expansion versus dimensionless distance from piston to cylinder head for each test case.	69
4.12	Prandtl number during expansion versus dimensionless distance from piston to cylinder head for each test case.	69

LIST OF FIGURES (Continued)

Figure		Page
4.13	Peclet number during expansion versus dimensionless distance from piston to cylinder head for each test case	71
4.14	Spatial average instantaneous heat transfer coefficient during expansion versus dimensionless distance from piston to cylinder head for each test case	73
4.15	Spatial average Nusselt number during expansion versus dimensionless distance from piston to cylinder head for each test case	75
4.16	Alternate Peclet number, using the length scale of *x*, the distance from the cylinder head to the piston	78
4.17	Alternate Reynolds number, using the length scale of *x*, the distance from the cylinder head to the piston	79
4.18	Alternate Nusselt number, using the length scale of *x*, the distance from the cylinder head to the piston.	80
4.19	Polytropic exponent and the characteristic Peclet number for each test case. The polytropic exponent was determined from experimental pressure-volume data and the characteristic Peclet number was calculated using Eq. 4.10-4.11.	84
4.20	Polytropic exponent normalized by the specific heat ratio at the beginning of expansion, versus the characteristic Peclet number calculated using Eq. 4.10-4.11.	87
4.21	Polytropic exponent normalized by the specific heat ratio at the beginning of expansion, versus the dimensionless mean piston speed defined by Eq. 4.14	91
4.22	Comparison of experimental results and the proposed heat transfer model (Eq. 4.1) for the Nusselt number during expansion, using Eq. 4.12 for *n* – Test Case A.	94
4.23	Comparison of experimental results and the proposed heat transfer model (Eq. 4.1) for the Nusselt number during expansion, using Eq. 4.12 for *n* – Test Case B.	95

LIST OF FIGURES (Continued)

Figure		Page
4.24	Comparison of experimental results and the proposed heat transfer model (Eq. 4.1) for the Nusselt number during expansion, using Eq. 4.12 for n – Test Case C.	95
4.25	Comparison of experimental results and the proposed heat transfer model (Eq. 4.1) for the Nusselt number during expansion, using Eq. 4.12 for n – Test Case D.	96
4.26	Comparison of experimental results and the proposed heat transfer model (Eq. 4.1) for the Nusselt number during expansion, using Eq. 4.12 for n – Test Case E.	96
4.27	Nusselt number during expansion versus the Reynolds number calculated using the mean piston speed (logarithmic scale)	100
4.28	Comparison of the proposed heat transfer model with models from other studies. Experimental data from Test Case D	103
4.29	Comparison of the proposed heat transfer model with models from other studies. Experimental data from Test Case B	104

LIST OF TABLES

Table		Page
3.1	Test Conditions.	49
3.2	Instrument Uncertainties.	51
3.3	Uncertainty in Measured Variables.	51
3.4	Polytropic Exponent	52
3.5	Propagated Uncertainties in Physical Variables.	53
3.6	Propagated Uncertainties in Non-Dimensional Parameters	54
4.1	Combustion Times	58
4.2	Polytropic Exponent for Each Test Case	88

LIST OF APPENDICES

Appendix		Page
A	Conservation Equations for Mass, Momentum, and Energy	119
B	Characteristic Expansion Velocity	121
C	Experimental Apparatus.	124
D	Position Transducer Calibration.	131
E	Wall Temperature Analysis.	134
F	Data Processing.	139
G	Experimental Uncertainties.	143
H	Experimental Data.	152
I	Thermophysical Fluid Properties.	169
J	Results of Applying Alternate Models for the Polytropic Exponent . . .	173

LIST OF APPENDIX FIGURES

Figure		Page
B.1	Geometry used to determine the characteristic fluid velocity during expansion	121
C.1	Image of test apparatus used for experiments	125
C.2	Image of test apparatus used for experiments, showing position of data acquisition instruments.	126
C.3	Screenshot of LabVIEW block diagram showing data collection system; Part 1 of 2	127
C.4	Screenshot of LabVIEW block diagram showing data collection system; Part 2 of 2	128
C.5	Screenshot of LabVIEW front panel showing data collection system; Part 1 of 2	129
C.6	Screenshot of LabVIEW front panel showing data collection system; Part 2 of 2.	130
D.1	Calibration curve for the cable-extension position transducer.	132
E.1	Schematic for wall temperature analysis.	134
E.2	Temperature distribution for aluminum using a semi-infinite solid analysis	137
E.3	Temperature distribution for steel using a semi-infinite solid analysis	137
F.1	Volume versus time for a single expansion in Test Case D, showing raw and filtered data	140
F.2	Volume versus time for Test Case D, showing individual runs and the polynomial curve fit	141
F.3	Pressure versus volume for Test Case D, showing individual runs and the power law curve fit.	142
G.1	Propagation of uncertainty for the number of moles of gas in the cylinder during expansion	147

LIST OF APPENDIX FIGURES (Continued)

Figure		Page
G.2	Propagation of uncertainty for the bulk gas temperature during expansion. .	147
G.3	Propagation of uncertainty for the gas density during expansion	148
G.4	Propagation of uncertainty for the heat transfer coefficient during expansion	149
G.5	Propagation of uncertainty for the Nusselt number during expansion	150
G.6	Propagation of uncertainty for the Prandtl number during expansion	150
G.7	Propagation of uncertainty for the Reynolds number during expansion	151
G.8	Propagation of uncertainty for the Peclet number during expansion	151
H.1	Bomb data for Test Case A	153
H.2	Bomb data for Test Case B	153
H.3	Bomb data for Test Case C	154
H.4	Bomb data for Test Case D	154
H.5	Bomb data for Test Case E	155
H.6	Combustion & expansion data for Test Case A, showing the end of combustion as obtained from bomb data and the beginning of expansion by 1% increase from initial volume.	156
H.7	Combustion & expansion data for Test Case B, showing the end of combustion as obtained from bomb data and the beginning of expansion by 1% increase from initial volume.	157
H.8	Combustion & expansion data for Test Case C, showing the end of combustion as obtained from bomb data and the beginning of expansion by 1% increase from initial volume	157
H.9	Combustion & expansion data for Test Case D, showing the end of combustion as obtained from bomb data and the beginning of expansion by 1% increase from initial volume	158
H.10	Combustion & expansion data for Test Case E, showing the end of combustion as obtained from bomb data and the beginning of expansion by 1% increase from initial volume	158

LIST OF APPENDIX FIGURES (Continued)

Figure		Page
H.11	Measured cylinder volume versus time during expansion for Test Case A	159
H.12	Measured cylinder pressure versus time during expansion for Test Case A	159
H.13	Measured pressure versus measured cylinder volume during expansion for Test Case A	160
H.14	Measured cylinder volume versus time during expansion for Test Case A, logarithmic scale	160
H.15	Measured cylinder volume versus time during expansion for Test Case B	161
H.16	Measured cylinder pressure versus time during expansion for Test Case B	161
H.17	Measured cylinder pressure versus measured cylinder volume during expansion for Test Case B	162
H.18	Measured cylinder pressure versus volume during expansion for Test Case B, logarithmic scale	162
H.19	Measured cylinder volume versus time during expansion for Test Case C	163
H.20	Measured cylinder pressure versus time during expansion for Test Case C	163
H.21	Measured cylinder pressure versus measured cylinder volume during expansion for Test Case C	164
H.22	Measured cylinder pressure versus volume during expansion for Test Case C, logarithmic scale	164
H.23	Measured cylinder volume versus time during expansion for Test Case D	165
H.24	Measured cylinder pressure versus time during expansion for Test Case D	165
H.25	Measured cylinder pressure versus measured cylinder volume during expansion for Test Case D	166
H.26	Measured cylinder pressure versus volume during expansion for Test Case D, logarithmic scale	166
H.27	Measured cylinder volume versus time during expansion for Test Case E	167
H.28	Measured cylinder pressure versus time during expansion for Test Case E	167
H.29	Measured cylinder pressure versus measured cylinder volume during expansion for Test Case E	168

LIST OF APPENDIX FIGURES (Continued)

Figure		Page
H.30	Measured cylinder pressure versus volume during expansion for Test Case E, logarithmic scale	168
I.1	Viscosity of the gas mixture for each test case during expansion	170
I.2	Thermal conductivity of the gas mixture for each test case during expansion	171
I.3	Specific heat at constant pressure of the gas mixture for each test case during expansion.	171
I.4	Thermal diffusivity of the gas mixture for each test case during expansion . .	172
J.1	Comparison of experimental results and the alternate heat transfer model for the polytropic exponent – Test Case A.	174
J.2	Comparison of experimental results and the alternate heat transfer model for the polytropic exponent – Test Case B.	175
J.3	Comparison of experimental results and the alternate heat transfer model for the polytropic exponent – Test Case C.	175
J.4	Comparison of experimental results and the alternate heat transfer model for the polytropic exponent – Test Case D.	176
J.5	Comparison of experimental results and the alternate heat transfer model for the polytropic exponent – Test Case E.	176

LIST OF APPENDIX TABLES

Table		Page
D.1	Calibration Data for the Cable-Extension Position Transducer	133
E.1	Thermal Properties Used for Wall Conduction Analysis	136
G.1	Bias Uncertainties for Each Measured Variable	143
G.2	Precision Uncertainties for Each Measured Variable	144
G.3	Total Uncertainties for Each Measured Variable	144
G.4	Propagated Uncertainties for Test Case A	145
G.5	Propagated Uncertainties for Test Case B	145
G.6	Propagated Uncertainties for Test Case C	146
G.7	Propagated Uncertainties for Test Case D	146
G.8	Propagated Uncertainties for Test Case E	146

NOMENCLATURE

Greek Letters and Symbols

α	Thermal diffusivity (m^2/s)
γ	Specific heat ratio, $\gamma = c_p/c_v$
θ	Non-dimensional temperature, $\theta = T_g/(T_g - T_{wall})$
κ	Thermal conductivity (W/m-K)
μ	Dynamic viscosity (Pa-s)
ρ	Gas density (kg/m^3)
ρ_{avg}	Average gas density (kg/m^3)
ϕ	Equivalence ratio
χ	Mole fraction

Roman

A_c	Cross-sectional area (m^2)
A_s	Surface area (m^2)
c	Acoustic velocity (m/s)
c_p	Specific heat at constant pressure (J/kg-K)
c_v	Specific heat at constant volume (J/kg-K)
D	Cylinder diameter (m)
f	Darcy friction factor
h	Heat transfer coefficient (W/m^2-K)
m	Mass (kg)
$\dot{m}$	Mass flow rate (kg/s)
n	Polytropic exponent
Nu_D	Spatial average Nusselt number using the cylinder diameter, $Nu_D = hD/\kappa$
$\overline{Nu_x}$	Spatial average Nusselt number using the distance x, $\overline{Nu_x} = hx/\kappa$
P	Gas pressure, absolute (Pa)
P_{air}	Air pressure, absolute (Pa)
P_{H2}	Hydrogen pressure, absolute (Pa)
P_T	Total initial pressure, absolute (Pa)

NOMENCLATURE (Continued)

Pe_D	Peclet number using the cylinder diameter, $Pe = v_p D/\alpha$
Pe^*	Characteristic Peclet number, $Pe^* = S_p D/\alpha_0$
Pe_x	Peclet number using the distance *x*, $Pe = v_p x/\alpha$
Pr	Prandtl number, $Pr = \mu c_p/\kappa$
Q	Heat lost (J)
$\dot{q}$	Heat loss rate (W)
$\dot{q}''$	Heat flux lost (W/m^2)
R	Gas constant (J/kg-K)
Re_D	Reynolds number using cylinder diameter, $Re_D = \rho v_p D/\mu$
Re_x	Reynolds number using the distance *x*, $Re_x = \rho v_p x/\mu$
St	Stanton number, $St = h/\rho c_p v_p$
S_p	Mean piston speed (m/s)
S_p^*	Dimensionless mean piston speed, $S_p^* = S_p/c_0$
T_g	Bulk gas temperature (K)
T_{wall}	Wall temperature (K)
t_{ex}	Expansion time (s)
U	Internal energy (J)
u	Fluid velocity (m/s)
u_m	Mean fluid velocity (m/s)
V	Cylinder volume (m^3)
v_p	Piston velocity (m/s)
x	Distance from cylinder head to piston face (m)
x^*	Non-dimensional distance, $x^* = x/D$

Chapter 1 – Introduction

The process of gas expansion in a piston-cylinder assembly is common in many applications, but the heat transfer which occurs during this process is not well understood. The expansion process itself is very complex; the expansions considered here are characterized by a turbulent flow field, and the process is inherently unsteady. These complexities make characterization of the heat transfer difficult, especially when time-dependent heat transfer rates during the expansion are required. Many previous studies have used a pseudo-steady state assumption to develop models for the heat transfer. While models of this form can be used to characterize average heat transfer rates for the expansion, these models do not capture the time dependence of the heat transfer. The expansion process is inherently unsteady; therefore, by neglecting the time dependence of the process, these models do not fully capture the fundamental forces driving heat transfer during this process. Other researchers have proposed various methods of including the time dependence of the expansion process in heat transfer models. Largely, these consist of modifications to pseudo-steady models which incorporate various transient elements of the process. Since the transient behavior of heat transfer is of interest in this study, the proposed method of addressing the problem is to develop a model based on the transient effects of expansion directly, rather than by first assuming a steady process.

1.1 General Problem Statement

The situation of heat transfer that occurs when hot gases are allowed to expand in a closed piston-cylinder assembly has many complexities, such as turbulence, spatially growing boundary layer regions and transient effects due to expansion. Since the gases are at a higher temperature than the walls of the piston-cylinder assembly, a temperature gradient exists to drive heat transfer. Gases are considered here to be non-radiating, and due to the bulk fluid motion that occurs, heat transfer is overwhelmingly dominated by convective heat transfer, meaning that it is governed by Newton's law of cooling:

$$\dot{q}'' = h\Delta T \tag{1.1}$$

This process is shown schematically below in Figure 1.1.

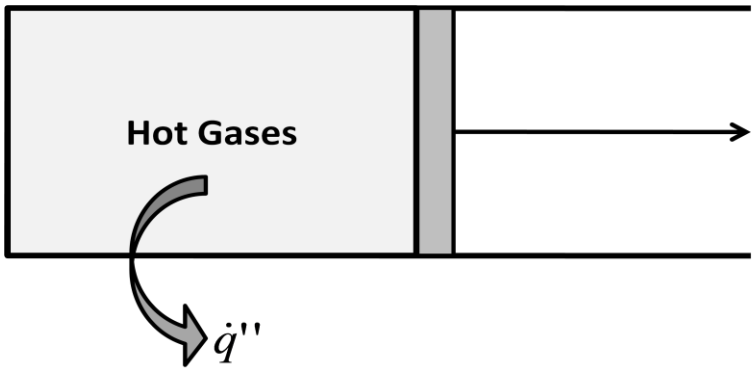

Figure 1.1 – Schematic of heat transfer during a piston-cylinder expansion process as currently studied

In this formulation of Newton's law of cooling, the temperature difference to be used is that between the bulk fluid and the wall, $\Delta T = T_g - T_{wall}$. The bulk fluid

temperature for the expansion process is most commonly defined using the ideal gas equation of state:

$$T_g = \frac{PV}{mR} \tag{1.2}$$

This differs from other bulk fluid temperature definitions; for flow in pipes, for example, the bulk temperature is defined based on the amount of thermal energy transport. In Eq.1.2, *P* refers to the absolute pressure of the gas and *V* is the volume which the gas occupies, while *m* refers to the mass of gas and *R* refers to the gas constant for the mixture. For a uniform pressure distribution within the cylinder, this expression yields a spatially averaged gas temperature used as the bulk temperature. However, since the pressure and volume of the gas change as the system expands the bulk temperature is not constant in time, although still evaluated from the ideal gas equation of state above.

The challenge in describing heat transfer for this process is in determining the appropriate heat transfer coefficient, *h*, to used in Eq. 1.1. In some other situations the heat transfer coefficient is directly calculable from the Navier-Stokes equations and the energy equations (see Appendix A), most notably for certain steady, laminar flows such as steady flow in a tube. This is not possible for the expansion of a gas however, because of the unsteady and potentially turbulent nature of the process. The conditions presently investigated all result in turbulent flow, characterized by unstable, highly three dimensional and transient flow patterns with large Reynolds numbers. This makes an analytic solution by solving the Navier-Stokes and energy equations impossible.

Therefore, the goal is to extract the most important physical processes driving the heat transfer, and incorporate these into a simplified model.

The expansion of a gas is also not a steady process, but gas pressure, temperature, and density, as well as the expansion rate, all may vary with time. This has several ramifications. Firstly, this means that the density, momentum, and energy content of the process varies with time, shown mathematically by the inclusion of the time derivatives of density, velocity, and temperature in the governing equations. Secondly, this also has consequences on what flow distributions can be assumed. When analyzing steady flows in tubes it is often assumed that the flow is fully developed, which means that axial variations in an appropriate temperature difference and velocity distributions can be neglected and that sufficient time has elapsed for momentum and heat to diffuse completely across the flow. In the expansion of a gas however, the flow certainly is not fully developed, and there may significant axial variations of fluid velocity and temperature distributions. Similarly, heat and momentum may not be able to diffuse across the flow in the time scales of expansion, meaning that both thermal and viscous boundary layers will exist at the wall edges and may be non-uniform in both space and time. These boundary layers are expected to be thin because the flow has not fully developed. This situation leads to increased heat transfer caused by these large temperature gradients. These boundary layers may be additionally affected as the gas pressure changes during the expansion (Lawton, 1987). Furthermore, because of the large changes in temperature and pressure, properties such as viscosity, thermal conductivity,

and specific heat are not constant, which further complicates the governing equations. Because of these complications, in order to calculate or predict the heat transfer certain simplifications or generalizations to the governing equations and processes must be made, and often experimental data is required to justify these simplifications or to determine empirical relationships.

Many other researchers have studied this general problem, in various forms and for different applications. Since the problem is inherently very complex, various assumptions must be made to arrive at a useable solution. These simplifications lead to different results depending on what parts of the governing processes are included as the most necessary physical factors influencing heat transfer. Some researchers have proposed discarding many transient elements of the problem, while others have included them in various forms. Examining what other researchers have proposed as models for the heat transfer allows one to explore how the various physical processes are incorporated into heat transfer models and how future improvements could potentially be made.

1.2 Literature Review

The problem of predicting the convective heat transfer to or from a hot, expanding gas is one which has already received considerable attention in the literature. Most research has been from the field of internal combustion engines, where knowledge of the heat transfer from the working fluid (combustion gases) to the engine wall is of

importance to understand the overall energy losses from the system, to determine the necessary cooling load, and in the development of computer models predicting engine performance (Heywood, 1988). Different researchers have approached the problem in different ways. One common approach has been to simplify the analysis by modeling the process as "pseudo-steady". In this approach, parameters such as temperature, pressure, and density still vary with time, but it is assumed that the mechanism driving the heat transfer is similar to that for a steady process. This allows for the functional form describing the heat transfer to be borrowed from the analysis of a simpler situation, such as flow in tubes. Others recognized that the transient nature of the flow is important, and have developed models that reflect transient effects such as the developing nature of the flow and the effect that expansion has on the boundary layer. Because of the complex nature of the problem however, other simplifications concerning the flow behavior must be made in order to obtain a useable expression for the heat transfer.

Most researchers choose to express the heat transfer using non-dimensional parameters that represent fundamental physical elements governing the process. The dimensionless parameters generally considered are: the Nusselt number, $Nu = \frac{hL_s}{\kappa}$, which represents the magnitude of convective heat transfer to conductive heat transfer; the Reynolds number, $Re = \frac{\rho u_s L_s}{\mu}$, which represents the ratio of inertial forces to viscous forces; and the Prandtl number, $Pr = \frac{\mu c_p}{\kappa}$, which represents the ratio of momentum diffusion to heat diffusion. While these are the parameters with which heat transfer

during the expansion of a gas is generally described, there are significant differences in what characteristic length scale, L_s, and characteristic velocity scale, u_s, are used to represent these parameters.

1.2.1 Pseudo-Steady State Models

Many researchers describing heat transfer during the expansion of a gas have assumed that the convective heat transfer can be modeled using the pseudo-steady state assumption described previously. This assumes that convective heat transfer behaves similarly as it does in related steady, fully developed flows. Such flow in tubes has been studied extensively, and the similarity between momentum and energy transport yields the Chilton-Colburn analogy relating flow characteristics (e.g. velocity) to heat transfer (Incropera, et al., 2007). For turbulent flows, this takes the form of the Colburn equation, given as:

$$Nu_D = 0.023 Re_D^{0.8} Pr^{0.33} \tag{1.3}$$

This commonly used heat transfer correlation holds for both liquids and gases. Since the Prandtl number is roughly constant for most gases near 0.7, this can be generalized as:

$$Nu_D = C Re_D^m \tag{1.4}$$

This functional form for convective heat transfer arises from turbulent flow in tubes, where it has been applied quite effectively to predict heat transfer rates (Bhatti & Shah, 1987).

Three important studies of heat transfer in internal combustion engines that have made use of this same functional form are by Annand, Woschni, and Hohenburg (Annand, 1963; Woschni, 1967; Hohenburg, 1980). In modeling the convective heat transfer during expansion, the starting point for each is the functional form for steady flow in tubes, Eq. 1.4. However, each differs in its application in several important points. In particular, they differ in the definition of the characteristic length scale associated with both the Nusselt and Reynolds numbers and in the characteristic velocity scale associated with the Reynolds number. Additionally, while Annand expresses his relation in dimensionless form, Woschni and Hohenburg both start from the dimensionless form of Eq. 1.4 but express their results dimensionally, allowing for the dependence of the heat transfer coefficient on the gas pressure and temperature to be shown explicitly.

Annand represents the characteristic length scales in both the Nusselt and Reynolds numbers with the cylinder diameter, D (Annand, 1963). Additionally the mean piston speed, S_p, is chosen as the characteristic velocity scale. While these may change for different geometries and operating conditions, once fixed they do not change during expansion. Thus, the main physical parameter affecting change in the heat transfer coefficient (via the Nusselt number) is the density of the gas (via the Reynolds number). The final form of Annand's expression was given as:

$$Nu_D = CRe_D^{0.7} \tag{1.5}$$

The constant *C* has a range given as *C=0.35-0.8*. The range in the constant *C* represents the range needed for the various engine types tested, and can be selected according to the best fit for one's particular geometry (Annand, 1963). As a constant multiplicative enhancement of heat transfer, this constant is meant to represent the strength of advection for the given engine geometry and operating conditions. The power 0.7 was selected empirically as the best fit to experimental data.

Woschni similarly started from Eq. 1.4 and used the cylinder diameter D as the characteristic length scale (Woschni, 1967). However, the characteristic velocity scale was modified to be the mean piston speed multiplied by a constant, c_1. The heat transfer coefficient is given directly, rather than non-dimensionally through the Nusselt number. To do this, the thermal conductivity and viscosity of a gas were taken as functions of temperature, $\kappa \propto T^{0.75}$ and $\mu \propto T^{0.62}$, together with the ideal gas law for density. These are substituted for the properties in both the Reynolds and Nusselt numbers, resulting in the expression shown in Eq. 1.6:

$$h = CD^{-0.2}P^{0.8}(c_1 S_p)^{0.8}T_g^{-0.53} \tag{1.6}$$

The power 0.8 reflects the original power on the Reynolds number used in the Colburn equation, Eq. 1.3, which was found to represent experimental data well. The other constants were given as $c_1 = 2.28$ and $C=0.085$ (for standard SI unit system, as this constant must take on units for the equation to be dimensionally consistent), chosen as the best fit to experimental data (Woschni, 1967).

Hohenburg took an identical approach to Woschni by expressing the result dimensionally rather than in terms of non-dimensional parameters (Hohenburg, 1980). However, the definition of the length scale is modified, choosing this as the diameter of a sphere with an equivalent volume to the current gas volume. In introducing this transient length scale, he introduced further time dependence on the heat transfer; however, this term does not explicitly represent any physical effect concerning transient heat transfer. Additionally, Hohenburg removed the constant multiplicative value on the mean piston speed, instead modifying the exponent for the temperature to reflect the gas velocity dependence on temperature. This equation is given as:

$$h = CV^{-0.06}P^{0.8}T_g^{-0.4}S_p^{0.8} \tag{1.7}$$

The constant *C* was determined by experimental data, and given as *C=0.013*.

These three authors represent efforts made to characterize the heat transfer using a pseudo-steady state model, and while their results are the most widely used, others have also presented correlations in similar forms (Sitkei, 1972; Chen & Karim, 1998; Chang et al., 2004). Each of these researchers began from a form of the Colburn analogy, Eq. 1.4, and while they differed in selection of the appropriate length scale and in the handling of the thermal properties, they notably all use a constant velocity scale in the Reynolds number. Additionally, none of these authors chose to include Prandtl number dependence. Instead, any Prandtl number effects were lumped into the empirical constant, which was justified by noting that the Prandtl number remains near 0.7 for most gases. While each requires individual tuning by way of constants, they have been widely used in

both industry and academia as tools to predict heat transfer for internal combustion engines as well as starting points for further analysis (Borman & Nishiwaki, 1987; Soyhan, et al., 2009; Demuynck, 2010).

An additional item of concern in using the aforementioned functional forms for heat transfer is the large temperature difference possible between the gas and the wall. Temperature affects the thermal conductivity, viscosity, and density for gases, raising questions as to what temperature should be used in evaluating these properties. Additionally, these variations can have an effect on temperature and velocity distributions, thereby affecting the heat transfer (Kakac, 1987). One option to account for this is to choose a reference temperature such as the average between the bulk and wall temperature at which to evaluate all properties; this is the method used in Annand's model. Another method is to evaluate all properties at the bulk temperature and then include a temperature correction factor. For gases, this is typically accomplished using the form (Kakac, 1987):

$$\frac{Nu}{Nu_{cp}} = \left(\frac{T_w}{T_g}\right)^a \tag{1.8}$$

In this expression, Nu_{cp} represents the Nusselt number evaluated using constant properties at the bulk temperature. The exponent *a* is negative and approximately equal to -0.5, thus for a hotter bulk temperature than wall temperature this modification increases the predicted Nusselt number. While this temperature correction is not used in many heat transfer equations for gas expansion, the importance of including this temperature

difference could perhaps be justified by its accuracy in modeling steady flows with large temperature differences.

1.2.2 Transient Models

While developing a model for heat transfer based on a pseudo-steady state assumption is attractive because of its relative simplicity, there are significant transient effects occurring in the expansion of a gas that call this assumption into question. This is especially true if one is interested in the time evolution of the heat transfer coefficient, rather than an expression that tends towards an average description of heat transfer during a single expansion. These transient effects can be seen in several ways. They are important because the time dependence of density, velocity, and temperature are included in the fundamental conservation equations, and reflect that density, momentum and energy, respectively, need not pass through the system at constant rates, but can change due to compressibility, applied forces, and energy storage capacities of the fluid, respectively. Additionally, their effects can be seen tangibly through the concepts of flow development and the boundary layer.

When pseudo-steady state is assumed in the form of Eq. 1.4, it is implicitly assumed that the flow is fully developed. This is because the Colburn analogy which forms the basis for pseudo-steady state models was derived for steady, fully developed flows. For turbulent flows the entry length typically lasts between 10 and 60 diameter

lengths ($10 \leq \frac{L_{fd}}{D} \leq 60$) (Incropera et al., 2007). While this is a generally short distance for flow in tubes, this is often much larger than the expansion distance experienced in piston-cylinder expansions. For example, automobile engines typically have a stroke to bore ratio (equivalent to the expansion length per diameter) of less than 1.3 (Heywood, 1988). The entry length is of importance because it typically exhibits higher amounts of heat transfer than the fully developed region, due to the fact that the boundary layer is thinner and allows for greater mixing (Molki, 1986). Often, the entry length is accounted for by using an expression that enhances the fully developed Nusselt number near the entry length (Incropera et al., 2007):

$$\frac{Nu_D}{Nu_{D,fd}} = 1 + C\left(\frac{x}{D}\right)^{-m} \tag{1.9}$$

An entry length correction was used in the model proposed by Irimescu (Irimescu, 2012). He also used a more elaborate expression for the steady heat transfer for turbulent flow in tubes due to Gnielinski (Gnielinski, 1976). This was modified to account for entry length in the fashion described above, as well as an additional modification to account for the wall to gas temperature difference:

$$Nu_D = \left(\frac{(f/8)(Re_D - 1000)Pr}{1 + 12.7(f/8)^{0.5}(Pr^{2/3} - 1)}\right) * \left(1 + \left(\frac{x}{D}\right)^{-\frac{2}{3}}\right) * \left(\frac{\mu_g}{\mu_w}\right)^{0.14} \tag{1.10}$$

In the above expression, f is the Darcy friction factor, μ_b the viscosity at the bulk gas temperature, and μ_w the viscosity at the wall temperature. Instead of using a constant velocity scale in the Reynolds number, Irimescu proposed using a velocity calculated by

using a simplified k-ϵ turbulence model, which varied during the cycle and is related to the instantaneous piston speed. By making these changes, Irimescu incorporated the effect of the entry length on heat transfer, as well as introducing time dependent velocity scale, reflecting the importance of the instantaneous velocity on heat transfer.

The expansion process has also been found to have an effect on the boundary layer. Lawton suggested that the expansion process tends to decrease the gas temperature in the boundary layer due to the decrease in pressure, thus effectively lowering the driving temperature difference for heat transfer near the cylinder walls (Lawton, 1987). This is in agreement with several published experimental and theoretical results, but is often considered to be of low significance in overall heat transfer calculations (Annand & Ma, 1970; Borman & Nishiwaki, 1987; Kornhauser & Smith, 1994; Ota, 2008). Nevertheless, by starting with the one-dimensional energy equation and making several simplifying assumptions (while keeping the essential time dependence relations intact), Lawton showed that pseudo-steady state correlations such as Annand's equation (Eq. 1.5) should be modified by an unsteady term reflecting the expansion of the gases (Lawton, 1987):

$$Nu_D = aRe_D^{0.7} - 2.75\left(\frac{T_w}{T_g - T_w}\right)L \quad \text{with} \quad L = \frac{\gamma-1}{V}\frac{dV}{dt}t_s \qquad (1.11)$$

For this expression, t_s is expressed as the combination of convective and diffusive time scales, or $t_s = \left(\frac{D^3}{\alpha S_p}\right)^{0.5}$. While this does not incorporate the effects of flow development directly, this formulation of the heat transfer during the expansion of a gas models the

transient behavior through means of the expansion process itself, through its effect on the boundary layer.

It should be mentioned that there has been considerable research in modeling the heat transfer during the expansion of a gas using computational fluid dynamics (CFD) codes. This is certainly a useful tool in studying the heat transfer in this complex process, and can be used to examine time dependent phenomenon. However, it does not replace the need for straightforward expressions that accurately model the heat transfer characteristics seen in the expansion of a gas. These expressions are useful for things such as overall computer codes modeling internal combustion engines or other similar devices, and to gain deeper understanding into the governing processes. Additionally, there are other concerns which exist in CFD models, such as how the wall heat transfer formulations are developed (Rakapoulos et al., 2010).

While the heat transfer models given by Eq. 1.5-1.7 and Eq. 1.10-1.11 have been used frequently to predict heat transfer, there is room for improvement in these models. Many of the models are highly dependent on experimental constants used in the equations. The values of these constants are not firmly established, and they can vary widely with different geometries and different operating conditions (Annand & Ma, 1970; Borman, 1987; Demuynck, 2010). This makes predicting heat transfer difficult unless one has experimental data to compare against. From a design perspective this is a large hindrance on thermal modeling. This is especially true in the development of novel engines, such as HCCI engines (Soyhan et al., 2009). Therefore one improvement which

could be made is to develop a model that is less dependent on ambiguously defined constants, or where the range of experimentally determined constants is small. Another area of improvement is in predicting the time dependence of heat transfer. While the previously mentioned models generally predict cycle-averaged heat transfer well, they often fail at describing the unsteady heat transfer effects (Borman & Nishiwaki, 1987). Accurate prediction of instantaneous heat transfer rates is essential for an understanding of heat transfer during gas expansion process. It is also important from a design perspective. For example, knowledge of the time dependence of heat transfer rates is important in the design and modeling of novel internal combustion engines, where steps could be taken to minimize heat loss based on knowledge of instantaneous heat transfer rates. In general, current heat transfer models lack universality and transient robustness, leaving considerable room for improvement.

1.3 Specific Problem Statement

Based on the foregoing discussion, the goal of this research is to develop a simple model for the time-dependent heat transfer during the expansion of a gas. The spatial distribution of heat transfer is not of interest in this research, but rather accurately modeling the time evolution of heat transfer. Additionally, this model must be able to accurately respond to changes in operating parameters (such as the initial pressure). To accomplish these objectives, the heat transfer during the expansion process must be

analyzed in a manner that incorporates the necessary physics driving the flow and heat transfer while avoiding excessive complication.

Many previous studies have assumed the same form of the heat transfer model between the expansion process and steady flow in tubes as the starting point for their analysis. While it may be useful to compare the expansion process with steady flow in tubes because flow in tubes is a well studied and more straightforward scenario, this assumption should not be used as a starting point for the analysis because it ignores the inherently transient nature of the expansion process. Instead, the expansion process should be analyzed independently in order to describe the transient heat transfer behavior and capture the fundamental physics driving the heat transfer in this process.

This study develops an analytical model for transient heat transfer during the expansion of a gas. The time dependence of this process is particularly emphasized, while spatial variation is not considered. Experiments are then carried out in order to evaluate the accuracy of this model. These experiments emphasize variations in the operating conditions of the expansion, in order to determine how universal the model developed is. The results from these experiments give insight into what further improvements could be made in the modeling of heat transfer during the expansion of a gas.

Chapter 2 – Analysis

The situation of heat transfer during the expansion of a gas in a piston-cylinder assembly is analyzed in order to develop a model for the heat transfer. The process is inherently complex, so in order to analyze it the process is simplified by restricting the analysis to the global system, without consideration of spatial variations of heat transfer within the cylinder. By restricting the analysis to the global system, a model is developed which predicts the transient heat transfer characteristics of the process. By expressing this model in a non-dimensional form, the key factors influencing heat transfer can be illuminated and the model compared against existing models. The analytical development and subsequent discussion of this model is presented in the following sections.

2.1 Model Development

Many different approaches are possible in order to analyze the heat transfer during the expansion of a gas. The differential form of the energy equation (see Appendix A) could be invoked, together with the continuity and the Navier-Stokes equations. This by itself forms a formidable set of coupled, non-linear partial differential equations to be solved, further complicated by the unsteady nature of the problem and that thermal properties (such as viscosity and thermal conductivity) are not constant over the wide range of expected bulk temperatures. Furthermore, the flows considered here are

turbulent, making an analytic solution to the Navier-Stokes equations impossible. Therefore, in order to conduct a mathematical analysis, the process must be simplified by some means. One such method is to examine the system globally rather than on a spatial basis. To do this, a control volume is placed around the entire gas present in the volume, as shown in Figure 2.1.

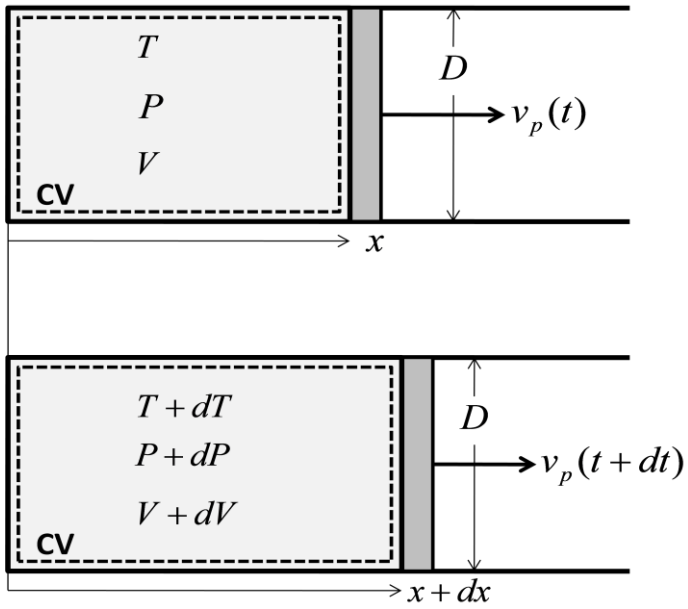

Figure 2.1 – Schematic showing control volume used for the analysis of the expansion process

The energy equation can be expressed globally as the first law of thermodynamics, written for a closed system (no inlets or exits):

$$\frac{dU}{dt} = \frac{dQ}{dt} - \frac{dW}{dt} \tag{2.1}$$

This is a statement of the conservation of energy principle, expressed on a rate basis. It reads that the change in internal energy (U) is balanced by any heat gain and work done

(following standard thermodynamic sign convention, heat lost from the system is represented by a negative *Q*, and work done by the system is represented by a positive *W*). With the assumption of an ideal gas and recognizing that the only way for work to be done is through the expansion of the piston, this equation becomes:

$$mc_v \frac{dT_g}{dt} = \frac{dQ}{dt} - P\frac{dV}{dt} \tag{2.2}$$

Where *m* is the mass of gas in the system, and c_v is the specific heat at constant volume of the gas mixture at its current temperature. The temperature is the bulk temperature as defined by Eq. 1.2 while the pressure is the average gas pressure. The ideal gas equation of state (used for the bulk temperature) gives:

$$mRT_g = PV \tag{2.3}$$

Taking the derivative with respect to time while assuming that the amount of gas in the cylinder is constant, the ideal gas equation of state becomes:

$$mR\frac{dT_g}{dt} = P\frac{dV}{dt} + V\frac{dP}{dt} \tag{2.4}$$

Upon substitution into Eq. 2.2 and using the relation $c_p = c_v + R$, the conservation of energy equation reads:

$$\frac{dQ}{dt} = \frac{c_p}{R}P\frac{dV}{dt} + \frac{c_v}{R}V\frac{dP}{dt} \tag{2.5}$$

If there is no heat input to the system (via combustion or external heating), then the quantity *dQ/dt* represents the rate of heat loss from the gas. Using the chain rule, Eq. 2.5 could be expressed as:

$$\frac{dQ}{dt} = \frac{c_p}{R} P \frac{dV}{dt} + \frac{c_v}{R} V \frac{dP}{dV} \frac{dV}{dt} \tag{2.6}$$

In this expression, *P*,*V*, c_p, and c_v are known based on the thermodynamic state of the gas. The term dV/dt is the rate of change of volume, which for this geometry is the velocity of the piston times the cross sectional area. However, the rate of change in pressure with volume, dP/dV, is unknown. To proceed with this analysis, some relationship between pressure and volume must be known or assumed. This is accomplished by assuming that the pressure and volume follow a polytropic relationship:

$$PV^n = constant \tag{2.7}$$

This assumption has been found to represent many gaseous expansion processes well and was verified experimentally for the test conditions used here (see Chapter 3 and 4) (Zucker & Bilbarz, 2002) . There is also a physical significance to the exponent *n*. An expansion at constant entropy (an isentropic expansion) has an exponent *n* equal to the specific heat ratio $\gamma = c_p/c_v$, so expansion at an exponent greater than γ indicates deviation from the isentropic, ideal expansion due to irreversibilities in the expansion such as heat loss. Conversely, an isothermal expansion is one where the exponent *n* is equal to unity, as indicated in Eq. 2.3 where if PV is constant, temperature must also be constant.

Assuming a polytropic expansion, the pressure volume derivative is:

$$\frac{dP}{dV} = -n \frac{P}{V} \tag{2.8}$$

Substituting this expression into Eq. 2.6 and rearranging (as well as invoking the definition of γ as given above), the rate of heat loss from the gas becomes:

$$\frac{dQ}{dt} = \left(1 - \frac{n}{\gamma}\right)\frac{c_P}{R}P\frac{dV}{dt} \tag{2.9}$$

Following standard thermodynamic sign convention, this quantity is negative for heat lost from the system. Changing convention to what is commonly used in heat transfer (heat lost is positive), the rate of total heat lost from the gas is given by the following equation.

$$\frac{dQ}{dt} = \left(\frac{n}{\gamma} - 1\right)\frac{c_P}{R}P\frac{dV}{dt} \tag{2.10}$$

The assumptions made in deriving Eq. 2.10 are:

- Spatially uniform temperature and pressure (bulk state)
- Ideal gas
- Constant mass (no leakage or inlets)
- Polytropic expansion, determined by the exponent *n*
- No heat input

The assumption of no heat input is required in order for this result to be interpreted as heat loss, otherwise the above expression gives the "apparent" heat loss or gain (Heywood, 1988).

Equation 2.10 is the basis for the proposed heat transfer model; however, it can be rearranged to provide more insight and utility. Recognizing that the time rate of volume

change is the piston velocity, v_p, times its cross sectional area, and expressing the heat loss as a flux, the expression becomes

$$\dot{q}'' = \left(\frac{n}{\gamma} - 1\right)\frac{c_p}{R}\frac{A_c}{A_s}Pv_p \tag{2.11}$$

Where A_c is the piston cross sectional area and A_s is the total surface area for heat transfer. For the geometry given in Figure 2.1 these quantities are $A_c = \left(\frac{\pi}{4}\right)D^2$ and $A_s = \pi Dx + 2A_c$. Introducing the definition of the heat transfer coefficient given by Newton's law of cooling, $\dot{q}'' = h\left(T_g - T_{wall}\right)$, and again invoking the ideal gas equation of state to rewrite pressure gives Eq. 2.12:

$$h = \left(\frac{n}{\gamma} - 1\right)\left(\frac{A_c}{A_s}\right)\left(\frac{T_g}{T_g - T_{wall}}\right)\rho c_p v_p \tag{2.12}$$

The quantity $\frac{T_g}{T_g - T_{wall}}$ is a non-dimensional temperature based on the driving temperature difference for heat transfer; this is defined as θ. This expression can be further non-dimensionalized by introducing the Nusselt number, $Nu_D = \frac{hD}{\kappa}$, the Reynolds number, $Re_D = \frac{\rho v_p D}{\mu}$, and the Prandtl number, $Pr = \frac{\mu c_p}{\kappa}$. Additionally, the term A_c/A_s can be rewritten for the geometry given in Figure 2.1 as $A_c/A_s = 1/(2 + 4x^*)$, where x^* is the piston position non-dimensionalized by the cylinder diameter, $x^* = x/D$. Given in this dimensionless form, the heat transfer during the expansion of a gas is equal to

$$Nu_D = \left(\frac{n}{\gamma} - 1\right)\left(\frac{1}{2 + 4x^*}\right)\theta Re_D Pr \tag{2.13}$$

The length scale for both Nusselt and Reynolds numbers is the cylinder diameter, *D*, while the velocity scale used in the Reynolds number is the instantaneous piston velocity, v_p. Since the derivation was based on the bulk gas temperature, properties such as thermal conductivity, viscosity, density, and specific heat must be evaluated at the bulk gas temperature (defined by the ideal gas equation of state). This analysis was not restricted to any particular gas, so is valid for any gas species provided that the thermal properties are evaluated for the species at hand. However, the gas must behave ideally, which is true for many gases over a wide range of thermodynamic states (Moran & Shapiro, 2008).

2.2 Alternate Expressions

The non-dimensional parameters in Eq. 2.13 could be expressed differently, and exploring these alternate expressions is helpful in understanding the underlying processes driving heat transfer. The product of the Reynolds number and Prandtl number is the Peclet number, $Pe = \frac{v_p D}{\alpha}$, which expresses the ratio of the advection (bulk fluid motion) rate to conduction (molecular motion) heat transfer rate:

$$Nu_D = \left(\frac{n}{\gamma} - 1\right)\left(\frac{1}{2 + 4x^*}\right)\theta Pe_D \qquad (2.14)$$

The expression of the heat transfer model in Eq. 2.14 emphasizes the direct relationship between the Nusselt and Peclet numbers for the expansion process. Since the Nusselt number represents the rate of convection to conduction heat transfer, what is seen is that

heat loss via convection is directly proportional to the strength of bulk fluid motion. The proportionality between these two is governed by the position along the expansion, the temperature of both the fluid and the wall, and the polytropic term which represents the deviation of the expansion from the isentropic ideal.

The Nusselt, Reynolds, and Prandtl numbers could also be combined to form the Stanton number:

$$St = \frac{Nu}{RePr} = \frac{h}{\rho c_p v_p} \tag{2.15}$$

As can be seen by its definition, the Stanton number represents the ratio of heat transfer by convection to the thermal energy storage of the fluid. Using this, Eq. 2.13 becomes

$$St = \left(\frac{n}{\gamma} - 1\right)\left(\frac{1}{2 + 4x^*}\right)\theta \tag{2.16}$$

This expression of the heat transfer model combines the information contained in Reynolds, Prandtl, and Nusselt numbers into one quantity. The ratio n/γ is roughly constant for the expansion, and since both $1/x^*$ and θ decrease monotonically during the expansion the Stanton number will also decay monotonically. In this form, the transient nature of the heat transfer characteristics is shown to be strongly dependent on the dimensionless position, x^*. It is noted that upon examining the expression for the heat transfer coefficient, Eq. 2.12, that the Stanton number emerges as the simplest non-dimensional form for the heat transfer coefficient.

These alternate expressions of the heat transfer model are useful in understanding the implications of the proposed model. Many other researchers have chosen to represent their results using the Nusselt, Reynolds, and Prandtl numbers, so the original form given in Eq. 2.13 is used frequently in order to draw comparisons between the proposed model and other models. However, as will be seen later, describing the heat transfer using the Peclet number as shown in Eq. 2.14 may be the most appropriate dimensionless form for understanding and modeling the expansion process because of the significance of the Peclet number to modeling the polytropic exponent.

2.3 Model Discussion

The expression in Eq. 2.13 relates the heat transfer characteristics to the physical characteristics of the expansion process in a dimensionless manner. No pseudo-steady state assumptions were made in the derivation, so the expression given is by nature fully transient, which was the objective. Because spatial non-uniformities were not considered in the analysis, the development of this model did not explicitly invoke the use of the boundary layer or developing flow phenomena. While this means that spatial information concerning the heat transfer is not expressed, this is not at the loss of transient accuracy since the other parameters represent these transient effects in the process.

By expressing the result in a dimensionless form the governing physical processes are illuminated, and the result can be compared with the results from other studies. Two important parameters in the heat transfer model are the Reynolds number, and the Prandtl

number. These dimensionless parameters are of importance in many heat transfer applications because they encapsulate much of the necessary information about the flow conditions (Incropera et al., 2007). The Reynolds number for the expansion contains information on the magnitude of inertial forces for this expansion compared to viscous forces. The Prandtl number is a combination of thermophysical fluid properties that compares the ratio of momentum diffusion to heat diffusion. The proposed form of the heat transfer model, Equation 2.13, suggests that the exponents on the Reynolds and Prandtl numbers for this process should each be unity. The common pseudo-steady state form which has been used to model the expansion process uses an exponent of 0.7 or 0.8 on the Reynolds number (Annand, 1963; Woschni, 1967; Hohenburg, 1980; Chang et al., 2004). This pseudo-steady state form comes from the Colburn equation for turbulent flow in tubes:

$$Nu_D = 0.023 {Re_D}^{4/5} Pr^{1/3} \tag{2.17}$$

This equation comes from a more general statement of similarity between fluid flow and heat transfer. This similarity stems from the processes of heat diffusion and fluid shear stress being identical, both representing the transport of a property (energy or momentum, respectively) across a spatial gradient of either temperature or velocity, respectively. When formulated mathematically by the energy equation and the Navier-Stokes equation, it can be shown that the governing equations and boundary conditions for heat and momentum transport in boundary layer flow have the same form; therefore the solutions to these equations must also be related (Incropera et al., 2007). This forms a

basis for relating the shear stress in a fluid to the heat flux. The Colburn analogy (or modified Reynolds analogy) relates the two processes for fully developed flow in tubes by the non-dimensional parameters governing each situation:

$$Nu = \left(\frac{f}{8}\right) RePr^{1/3} \tag{2.18}$$

The analogy of Eq. 2.18 has proved to be very useful and accurate in predicting heat transfer for flows such as pipe flow, even when the flows are turbulent. This analogy is also at the heart of the pseudo-steady state models discussed in Chapter 1. In pipe flows, the Darcy friction factor, *f*, is often replaced by a function of the Reynolds number, $f \propto Re^{-0.2}$. This is gives the power of 0.8 on the Reynolds number used by many pseudo-steady models.

However, while fluid flow and heat transfer are undoubtedly related during an expansion process, Eq. 2.18 is not strictly applicable for the expansion process. This is because the assumptions in the Colburn analogy leading to Eq. 2.18 include assumptions invalid for the expansion process, such as steady flow and constant thermal properties. These assumptions are not valid for the expansion process currently studied, so the direct application of Eq. 2.18 is not valid. Therefore, from a fundamental perspective, the difference between the exponent on the Reynolds number for the model proposed by Eq. 2.13 and the exponent used in pseudo-steady state models results from how similarity between the flow and the heat transfer is imposed. While the processes of momentum and energy transport are undoubtedly still connected due to their inherent natures, the

relationship between the two is not governed by the simple Colburn analogy in Eq. 2.18 for the process of gas expansion.

The heat transfer expression given in Eq. 2.13 also contains information on both the expansion distance and the gas to wall temperature difference. The term $1/(2 + 4x^*)$ comes from the ratio of cross sectional area to total surface area; however, it resembles the entry length correction often used for turbulent flow in tubes (Eq. 1.9). It similarly functions to enhance heat transfer near the inlet or beginning of expansion. The non-dimensional temperature term is $\theta = T_g/(T_g - T_{wall})$; this bears some resemblance to the correction factor often used to model flows with large gas to wall temperature differences (Eq. 1.8). However, the term shown above tends towards unity for large temperature differences, while the factor used in Eq. 1.8 serves to enhance heat transfer for large temperature differences. Since the factor used in Eq. 1.8 is used to model flow in tubes, this seems to be another difference between heat transfer during an expansion process and in pipe flow.

The Reynolds number, Prandtl number, and the non-dimensional temperature and distance quantities in Eq. 2.13 are known from the thermodynamic state of the gas and the geometric considerations of the piston-cylinder assembly. What is unknown is the term *n*, which is the polytropic exponent governing the expansion process, as defined in Eq. 2.8. If this parameter is equal to the specific heat ratio γ, the Nusselt number calculated by Eq. 2.13 goes to zero. This is in agreement with an adiabatic and reversible expansion, which by definition has no heat loss and has the pressure-volume relationship

given by $n = \gamma$ (Moran & Shapiro, 2008). What remains to complete the development of the heat transfer model is a method for predicting the value of *n*.

2.4 Flow Considerations

Before investigating methods of determining the polytropic exponent *n*, it is important to discuss more of the differences between an expansion process and a flow. The term "flow" describes continuous bulk motion of a fluid, driven most commonly by spatial pressure gradients or gravitational forces. An expansion process is not a flow, but describes a fixed mass of fluid whose volume increases due to a pressure differential between the contained fluid and ambient conditions. While this has characteristics certainly similar to some flows, the processes are not identical.

In order to examine the flow characteristics of the expansion, an analysis is done comparing flow in tubes with an expansion by way of their characteristic fluid velocities. From the geometric arrangement examined here, the expansion process seems to resemble flow in a tube. For flow in tubes, the characteristic velocity can be defined as the spatial average velocity needed to achieve the given flow rate (Incropera et al., 2007):

$$u_m = \frac{\dot{m}}{\rho A_c} \tag{2.19}$$

For a piston-cylinder expansion, an obvious choice for the characteristic velocity would be the piston velocity. However, this velocity is not a uniform fluid velocity. Simply by imposing a no-slip boundary condition on the walls, one can infer that the

fluid velocity at the piston face in Figure 2.1 would equal the piston speed, while the fluid velocity at the opposite end of the chamber ($x = 0$) would remain zero for the duration of the expansion. An estimate of the fluid velocity distribution between these points can be made by using the differential form of the continuity equation:

$$\frac{D\rho}{Dt} + \rho\frac{\partial u}{\partial x} + \rho\frac{\partial v}{\partial y} = 0 \tag{2.20}$$

This can be simplified by restricting the analysis to along the centerline and assuming symmetry, which eliminates the gradients in *y*. Under the assumptions of uniform pressure and temperature (as used in developing the heat transfer model), spatial variations in density may also be neglected. These assumptions lead to a linear velocity distribution (see Appendix B):

$$u = \frac{v_p}{L}x \tag{2.21}$$

While these assumptions may be too restrictive for a detailed model of the velocity distribution, this analysis gives a rough idea of what the gas velocities within the cylinder are. Assuming the velocity distribution of Eq. 2.21, the maximum gas velocity is the piston speed while the average gas velocity is half of the piston speed. This justifies the velocity scale used in the Reynolds number for the previous analysis (the piston speed), since this is the quantity that characterizes the fluid velocity within the cylinder. If it was desired to use an average gas velocity in modeling the expansion process, simply half the piston speed could be used. Since this would result in an extra factor of two in the model shown by Eq. 2.13, the current study leaves the characteristic velocity as the

piston speed. The presence of this axial velocity gradient by Eq. 2.21 illustrates one of the differences between the expansion process and steady flow in tubes, which has uniform velocity in the axial direction (assuming a constant cross sectional area).

2.5 Polytropic Exponent

The heat transfer model developed for the expansion process and shown by Eq. 2.13 includes the parameter *n*, the polytropic exponent. This parameter is not known *a priori* for an expansion process. Therefore, in order for the heat transfer model to be useful in predicting heat transfer, this unknown parameter must be related to other, known parameters concerning the expansion process.

The analysis of the expansion process conducted thus far has shown the importance of transient characteristics of the expansion on heat transfer. This will also be seen in Ch. 4 when the results from the proposed heat transfer model are compared with experimental data. Also seen in this analysis is the importance of the polytropic exponent, *n*, in characterizing the expansion process, as this parameter governs the pressure decay with volume during expansion. Since the expansion process is inherently transient, it is reasonable to suggest that *n* is related to the transient nature of the process and could be characterized by some time or rate scale associated with the expansion.

Examining the limiting cases of long and short expansion time scales provides evidence that the polytropic exponent is indeed related to the time scale associated with

the expansion process. As the expansion process becomes very slow (a long expansion time scale), the rate of change of pressure with volume, dP/dV, becomes large as pressure decreases due to heat transfer while the volume changes very little. In the limit of an isochoric (constant volume) process, the polytropic exponent approaches infinity (Zucker & Bilbarz, 2002). In the other limit, as the expansion process becomes very fast the process becomes nearly adiabatic, as the time for heat transfer to occur becomes negligibly small. This limit suggests that $n \to \gamma$, as this would cause the heat transfer by Eq. 2.10 to approach zero. Thus, by examining the limiting cases, it can be seen that the polytropic exponent is affected by the expansion rate. Examining the time scales associated with the expansion process can then provide a basis for a functional form used to determine the polytropic exponent.

One way to characterize the time associated with the expansion process is by comparing the expansion rate with the rate at which heat can diffuse through the cylinder gases. This results in the Peclet number, which can also be viewed as a combination of the Reynolds and Prandtl numbers for the expansion process:

$$\frac{v_p D}{\alpha} = Pe = RePr \tag{2.22}$$

The Peclet number shown in Eq. 2.22 is an instantaneous value, since both the piston speed, v_p, and the thermal diffusivity, α, change during the expansion. Since the polytropic exponent, *n*, is a constant value for an expansion, the parameter used to characterize it should also be a constant value which describes the expansion. A

characteristic Peclet number describing the expansion process can be obtained by using the mean piston speed, S_p, as the characteristic expansion velocity. This results in the following definition of the characteristic Peclet number for the expansion process:

$$Pe^* = \frac{S_p D}{\alpha_0} \tag{2.23}$$

Where α_0 is the thermal diffusivity of the gas, taken at the initial conditions of the expansion so that it is a known quantity. Comparing the expansion speed with the heat diffusion speed effectively references the magnitude of the expansion time to the time required for heat to diffuse through the gas. Therefore, it is proposed that the polytropic exponent can be determined as a function of the characteristic Peclet number for the expansion:

$$n = f(Pe^*) \tag{2.24}$$

Describing the polytropic exponent with the characteristic Peclet number emphasizes the ratio between the time scale associated with heat diffusion and with the expansion. The importance of the Peclet number in determining the polytropic exponent suggests that the most appropriate non-dimensional form of the overall heat transfer model is the form given by Eq. 2.14 (reproduced below as Eq. 2.25):

$$Nu = \left(\frac{n}{\gamma} - 1\right)\left(\frac{1}{2 + 4x^*}\right)\theta Pe_D \tag{2.25}$$

The Peclet number used in Eq. 2.25 is the instantaneous value based on the time-dependent piston velocity and thermal diffusivity (Eq. 2.22), as opposed to the constant

value used in Eq. 2.23 to model the polytropic exponent. Because of the importance of the Peclet number to describing the polytropic exponent, Eq. 2.25 is suggested as the most appropriate form of the proposed heat transfer model.

In characterizing the time associated with the expansion process, the expansion rate could also be compared with other rates relevant to the expansion process. Another rate relevant to the expansion process is the acoustic velocity, which describes the speed at which pressure waves can propagate through the gas mixture. For an ideal gas, the acoustic velocity can be calculated as:

$$c = \sqrt{\gamma RT} \tag{2.26}$$

From Eq. 2.26, it is seen that the acoustic velocity is a state variable; therefore, using this is also a means of comparing the expansion process with the thermodynamic state of the gas mixture. Comparing the expansion speed to the acoustic velocity gives the following definition for a parameter describing the characteristic time scale of the expansion:

$$S_P^* = \frac{S_P}{\sqrt{\gamma_0 RT_0}} \tag{2.27}$$

Where S_P^* is a dimensionless mean piston speed. Since both γ and T change during the expansion, their values are taken at the initial conditions so that they are known at the beginning of the expansion. Eq. 2.27 emphasizes the importance of the mean piston speed and the thermodynamic state of the gas on characterizing the expansion process, and leads to the following functional form for the polytropic exponent:

$$n = g\left(S_p^*\right) \tag{2.28}$$

In order to determine the functional relationships, f and g in Eq. 2.24 and Eq. 2.28, experiments were conducted. The results of these experiments also produced heat transfer data for the expansion, which were used to test the accuracy of the proposed model for heat transfer, Eq. 2.25. The experimental methodology used to conduct these tests is discussed next in Ch. 3, and the results are presented in Ch.4.

Chapter 3 – Experimental Methodology

Experiments were performed in order to test the analytic model developed for heat transfer during the expansion of a gas. As shown in Ch. 2, the polytropic exponent is related to the characteristic time scales associated with the expansion process, such as the characteristic Peclet number and a dimensionless form of the mean piston speed. The exact forms of these relationships, however, are not known. Therefore, one purpose of the experiments is to establish the relationship between the polytropic exponent and both the characteristic Peclet number and the mean piston speed. It is also necessary to test the overall accuracy of the analytic model developed for heat transfer during the expansion of a gas. This is done by experimentally determining the heat transfer coefficient and comparing this result to the value predicted by the model. The spatial variance of the heat transfer coefficient is not considered, but its time evolution is to be determined. In order to determine the heat transfer coefficient, as defined by Newton's law of cooling (Eq. 1.1), the total heat flux from the gas to the wall and the bulk gas temperature (as defined by Eq. 1.2) is required. The bulk gas temperature is determined by measuring the average pressure and the cylinder volume, relating these to temperature using the ideal gas equation of state, Eq. 1.2. Heat flux is determined by an energy balance, again relying on the measured pressure and volume.

The experimental test facility, built in 2009, used a single shot, single piston-cylinder assembly, located at the laboratory of Long Haul Power, LLC, in Corvallis, OR.

This apparatus allows for recording pressure, volume, and time data for a single expansion event. In order to evaluate the applicability of the heat transfer expression, tests conditions were varied to produce a range of conditions on the expansion. In particular, test conditions were controlled in order to produce a range of Reynolds numbers. This was done because it will allow characterizing the polytropic exponent over a range of Peclet numbers and piston speeds. An uncertainty analysis was conducted in order to ascertain the level of confidence in the final results.

3.1 Experimental Setup

The experimental setup was used to extract necessary information to evaluate the heat transfer that occurs during the expansion of a gas. Prior to its expansion however, the gas mixture undergoes a combustion reaction. Understanding and investigating the energy release via combustion and the heat transfer associated with this reaction are not topics of this present research. Instead, the combustion reaction is used primarily to generate the initial conditions needed for the expansion, which are high pressures to drive the expansion and high temperatures to drive heat transfer from the gas to the cylinder walls and piston head. The data of interest to this study begins after combustion, once the piston starts expanding.

An experimental test facility had been constructed at Long Haul Power, LLC for other experimental purposes but was found to be suitable for the current study. A

schematic of the test apparatus is shown below in Figure 3.1; photographs of the facility are included in Appendix C.

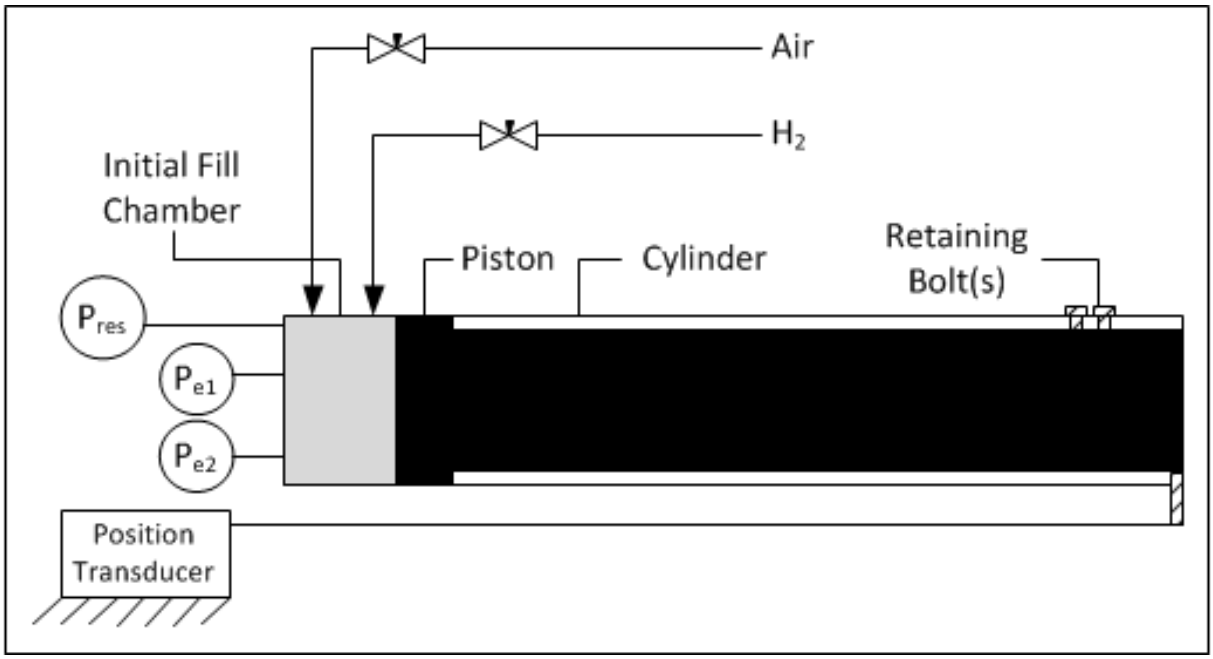

Figure 3.1 – Schematic of experimental apparatus used to conduct tests

This test apparatus is a single piston-cylinder assembly, which is used for a single expansion event (it does not reciprocate). An initial fill chamber is attached to one end of the assembly, and forms a seal with the piston and cylinder. The cylinder diameter is 4 inches. The piston is initially held in place by one to three retaining bolts (depending on the test requirements), as shown in Figure 3.1. To operate, the initial fill chamber is filled with a mixture of air and hydrogen. Air is added first, controlled by a needle valve until the desired initial air pressure is reached. Hydrogen is then added, similarly controlled by

a needle valve, until the desired mixture composition is reached. The final mixture composition can be described using the mole fraction, χ, of each species, which can be determined by the partial pressure of each gas as the chamber is filled:

$$\chi_{air} = \frac{P_{air}}{P_T}; \quad \chi_{H_2} = \frac{P_{H_2}}{P_T}$$

The air pressure, P_{air}, was known from the initial air fill pressure since air was the first species added. The hydrogen pressure, P_{H_2}, was the difference between the total pressure in the system after both hydrogen and air had been added, and the initial air pressure. The total pressure of the mixture is P_T. This mixture is then ignited by spark-plug type electrodes located the initial fill chamber. The piston is held immobile while the mixture undergoes a combustion reaction by the retaining bolt(s) holding it in place, and the pressure in the initial fill chamber rises very rapidly. Once the pressure reaches a certain value, the bolt(s) shear, allowing the piston to accelerate rapidly. As the piston expands, some of the energy in the gas is lost as heat while the rest goes into expansion work. This work is dissipated by the raising of a weight (not shown). The expansion that occurs immediately following the shearing of the bolts is the expansion of interest for these tests.

The initial air pressure and the initial mixture pressure (prior to ignition) was recorded by an Omega model PX309 piezo-resistant type pressure transducer (shown in Figure 3.1 as P_{res}). In order to record the rapid pressure rise during combustion and the subsequent rapid pressure drop during expansion, two piezoelectric pressure transducers,

by PCB Piezotronics model 102B04 (shown in Figure 3.1 as P_{e1} and P_{e2}), were used. Piston position was known from the cable-extension position transducer, Celesco model PT5A. The output from these sensors was read by a LabVIEW controlled data acquisition system. The block diagram and the front panel of this system are shown in Appendix C. Data were sampled and recorded at a rate of 25,000 Hz in order to capture the expansion event in detail, as the expansion process was very rapid, lasting less than 50ms. The experimental setup and data acquisition system were built and assembled by Long Haul Power prior to this author's involvement.

3.2 Data Reduction

The output from the piston-cylinder assembly used for these experiments was pressure, position, and time data. Position data was a voltage output from the position transducer directly proportional to the piston displacement. The calibration to convert voltage to position for this was performed *in situ* (see Appendix D). Since the geometry was a right cylinder, the volume was determined from $V = \frac{\pi}{4} D^2 x$, where x is the piston position and D is the cylinder diameter.

The polytropic exponent of the expansion process is determined by the pressure-volume relationship:

$$PV^n = constant \tag{3.1}$$

This can be rewritten in a linear fashion using logarithms as:

$$\log(P) = -n\log(V) + \log(C) \tag{3.2}$$

The value of *n* was determined using a least squares fit of pressure versus volume data based on Eq. 3.2. The polytropic exponent is the slope of this line.

The pressure-volume data was also used to obtain the heat transfer coefficient for the expansion process. This was done by means of a global energy balance. The analysis used to determine this begins identically as the global energy balance used to analyze this process in Ch. 2, and has been used by other researchers to obtain time-dependent heat transfer information (Chen & Karim, 1998; Ota, 2008).

Using the same terminology as in Figure 2.1, a global energy balance of the gas within the cylinder can be written as:

$$dU = dQ - dW \tag{3.3}$$

By assuming that the gas behaves ideally, this can be rewritten in terms of solely pressure and volume (see Eqns. 2.1-2.4 for this derivation), and rearranged to give:

$$dQ = \frac{c_p}{R}PdV + \frac{c_v}{R}VdP \tag{3.4}$$

In Eq. 3.4, *dQ* represents a differential amount of heat lost from the gas. To obtain the total, accumulated heat lost as a function of time, this expression is integrated from the start (t_0) to the time of interest:

$$Q(t) = \int_{V(t_0)}^{V(t)} \frac{c_p}{R}PdV + \int_{P(t_0)}^{P(t)} \frac{c_v}{R}VdP \tag{3.5}$$

Pressure and volume were measured directly, and the specific heats were calculated based on the bulk temperature determined through the ideal gas equation of state. The quantity *Q(t)* was obtained from the experimental data by numerically evaluating the integrals in Eq. 3.5.

The key assumptions necessary to use this method to experimentally determine the heat transfer coefficient are that the gas follows the ideal gas equation of state, that the mass in the cylinder is constant, and that there is no heat input/combustion during the expansion. The assumption of no heat input is necessary so that the quantity calculated in Eq. 3.5 is the heat loss, rather than a net heat transfer (heat loss minus heat input). As was previously described, the high pressures and temperatures needed at the beginning of the expansion were obtained by burning hydrogen with air (forming water vapor and nitrogen) in a constant volume vessel. Therefore, the assumption of no combustion during the expansion was also necessary in order to determine the gas composition, which was calculated assuming complete combustion. Because of the importance of this assumption to the data reduction, constant volume ("bomb") tests were conducted to justify combustion completeness. To do this, the piston was restrained with additional retaining bolts so that it could not move. Combustion time was then determined, defined as the time from the beginning of pressure rise to the peak pressure. This information was then used to determine whether it was justified in assuming that the reaction had completed by the time expansion began. Combustion times typically lasted around 2ms. By defining the start of expansion by a 1% volume increase, sufficient time was allowed for combustion

to complete prior to expansion. This is discussed further in Chapter 4 when the experimental data is presented and discussed.

In order to obtain the desired heat transfer coefficient the rate of heat loss is necessary. This was done simply by evaluating the time derivative of Eq. 3.5, $\dot{q} = dQ/dt$. Using the definition of bulk temperature given in Eq. 1.2, the heat transfer coefficient was calculated using Newton's law of cooling as:

$$h = \frac{\dot{q}}{A_s\left(T_g - T_{wall}\right)} \tag{3.6}$$

Surface area A_s includes the cylinder wall and piston face and was calculated as $A_s = \pi Dx + 2(0.25\pi D^2)$, given the geometry shown in Figure 2.1. The wall temperature used in Eq. 3.6 was assumed to be constant and uniform wall temperature. This was justified by a transient conduction analysis assuming that the cylinder walls and piston face could be modeled as a semi-infinite solid. This analysis imposes a step change in heat transfer coefficient and then holds both the gas temperature and the heat transfer coefficient constant, and the time response of the wall temperature was determined. In reality the temperature and the heat transfer coefficient are not constant, consequently this analysis provides a worst case scenario. The results of this analysis show that for the small time durations seen in this expansion process the semi-infinite approximation is valid and the wall temperature is very nearly constant, with a maximum increase of 3% from the initial wall temperature. This increase in wall temperature would change the gas to wall temperature difference by a maximum of 2.25%. Since this is a small change and

represents an over-statement of the wall temperature rise (due to being a worst-case scenario analysis), the assumption of constant and uniform wall temperature is justified. Details of the conduction analysis are included in Appendix E. The experimentally determined heat transfer coefficient calculated using Eq. 3.6 is a spatially averaged value, as the temperature used for the gas is the bulk temperature, the expression for the heat loss rate is for the entire gas volume, and the heat transfer occurs over the entire exposed wall surface area.

Since this research is focused solely on the heat transfer while the gas expands, a method of uniquely and consistently defining the beginning of expansion was necessary. Additionally, it was required that this point be sufficiently past the ignition point such that combustion was completed by the beginning of expansion. This was done by defining the beginning of expansion as the point where the cylinder volume has increased by 1% from its original volume. The time associated with this amount of expansion was then compared to the combustion time measured in the bomb. The cutoff value chosen could be arbitrary, but it was desirable to have this as small as possible so that information on the early expansion period was not lost, and necessary for this value to consistently represent a time that is beyond the combustion time. The value of 1% increase from the original volume was selected because it ensured enough time had elapsed for combustion to be complete without sacrificing very much information on the expansion heat transfer. This is further discussed in the Ch.4 .

Other parameters concerning the expansion are also of interest, and can be calculated from the experimental data. The bulk gas temperature used in Eq. 3.6 was calculated using the ideal gas equation of state:

$$T_g = \frac{PV}{mR} \tag{3.7}$$

In this expression, *P* is the measured gas pressure, *V* is the measured cylinder volume, *R* is the gas constant for the mixture, and *m* is the mass of the gas. The quantity *m* was known similarly from the ideal gas equation of state, applied at the initial fill conditions where the gas temperature was assumed to be ambient temperature.

$$m = \frac{P_T V_i}{R T_{amb}} \tag{3.8}$$

This mass is constant (no inlet or exits), so the density throughout the expansion is calculated using its definition:

$$\rho = \frac{m}{V} \tag{3.9}$$

Finally, the piston speed was calculated from the time derivative of volume (this was approximated numerically with a five-point finite difference):

$$v_p = \frac{1}{A_c}\frac{dV}{dt} \tag{3.10}$$

3.3 Test Conditions

In order to test the validity of the heat transfer model developed, it was necessary to test over a range of parameters. Based on the form of Eq. 2.13, the main parameters of interest to vary are the Reynolds number (which could be varied by varying density or piston speed), gas temperature, and the gas composition (which affects the Prandtl number and specific heat ratio). Variations in the Reynolds and Prandtl numbers will also produce variations in the Peclet number, which is also desired to characterize the polytropic exponent. The two main parameters which could be varied in the described experimental apparatus are the initial fill pressure, and the mixture composition (via the equivalence ratio, discussed below).

Changing the initial fill pressure while maintaining a constant equivalence ratio changes the peak pressures (and therefore piston speed) and gas densities attained during the expansion. Increasing the fill pressure increases both the piston speed and the density, thereby increasing the Reynolds number during the expansion process. By varying the fill pressure, a range of Reynolds numbers experienced during the expansion process could be obtained. Changing the initial fill pressure would have little effect on the subsequent peak bulk gas temperatures, since the energy released per mass is governed by the mixture composition, which is constant.

The mixture composition of hydrogen and air is best understood through use of the equivalence ratio, ϕ, which compares the amount of hydrogen mass inputted to the amount needed for complete combustion with no excess fuel or oxidant (stoichiometric

combustion). An equivalence ratio of one is combustion with no excess oxygen or fuel, as seen by the following:

$$H_2 + \frac{0.5}{0.21 * \phi}\,(0.21O_2 + 0.79N_2) \rightarrow H_2O + \frac{1.88}{\phi}N_2 + 0.5 * \left(\frac{1}{\phi} - 1\right)O_2 \quad (3.11)$$

By making changes to the equivalence ratio, the product gas composition is varied. Equivalence ratios less than one result in oxygen remaining in the exhaust, while equivalence ratios greater than one lead to unburned hydrogen or the presence of other species in the exhaust. Since energy is released via the combustion reaction, changing the equivalence ratio changes the amount of energy released into the system. This affects the temperatures and pressures attained at the beginning of the expansion, causing changes in the Reynolds number and temperatures experienced during the expansion, as well as affecting the gas composition.

One purpose of these experiments was to establish the relationship between the polytropic exponent and the characteristic Peclet number, and the relationship between the polytropic exponent and the mean piston speed, as proposed in Ch. 2. Variation in both of these parameters can be achieved by conducting the experiments over a range of Reynolds numbers. This was accomplished by changing the initial fill pressure while holding the equivalence ratio constant. While changing the equivalence ratio also changes the Reynolds number during the expansion, it also affects the gas temperature and composition, while changing fill pressure has very little effect on gas temperature and no effect on gas composition. Therefore by keeping the equivalence ratio constant and

increasing the fill pressure, the effect of increased Reynolds number could be isolated. The test cases conducted are shown in Table 3.1. Each test consisted of a single combustion and expansion event. In order to reduce the uncertainties associated with these experiments, multiple tests were conducted for each test condition, as listed in Table 3.1.

Table 3.1 – Test Conditions

Test Case	Air Fill Pressure (psia)	Equivalence Ratio (ϕ)	Number of Tests
Case A	14.7	1	7
Case B	20.0	1	6
Case C	27.4	1	6
Case D	34.7	1	6
Case E	44.7	1	9

The test cases listed in Table 3.1 provided for a wide range of Reynolds numbers to be tested, with mean Reynolds numbers ranging from 2400-12,200. Some tests were conducted at higher pressures than listed in an attempt to extend the test boundaries. It was found however that tests at higher fill pressures could not be conducted confidently because of leaks in the initial fill chamber. The amount of gas present in the cylinder during expansion was determined using Eq. 3.8. In order for this to be valid, the filling process must be slow to allow for the gas to come to an equilibrium temperature. This was incompatible with the higher leak rates present at fill pressures greater than those listed in Table 3.1, so these tests were not considered.

Each operating condition for the tests was repeated 6-9 times, as listed in Table 3.1. The results of these individual runs were then combined to form a single representative data set for that operating condition. While processing the data, it was found that the method outlined in Eqns. 3.3-3.6 required that the data be smooth. Therefore the representative data set for each operating condition was determined by fitting a smooth curve through the combination of all data sets for that operating condition. This was done using least-squares regression models. Details concerning this procedure are given in Appendix F.

3.4 Uncertainty Analysis

An uncertainty analysis was conducted in order to make an estimate of the uncertainties in the overall results. Bias errors for each instrument were taken from the manufacturer's specifications or from calibration, as given in Table 3.2. The piezoelectric sensors used for cylinder pressure during the combustion of the gas and the piston expansion had a calibration certificate from the manufacturer, Piezotronics, and calibration for the position transducer was performed *in situ* by the author (see Appendix D). Precision errors were calculated using the sample standard deviation between all the tests conducted for each test case and assuming 95% confidence. These precision errors were found to vary from test to test, as well as during the expansion; the values used were mean values of these precision errors for each test condition. The bias and precision

errors were then combined in a root-sum-square manner to produce the total uncertainty in measured parameters. This is shown in Table 3.3.

Table 3.2 – Instrument Uncertainties

Parameter	Instrument	Manufacturer	Model #	Nominal Value	Bias Error
Cylinder Diameter	Calipers	Mitutoyo	CD-6”CSX	4 in.	0.0005 in.
Piston Position	Cable-Extension Position Transducer	Celesco	PT5A	1.5 -12 in.	0.051 in.
Fill Pressure	Piezo-Resistant Transducer	Omega	PX309	27.4-91.9 psia	0.55 psia
Cylinder Pressure	Piezo-Electric Transducer	Piezotronics	102B04	varies	1.3 % of reading
Ambient Temperature	Thermometer	Honeywell	FocusPRO 5000	286-289 K	0.28 K

Table 3.3 – Uncertainty in Measured Variables

Test Case	Diameter	Initial Volume	Initial Fill Pressure	Ambient Temperature	Pressure	Volume
Case A	0.58%	6.09%	2.88%	1.39%	5.71%	3.84%
Case B	0.58%	6.06%	2.09%	0.26%	8.99%	6.70%
Case C	0.58%	6.40%	1.65%	0.10%	10.92%	8.85%
Case D	0.58%	5.35%	1.29%	1.09%	5.56%	4.59%
Case E	0.58%	3.64%	1.07%	0.54%	16.07%	13.32%

It was found that the precision errors were much larger than the bias errors of the instruments, especially for the cylinder pressure and volume. Thus, while the uncertainties listed in Table 3.3 are total (bias and precision) uncertainties, it is

dominated by the precision uncertainties. The breakdown between bias and precision uncertainties is shown in Appendix G.

The polytropic exponent is a measure of the non-dimensional pressure gradient during an expansion. This was calculated for each individual expansion test using the method shown in Eq. 3.1 and 3.2. For each test case, the uncertainty in the polytropic exponent was calculated from the deviation of the polytropic exponent between individual expansion tests, assuming 95% confidence, combined with uncertainties from instrument errors (which were relatively small). The uncertainty in the polytropic exponent ranged from 4%-10%, as shown in Table 3.4.

Table 3.4 – Polytropic Exponent

Test Case	**Polytropic Exponent**	**Uncertainty**
Case A	1.71	7.26%
Case B	1.52	3.59%
Case C	1.36	4.72%
Case D	1.36	6.27%
Case E	1.32	10.84%

Uncertainties were also estimated for other calculated parameters of interest. In particular, these were the gas temperature and density, piston speed, the heat transfer coefficient, and the dimensionless numbers characterizing the process. The total uncertainties in these calculated parameters were determined by the Kline and McClintock method. This method propagates the uncertainty in a measured parameter, u_x, to the uncertainty in a calculated parameter, u_y, as follows:

$$u_y = \frac{\partial y}{\partial x} u_x \tag{3.12}$$

The measured parameters for these tests are listed in Table 3.3. The uncertainties in calculated parameters from each measured variable were combined using the root-sum-square method to determine the total uncertainty in the dependent variable. The propagation of uncertainty from measured parameters to final parameters is shown graphically in Appendix G. Since the uncertainties were found to vary during expansion, the values presented in Table 3.5 are mean values for each test case for physical variables, while Table 3.6 has the mean values for each test case for non-dimensional parameters. The minimum and maximum uncertainties are included in Appendix G.

Table 3.5 – Propagated Uncertainties in Physical Variables

Test Case	**Moles**	**Temperature**	**Density**	**Piston Speed**	**Heat Transfer Coefficient**
Case A	7.12%	9.90%	8.09%	3.57%	13.38%
Case B	6.55%	12.99%	9.37%	3.79%	17.44%
Case C	6.69%	15.57%	11.10%	6.39%	26.68%
Case D	5.67%	9.17%	7.30%	2.42%	13.91%
Case E	3.89%	21.23%	13.88%	16.64%	48.67%

Table 3.6 – Propagated Uncertainties in Non-Dimensional Parameters

Test Case	**Reynolds Number**	**Prandtl Number**	**Peclet Number**	**Nusselt Number**
Case A	10.68%	9.89%	14.6%	15.40%
Case B	12.01%	12.97%	17.7%	20.12%
Case C	15.12%	15.55%	21.7%	29.44%
Case D	8.87%	9.16%	12.8%	15.62%
Case E	24.68%	21.21%	32.5%	52.18%

The uncertainty in total moles of gas is dictated solely by the initial fill conditions; the initial pressure, volume, and the ambient temperature. This was a manageably small uncertainty for each test case. The dominant sources of uncertainty for all other parameters were the cylinder pressure and volume, as shown previously in Table 3.3. Uncertainties in heat transfer coefficient ranged from 13% to 27% for test cases A-D, which were considered reasonable values for this study. However, the uncertainty in heat transfer coefficient reached nearly 50% for Case E. This was due to an increase in scatter in the data for this test case. It is unclear what caused this increase in scatter for this test case, but it is possible that this is from increased leaks in the initial fill chamber when filling to higher pressures. While this is a large uncertainty in the heat transfer coefficient, the uncertainty in the polytropic exponent was much less, as shown in Table 3.4. The value of the polytropic exponent was one of the primary goals of these experiments, as previously discussed, so even with large uncertainties in the heat transfer coefficient this test case was still useful in developing a model for heat transfer during the expansion of a gas.

The results of these experiments were compared with the analytic model previously developed in Ch.2. The presentation and discussion of these results is done next in Ch. 4.

Chapter 4 – Results & Discussion

An analytic model was developed in order to study the heat transfer that occurs during the expansion of a gas, as described in Ch. 2. The result of the analysis provided a form for the heat transfer model:

$$Nu = \left(\frac{n}{\gamma} - 1\right)\left(\frac{1}{2 + 4x^*}\right)\theta Pe_D \qquad (4.1)$$

Other forms of this model were given by Eq. 2.12-2.16; however, because the Peclet number is also significant in characterizing the polytropic exponent, the form given by Eq. 4.1 is suggested as the most appropriate form. This model assumed that the expansion process could be modeled as a polytropic process, $PV^n = constant$, where the polytropic exponent *n* is an unknown constant. By analyzing the time scales associated with this process and their implications on the polytropic exponent, it was proposed in Ch. 2 that *n* could be related to the characteristic Peclet number during the expansion, or to a dimensionless form of the mean piston speed. This model was tested by conducting experiments as described in Ch.3. These experiments were designed to determine the relationships concerning polytropic exponent suggested in Eq. 2.24 and 2.28, and to also determine the spatially averaged, instantaneous heat transfer coefficient during the expansion process.

The results of these experiments show that the pressure-volume relationship in the expansion matches the assumed polytropic expansion very closely, and that the

polytropic exponent can be modeled based on the characteristic Peclet number or the dimensionless form of the mean piston speed proposed in Ch. 2. The experimentally determined heat transfer coefficient for the expansion is then compared with the proposed overall heat transfer model as well as with previously established models. It is found that the proposed model is a good match for the experimental data, and accurately predicts the time evolution of the heat transfer coefficient during the expansion.

4.1 Experimental Results

The first component of experimental data was the constant volume ("bomb") combustion data. These tests were conducted because the high pressures and temperatures needed to drive the expansion process are created by an initial constant-volume combustion reaction in the expansion tests. Therefore, it was necessary to ascertain whether combustion had completed by the beginning of expansion. This was done by determining the combustion time from the bomb tests (no expansion), where combustion time is defined here as the time from the beginning of the measured pressure rise to the peak pressure. This time was compared to justify whether combustion was complete at the beginning of expansion, which was defined as the point where volume had increased from the initial volume by 1%. A sample output from the bomb experiments is shown in Figure 4.1 for Test Case D; other test conditions are included in Appendix H.

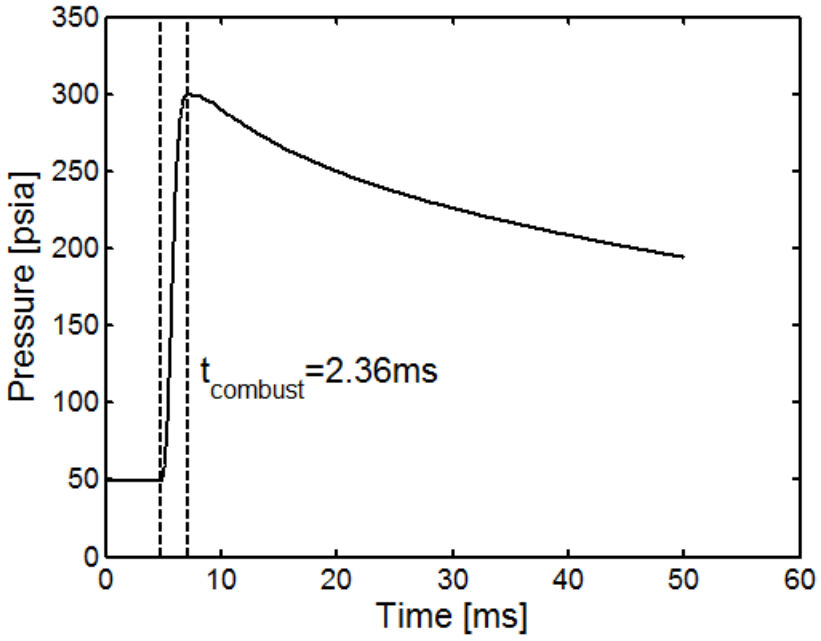

Figure 4.1 – Bomb data for Test Case D, used to determine combustion time

The measured combustion times for each of the tests conditions are reported in Table 4.1. Combustion times vary slightly for the conditions tested, which had a constant equivalence ratio of unity with various initial pressures.

Table 4.1 – Combustion Times

Test Case	**Initial Air Pressure**	**Equivalence Ratio**	**Combustion Time (ms)**
Case A	14.7 psia	1	1.84
Case B	20.0 psia	1	2.04
Case C	27.4 psia	1	2.04
Case D	34.7 psia	1	2.36
Case E	44.7 psia	1	3.20

This information was used to determine whether the combustion reaction was complete at the beginning of expansion. This is shown graphically in Figure 4.2, which

shows pressure and volume for a single combustion and expansion event, with the times corresponding to the end of combustion and the beginning of expansion marked. These representative data were taken from Test Case D, with other test conditions included in Appendix H. It can be seen that choosing to start the expansion at a 1% increase in volume from the initial fill volume gave ample time for combustion to complete before expansion data were collected.

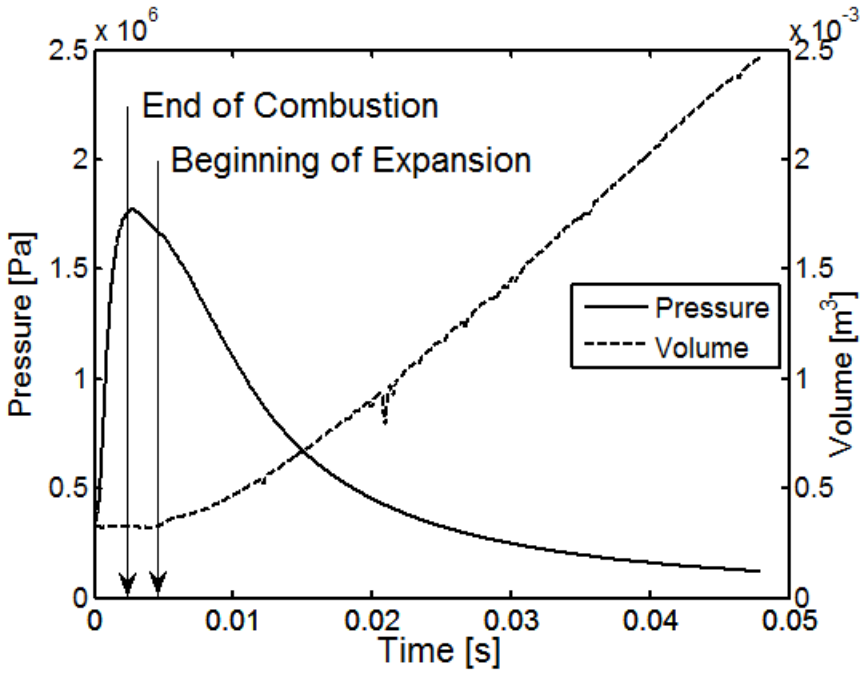

Figure 4.2 – Pressure and volume versus time for a combustion and expansion event, showing that combustion is complete by the time expansion begins. Data shown is from Test Case D.

Figure 4.2 justifies the assumption that combustion is complete when expansion begins by showing that the time at which the volume has increased by 1% of its original

value is beyond the measured combustion time. This is important because it was assumed that combustion is complete in the energy balance method used to extract heat transfer information, as discussed in Ch.3.

Multiple expansion tests were conducted for each test condition, as previously reported in Table 3.1. These tests were combined to form a single data set representative of that test condition by fitting a least squares curve through the combined data set. Figures 4.3-4.5 show the data from the expansion tests conducted for Test Case D. The experimental data from other tests conditions is included in Appendix H.

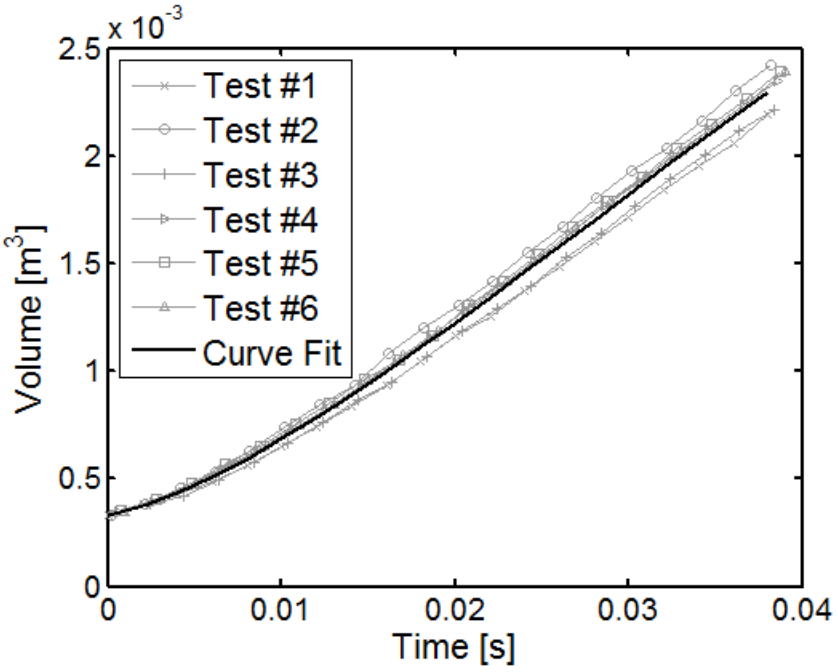

Figure 4.3 – Measured cylinder volume versus time during expansion for Test Case D

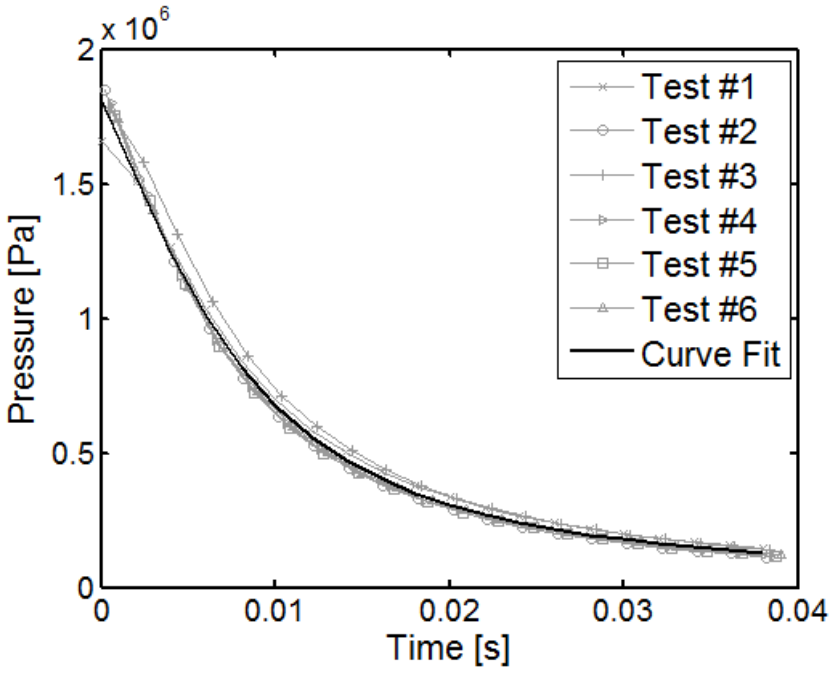

Figure 4.4 – Measured cylinder pressure versus time during expansion for Test Case D

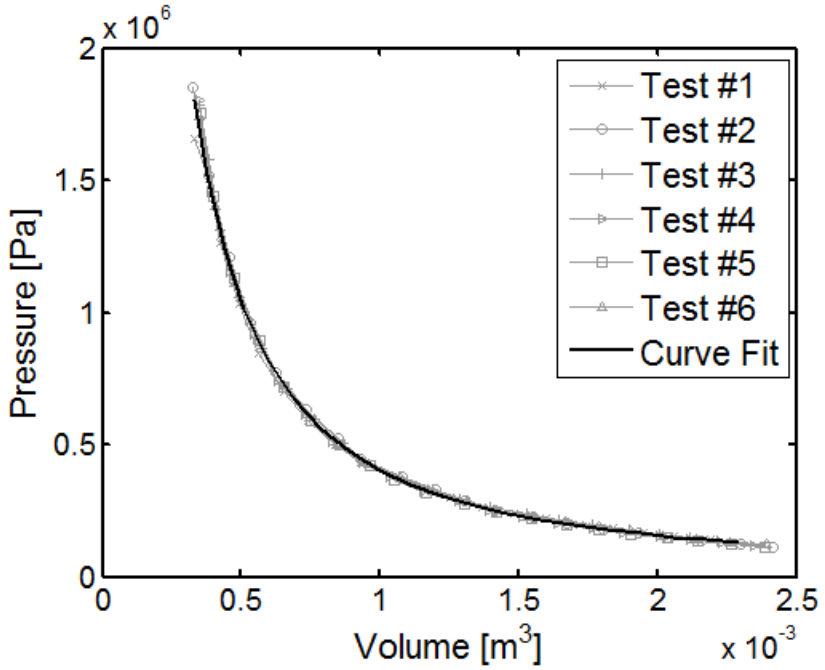

Figure 4.5 – Measured cylinder pressure versus volume during expansion for Test Case D

Figures 4.3 and 4.4 show the time evolution of volume and pressure, respectively. The piston velocity can be seen to approach a constant value midway through the expansion, as evidenced by the volume time trace becoming approximately linear in Figure 4.3. Pressure decays rapidly as the piston expands, as expected and shown in Figure 4.4. Of primary importance, however, is the pressure-volume relationship present in the expansion process (Figure 4.5). This is because the expansion process through the pressure-volume relationship determines the exponent *n* given in Eq. 4.1. Figure 4.5 shows that the individual expansion tests collapse onto a single curve on the pressure-volume diagram, showing good repeatability between tests. The curve fit shown in Figure 4.5 is a power law curve fit, meaning that the data follows a polytropic expansion (Eq. 2.7) very closely. This justifies the polytropic assumption made in developing the heat transfer model in Ch. 2.

Plotting the pressure-volume data on a logarithmic scale further illustrates the validity of the polytropic assumption. The pressure-volume data should be linear on a logarithmic scale, as suggested by Eq. 3.2, with the slope equal to the negative of the polytropic exponent. This is shown in Figure 4.6.

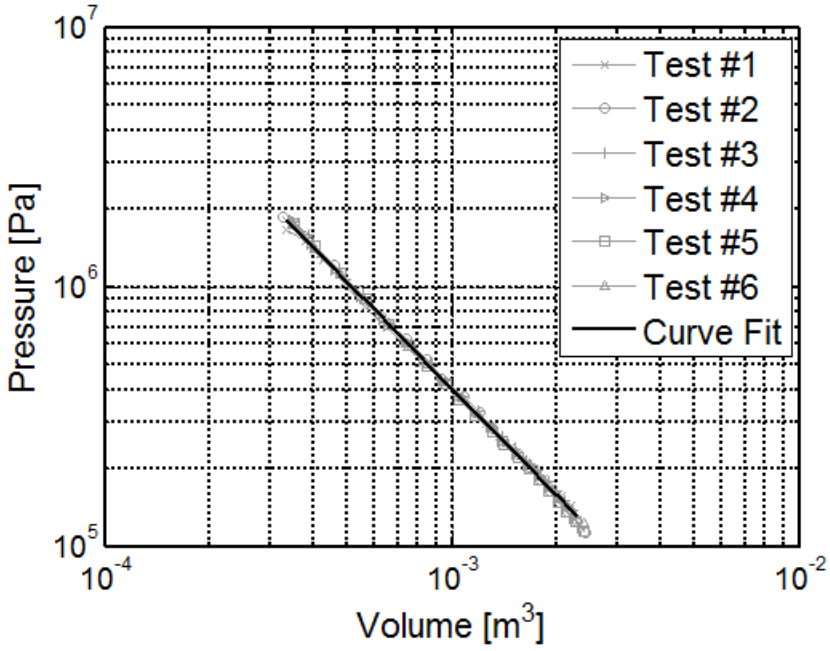

Figure 4.6 – Measured cylinder pressure versus volume during expansion for Test Case D, logarithmic scale

The experimental pressure-volume data were used to calculate the heat transfer characteristics and other relevant parameters during the expansion. These parameters are then used to describe the heat transfer in a dimensionless fashion and establish relationships for the polytropic exponent.

4.2 Expansion Characteristics

The experimental data were used to calculate parameters relevant to the expansion, such as the gas temperature, density, and piston speed. The data presented below is plotted along a non-dimensional distance, $x^* = x/D$. Plotting the results using

distance rather than time allows for direct comparisons between test conditions. This is because the total expansion time varied between test conditions, and because the thermodynamics of the expansion are more inherently linked to changes in volume (or position) rather than changes in time. Additionally, the non-dimensional distance, $x^* = x/D$, is an important factor in the heat transfer model, as seen in Eq. 4.1. Since the test apparatus included an initial fill chamber with a depth of approximately 1.5 inches and the cylinder diameter was 4 inches, the term x^* does not start at zero but near $x^* = 0.38$ since the initial volume at the initial time is not zero.

The gas pressure and the bulk temperature during the expansion for each test condition are presented below in Figures 4.7 and 4.8, respectively. The pressure reported is from the smooth curve combining the individual tests, and the bulk temperature was calculated using the ideal gas equation of state (Eq. 3.7).

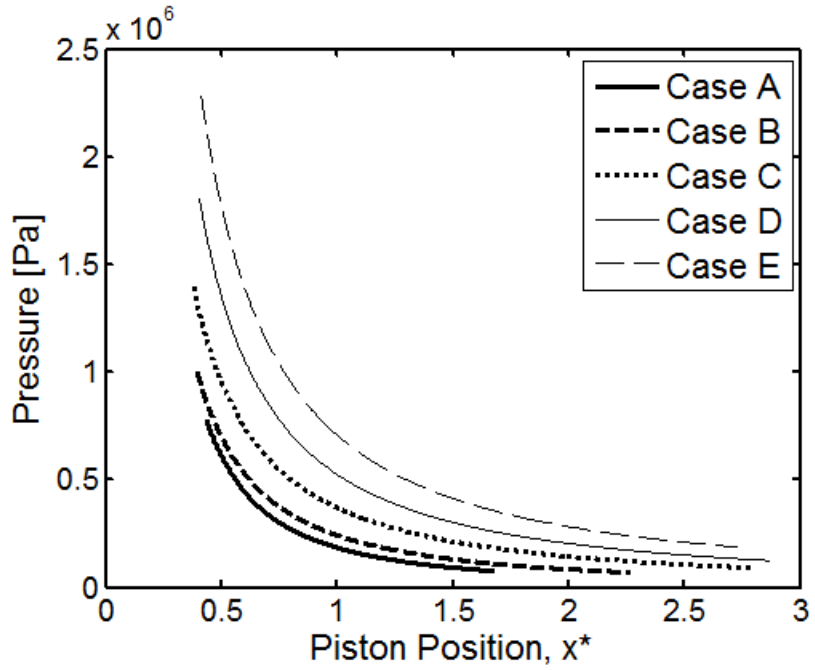

Figure 4.7 – Measured gas pressure during expansion versus dimensionless distance from piston to cylinder head for each test case

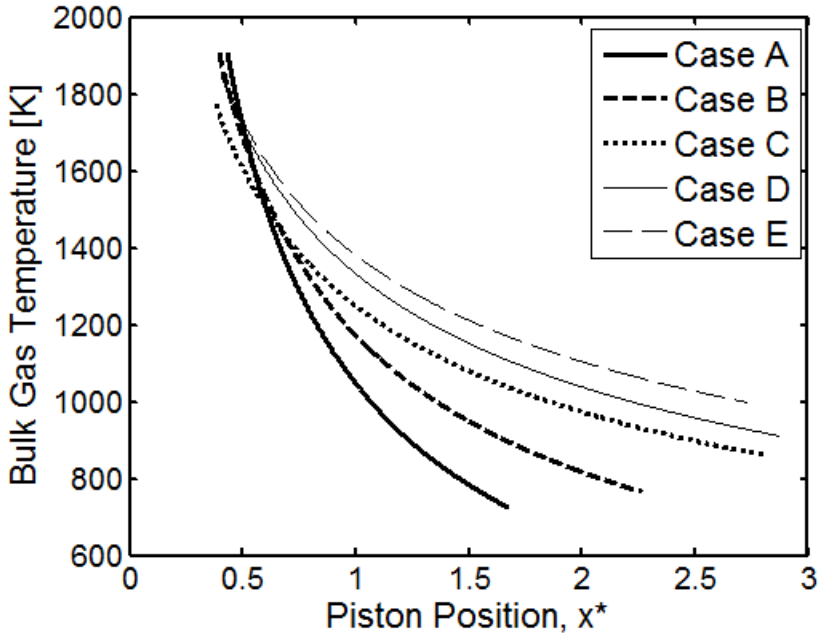

Figure 4.8 – Bulk gas temperature during expansion versus dimensionless distance from piston to cylinder head for each test case

The gas pressure decays rapidly during the initial expansion, with the decay slowing as the expansion progresses. By changing the initial fill pressure, the peak pressure at the beginning of expansion also increases, as expected. The peak temperature is almost invariant between test conditions. This is because the equivalence ratio is kept constant. By keeping this fixed, the amount of energy per mass originally inputted to the system in order to attain the peak expansion conditions is constant. Since the initial fill temperature is roughly constant between test conditions, the peak temperature at the beginning of expansion should similarly be the same among test conditions.

As shown in Ch. 2, the Reynolds number for the expansion plays an important role in modeling the heat transfer. The Reynolds number for this study is defined as:

$$Re_D = \frac{\rho D v_p}{\mu} \tag{4.2}$$

Where ρ is the gas density, v_p is the instantaneous piston velocity, D is the cylinder diameter, and μ is the viscosity of the gas. Since both the density and piston velocity are key physical variables in describing this process, these parameters are shown for each of the test conditions in Figures 4.9 and 4.10. The piston velocity was calculated numerically by evaluating the time derivative of position with a five-point central differencing scheme (Eq. 3.10), while the gas density was calculated from the mass and instantaneous volume of the system (note that the mass is constant during the expansion), according to Eq. 3.9.

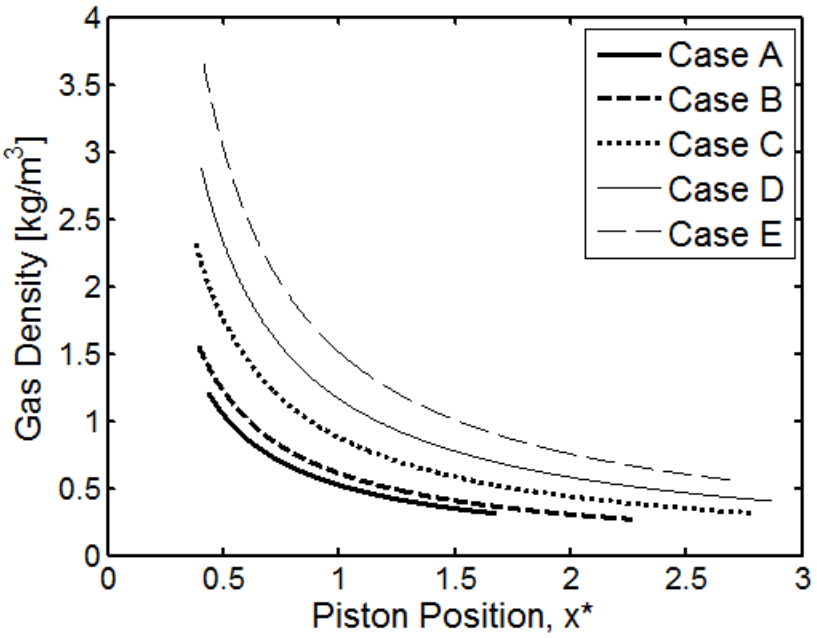

Figure 4.9 – Gas density during expansion versus dimensionless distance from piston to cylinder head for each test case

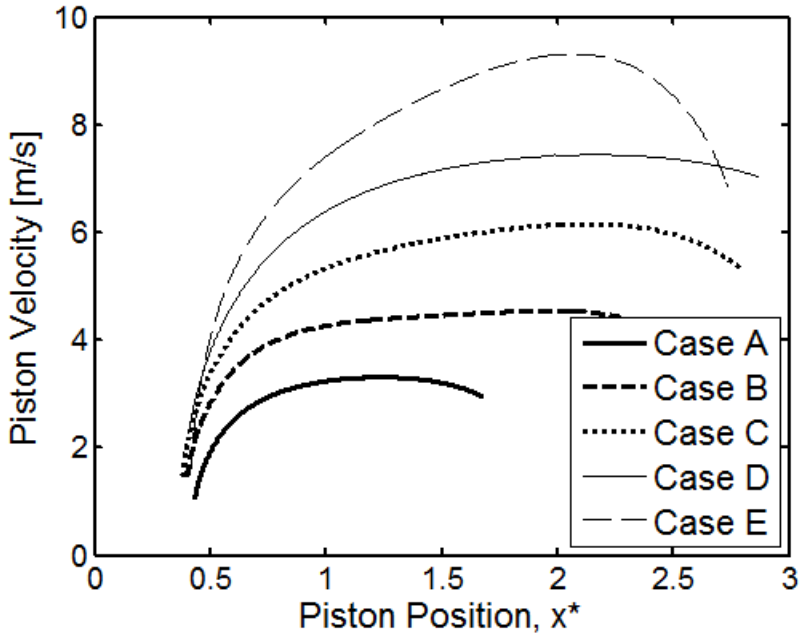

Figure 4.10 – Piston velocity during expansion versus dimensionless distance from piston to cylinder head for each test case

Since the mass of the gas is constant the density decays inversely with volume. Piston velocity starts low, however it is non-zero because the beginning of expansion was set at 1% change in volume, indicating that expansion has already begun. Piston velocity initially increases rapidly, approaches a constant value, and eventually slows as energy is dissipated by raising a weight.

The Reynolds number and Prandtl number during the expansion are shown in Figure 4.11 and 4.12, respectively, for each of the test cases. The Reynolds number was calculated using Eq. 4.2, while the Prandtl number was calculated using:

$$Pr = \frac{\mu c_p}{\kappa} \tag{4.3}$$

The thermophysical properties viscosity, μ, thermal conductivity, κ, and specific heat, c_p, were determined as functions of temperature during the expansion from tabular values compiled using the program *EES* (see Appendix I).

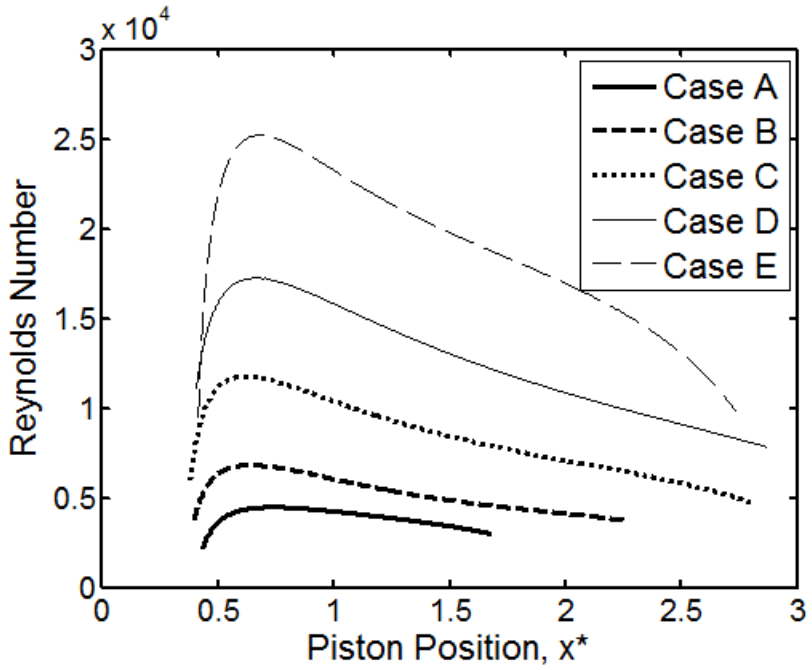

Figure 4.11 – Instantaneous Reynolds number during expansion versus dimensionless distance from piston to cylinder head for each test case

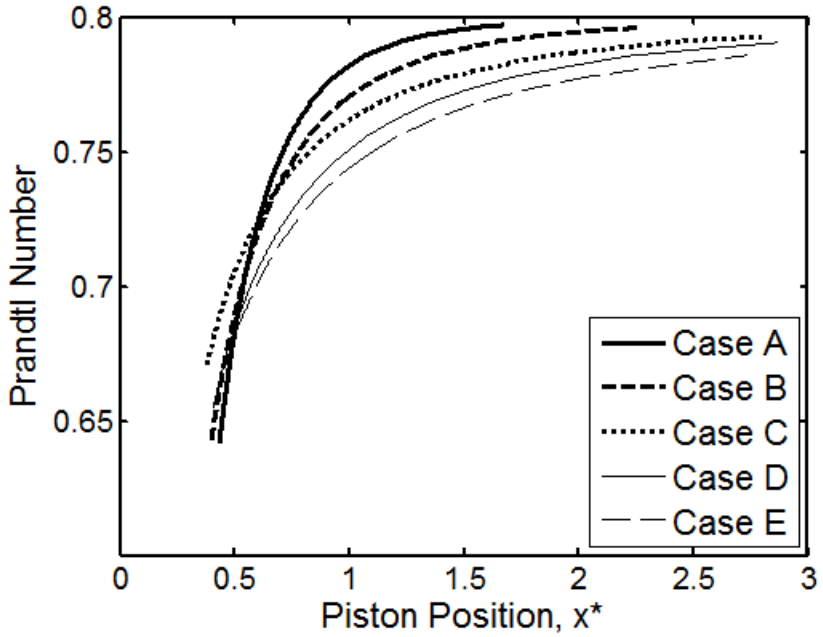

Figure 4.12 – Prandtl number during expansion versus dimensionless distance from piston to cylinder head for each test case

The length scale used in the Reynolds number is the cylinder diameter, which is a constant for this expansion. The viscosity of the gas varies with temperature during the expansion; however this variation is generally not as large as the variations in gas density and piston speed. The gas density decreases monotonically, as shown in Figure 4.9. Piston velocity, shown in Figure 4.10, is initially low but increases rapidly, followed by eventual slowing. This interplay between these variables causes a rapid rise in the Reynolds number shortly after expansion begins, followed by a gradual decay, as shown in Figure 4.11. This will be seen to have a significant effect on the behavior in the heat transfer during this process, as shown through the Nusselt number. In many situations the Prandtl number is taken as a constant for gases, such as in the pseudo-steady state models discussed in Ch.1. While it does not vary as widely as the Reynolds number does, Figure 4.12 shows that the Prandtl number varies by approximately 20% from the beginning to the end of expansion. This is due to the changes in temperature during the expansion, which affects the Prandtl number through changes in the thermal conductivity, viscosity, and specific heat. Since the Nusselt number is directly proportional to the Prandtl number in the proposed heat transfer model, Eq. 2.13, it follows that incorporating the time dependence (through temperature) of the Prandtl number is important to modeling the transient behavior of the heat transfer.

The Reynolds number and the Prandtl number are important dimensionless parameters characterizing the expansion process, and the original form of the heat transfer model, Eq. 2.13, shows their importance in predicting heat transfer. Many heat

transfer models are formulated in terms of these parameters, including many of the models discussed in Ch. 1, so it is useful to examine these quantities in the present study. However, it was found in Ch.2 that the proposed heat transfer model can best be characterized using the Peclet number, because this parameter is also significant in characterizing the polytropic exponent. The Peclet number can be formed by combining the Reynolds and Prandtl numbers:

$$Pe_D = Re_D Pr = \frac{\rho c_p v_p D}{\kappa} = \frac{v_p D}{\alpha} \tag{4.4}$$

The Peclet number during the expansion process is shown in Figure 4.13.

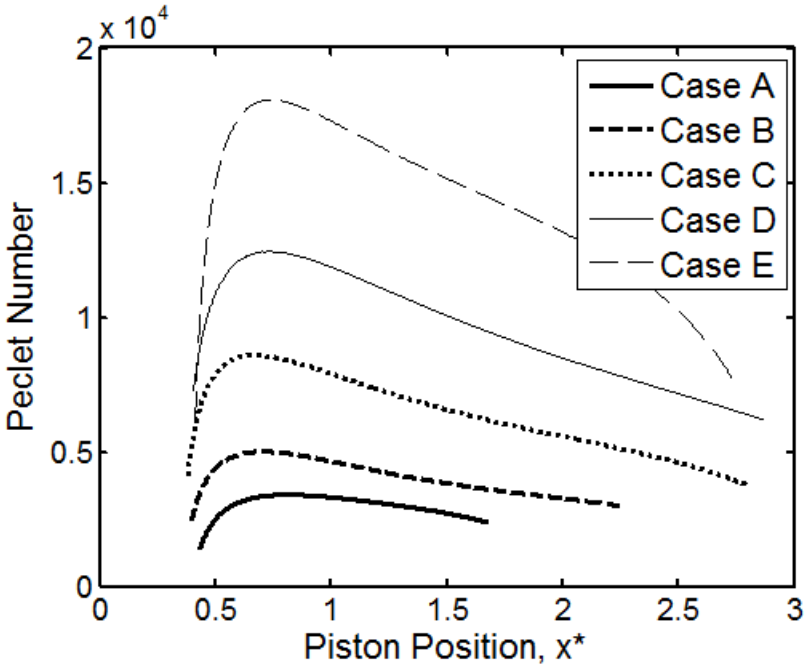

Figure 4.13 – Peclet number during expansion versus dimensionless distance from piston to cylinder head for each test case

Upon comparing Figure 4.13 with 4.11, it is seen that the Peclet number is very similar to the Reynolds number. This follows from Eq. 4.4, and can be understood by noting that while the Reynolds number compares inertial forces to viscous (momentum diffusion) effects, the Peclet number compares inertial forces to conduction (heat diffusion) effects. However, it is noticed that the Peclet number exhibits less abrupt changes during the expansion, and is slightly more leveled during the expansion. This is due to the effect of the Prandtl number not being constant, but changing during the expansion, as seen in Figure 4.12. Just as the peak in the Reynolds number was noted because of its future implications on heat transfer, the peak in the Peclet number shares a similar significance.

4.3 Heat Transfer Characteristics

The heat transfer characteristics associated with the expansion of a gas were calculated from the experimental data using the data reduction process developed and described in Ch.3. This results in a spatially averaged, instantaneous heat transfer coefficient, which is defined by:

$$h = \frac{\dot{q}''}{T_g - T_{wall}} \tag{4.5}$$

Where T_g is the bulk gas temperature, as defined by the ideal gas equation of state (Eq. 3.7). This results in values for the heat transfer coefficient versus piston position as shown in Figure 4.14.

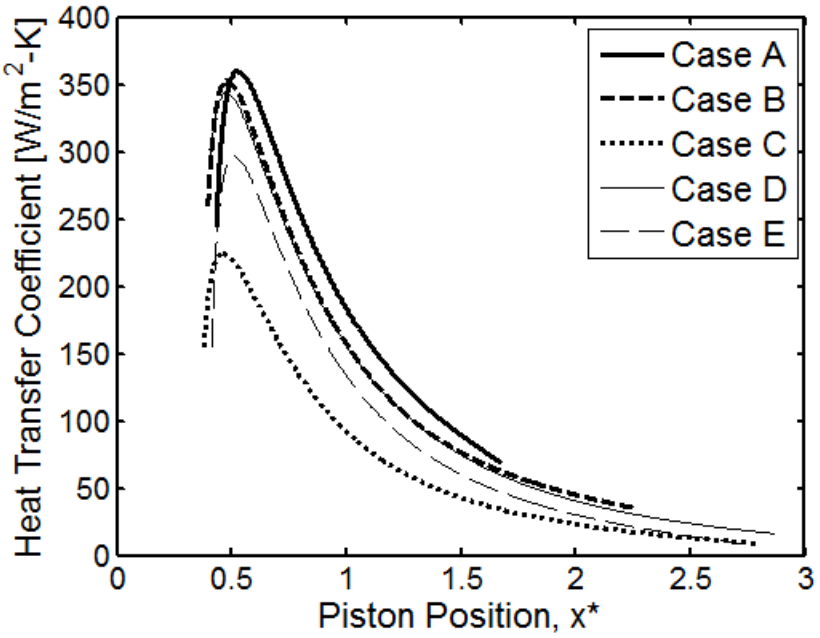

Figure 4.14 – Spatial average instantaneous heat transfer coefficient during expansion versus dimensionless distance from piston to cylinder head for each test case

The heat transfer coefficients shown in Figure 4.14 start at some finite value and increase rapidly to a peak value, occurring near $x^* = 0.5$. After this the heat transfer coefficient decays, approaching zero at the end of expansion. It is noted that all test cases produced heat transfer coefficients very similar in magnitude, and that the trend during expansion in this heat transfer coefficient is the same for all cases. While the magnitude of the heat transfer coefficient is very similar between test cases, it is seen that it is somewhat higher for cases at low initial fill pressures (Case A) than at higher initial fill pressures (Case E). The exception is Case C; here the heat transfer coefficient is lower than expected, and does not follow the trend present in the other cases. This however is

consistent with other results from this study, namely that the relationship between the polytropic exponent and the characteristic Peclet number changes when $Pe^* \approx 15{,}000$, which corresponds closely to the conditions of Case C (this is discussed further when the model for the polytropic exponent is developed).

It was noted previously that increasing the Reynolds number (or Peclet number) should increase the Nusselt number (or the heat transfer coefficient) since the proposed model suggests they are directly proportional. Figure 4.14 however, shows that the heat transfer coefficient is similar in magnitude between all tests. The reason for this is apparent when examining the relationship between the characteristic Peclet number and the polytropic exponent, and is discussed later. The peak magnitude of the heat transfer coefficient for all tests was approximately $h = 350\ W/m^2K$.

The experimentally determined heat transfer coefficient was non-dimensionalized by expressing it as the Nusselt number:

$$Nu_D = \frac{hD}{\kappa} \tag{4.6}$$

The Nusselt number during the expansion is shown in Figure 4.15.

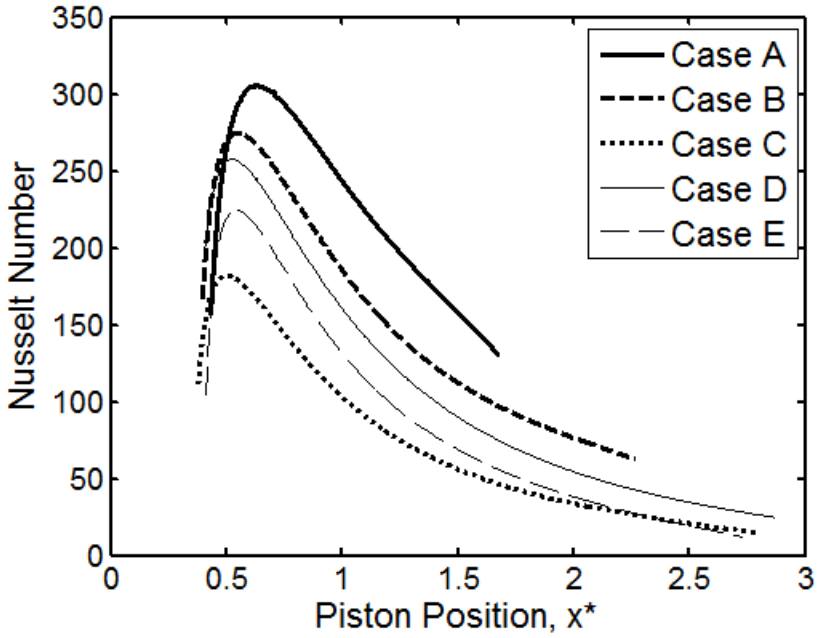

Figure 4.15 – Spatial average Nusselt number during expansion versus dimensionless distance from piston to cylinder head for each test case

It is seen that the Nusselt number follows a similar trend as the heat transfer coefficient. At the beginning of the expansion it is small, but it increases rapidly to form a peak near $x^* \approx 0.5$. Subsequently, the Nusselt number decays until the end of the expansion. Previously, it was noted that there was a distinct peak in the Peclet (and Reynolds) number (Figure 4.13 and 4.11, respectively), also occurring near $x^* \approx 0.5$. This peak was caused by the decay in density accompanied by the rapid increase in piston velocity. The Nusselt number shares a similar peak, illustrating the importance of the Peclet number on heat transfer during the expansion process. It also illustrates the importance of using the instantaneous piston speed, v_p, as the velocity scale in the Peclet

number used to model the heat transfer. If an average value, such as the mean piston speed, S_p, were used instead, this peak in the Peclet number would have been missing, and the model would subsequently not capture the peak in the Nusselt number shown in Figure 4.15.

The dimensionless parameters used in this study use a length scale of *D*, the cylinder diameter. This was defined in Ch.2 when the expansion process was analyzed, and reflects the importance of the diameter to the expansion process, as well being a simple length scale used in many other studies (Annand, 1962; Woschni, 1967; Lawton, 1987; Chen & Karim, 1998; Irimescu, 2012). However, other, equally valid, length scales could have been chosen instead. This would then influence the values and trends in the Reynolds, Peclet, and Nusselt numbers reported. The effect of using other length scales is investigated in the following section.

4.4 Alternative Length Scales

In the original development of the heat transfer model, it is seen that the non-dimensionalization of the model in Eq. 2.13 introduced the length scale as *D*, the cylinder diameter. This is consistent with the length scales used by many other researchers, and describes an important, constant dimension that governs the expansion process. However, other choices could have been made for the length scale without invalidating the form of the heat transfer model, as long as the same scale is applied to both the Peclet (or

Reynolds) and Nusselt numbers. This length scale could potentially be selected to represent the transient nature of the expansion.

One such possibility as an alternative length scale is the distance from the cylinder head to the piston, *x*. While the cylinder diameter is the radial dimension of importance to the expansion (and is constant), the expansion distance *x* is the axial dimension, and changes during the expansion. Applying this length scale, the Peclet, Reynolds, and Nusselt numbers become:

$$Pe_x = \frac{v_p x}{\alpha} \tag{4.7}$$

$$Re_x = \frac{\rho v_p x}{\mu} \tag{4.8}$$

$$\overline{Nu_x} = \frac{hx}{\kappa} \tag{4.9}$$

The overbar has been added to the Nusselt number to emphasize that it is still a spatially averaged value, not a local value. In this manner, $\overline{Nu_x}$ can be thought of as the spatially averaged Nusselt number up to the position *x*.

The Peclet number during the expansion using this alternative length scale is shown in Figure 4.16.

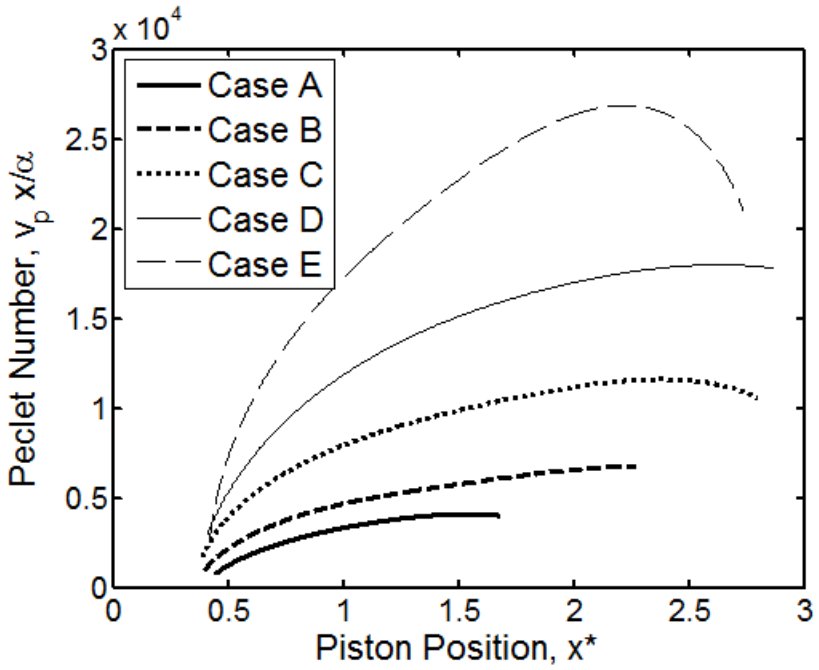

Figure 4.16 – Alternate Peclet number, using the length scale of *x*, the distance from the cylinder head to the piston

The Peclet number shown in Figure 4.16, using a length scale of *x*, is very different from the Peclet number shown in Figure 4.13, which uses the cylinder diameter as the length scale. Previously, there was a peak in the Peclet number early in the expansion, which was related to a similar peak the Nusselt number. Introducing the length scale of *x* makes the expansion distance a dominant factor in determining the Peclet number, and washes out the peak previously reported. Instead, the Peclet number increases monotonically for most of the expansion, decreasing only near the end as the piston velocity decreases. While the behavior of this alternative Peclet number is very

different from the Peclet number shown in Figure 4.13, the overall magnitudes are similar, although slightly larger.

The Reynolds number during the expansion using this alternative length scale is shown in Figure 4.17.

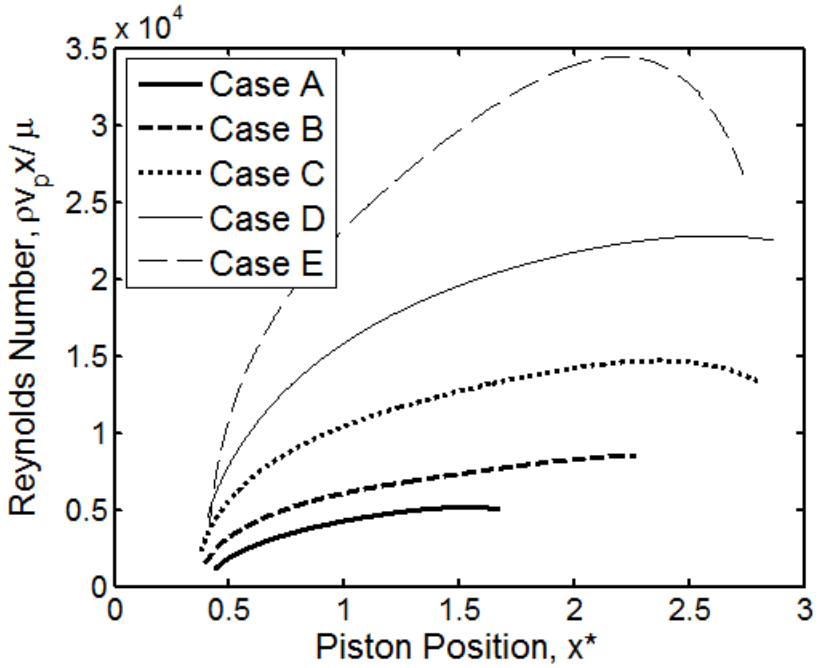

Figure 4.17 – Alternate Reynolds number, using the length scale of *x*, the distance from the cylinder head to the piston

The Reynolds number shown in Figure 4.17, using a length scale of *x*, is very similar to the Peclet number shown in 4.16, as could be inferred by Eq. 4.4. It, too, changes significantly when using the length scale of *x* rather than *D*, as seen by comparing Figure 4.17 with 4.11. Most significantly, the early peak previously noted in the Reynolds number disappears when using this length scale for the Reynolds number.

The Nusselt number during the expansion calculated using *x* as the length scale is shown in Figure 4.18.

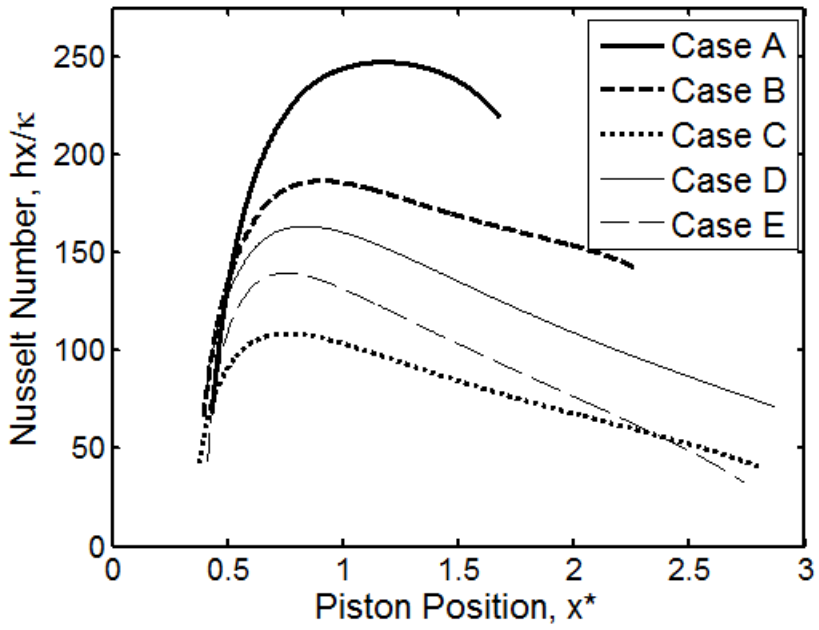

Figure 4.18 – Alternate Nusselt number, using the length scale of *x*, the distance from the cylinder head to the piston

Comparing Figure 4.18 with Figure 4.15, it is seen that using the expansion distance rather than the cylinder diameter as the length scale has a strong effect on the calculated Nusselt number. While the Nusselt number still has a peak early in the expansion, the peak is much weaker and occurs later than in Figure 4.15. Additionally, the magnitudes of the Nusselt numbers in Figure 4.18 are slightly lower than those in Figure 4.15.

When the cylinder diameter is used as the length scale (Figures 4.13 and 4.15), both the Peclet and Nusselt numbers have a peak early in the expansion ($x^* \approx 0.5$), and subsequently decay for the duration of the expansion. When the expansion distance is used (Figures 4.16 and 4.18), the Peclet number shows little to no peak, except possibly towards the end of the expansion, instead increasing for most of the expansion. The Nusselt number, however, still has a peak early in the expansion, although it is much less pronounced. After this peak, the Nusselt number decays for the duration of the expansion. When applying the cylinder diameter as the length scale, the direct importance of the Peclet number on predicting the Nusselt number is emphasized. This can be seen by comparing their graphs in Figures 4.13 and 4.15 and noting the similar behavior of each. This similar behavior vanishes when applying the expansion distance as the length scale. Instead, Figures 4.16 and 4.18 indicate that the other terms in the heat transfer model, Eq. 4.1, are also important to predicting the Nusselt number accurately.

Applying the expansion distance as the length scale in the Peclet, Reynolds and Nusselt numbers illustrates the effect of the selected length scale on the resulting dimensionless parameters. Since these parameters are used to characterize the heat transfer, the selection of the length scale influences how heat transfer during the expansion process is understood and discussed. However, the choice of this length scale does not affect the validity of the heat transfer model given by Eq. 4.1, assuming that the same length scale is used in both the Peclet and Nusselt numbers. The cylinder diameter was chosen as the length scale during this study because it is an important dimension

governing the expansion process and has been used by many other researchers as the length scale. However, future studies could determine whether a different dimension, such as the expansion length, *x*, is a more appropriate length scale for the expansion process. While this does not change the validity of Eq. 4.1, this will affect the interpretation of the heat transfer characteristics.

4.5 Model for the Polytropic Exponent

In Ch.2 it was proposed that the polytropic exponent *n* could be related to the characteristic time scale associated with the expansion process. After analyzing the time scales associated with the expansion process, two functional forms were proposed. One functional form suggested that a characteristic Peclet number, representing the ratio of the expansion rate to the heat diffusion rate, is an appropriate parameter upon which to base a model for *n*. The other functional form suggested that the mean piston speed, normalized by the acoustic velocity, is an appropriate parameter for use in modeling the polytropic exponent. Since the acoustic velocity is a state variable, this parameter compares the expansion time scale to a time scale associated with the thermodynamic state of the gas. It is found in this study that both functional forms can be used as the basis for developing models for the polytropic exponent, as shown in the following discussion.

4.5.1 Model Based on the Characteristic Peclet Number

It was proposed in Ch.2 that the polytropic exponent could be modeled using the characteristic Peclet number of the expansion. For this study, the characteristic Peclet number is defined as:

$$Pe^* = \frac{S_p D}{\alpha_0} \tag{4.10}$$

The velocity used in the characteristic Peclet number is the mean piston speed, S_p:

$$S_p = \frac{V_{max} - V_{min}}{A_c t_{ex}} \tag{4.11}$$

Where t_{ex} is the total expansion time, and A_c is the cross sectional area, $A_c = \frac{\pi}{4} D^2$. While the thermal diffusivity changes during the expansion (see Appendix I), its value is taken at the beginning of the expansion so that it is a readily known quantity. The relationship between the polytropic exponent and the characteristic Peclet number is shown in Figure 4.19.

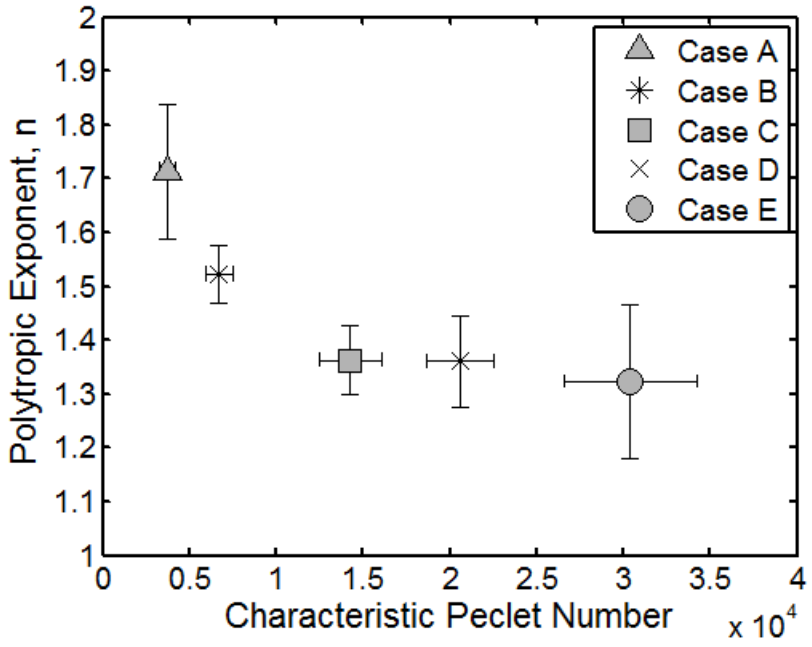

Figure 4.19 – Polytropic exponent and the characteristic Peclet number for each test case. The polytropic exponent was determined from experimental pressure-volume data and the characteristic Peclet number was calculated using Eq. 4.10-4.11

The results presented in Figure 4.19 show a strong link between the characteristic Peclet number and the polytropic exponent, as was hypothesized in Ch. 2. The polytropic exponent increases significantly at low Peclet numbers, while changing only slightly at high Peclet numbers. An increase in the polytropic exponent indicates an increase in heat transfer by Eq. 4.1. However, also by Eq. 4.1, heat transfer is also directly dependent on the Peclet number, and a decrease in the Peclet number causes a decrease in heat transfer. This explains why the heat transfer coefficients and Nusselt numbers seen in Figures 4.14 and 4.15, respectively, have similar magnitudes between test cases, while the Peclet numbers differ substantially between test cases, as shown in Figure 4.13. Test cases with

low Peclet numbers (such as Case A) have decreased heat transfer due to the Peclet number directly, but increased heat transfer due to the polytropic exponent. Test cases with high Peclet numbers (such as Case E) have increased heat transfer due to the Peclet number directly, but decreased heat transfer due to the polytropic exponent. This tends to keep the heat transfer coefficients and Nusselt numbers similar between test conditions, even though the Peclet numbers may differ significantly.

In order to establish a relationship between the polytropic exponent and the characteristic Peclet number, the behavior of the polytropic exponent in some limiting cases is examined. First, the polytropic exponent was normalized by the specific heat ratio at the beginning of expansion, γ_0. This normalization is suggested by the form of the proposed heat transfer model, Eq. 4.1. Additionally, an isentropic expansion is characterized by $n = \gamma$, so this normalization reflects the deviation of the expansion from the ideal. If γ were a constant, the lower limit for this normalized polytropic exponent would be one. If it were less than one, it would imply that heat is being added to the expansion, which would be heat transfer from a cold wall to a hot gas according to Eq. 4.1. However, γ changes with temperature during the expansion, and the value used to normalize the polytropic exponent is taken at the beginning of expansion when γ is lowest. This means that when *n* is normalized by the initial γ, the lower limit on n/γ_0 must be something slightly greater than one. Referring to Figure 4.19, an upper limit on the normalized polytropic exponent would be caused by very low characteristic Peclet numbers, meaning a very slow expansion. In the limit of the characteristic Peclet

number going to zero, the expansion becomes an isochoric (constant volume) process. An isochoric process can be modeled as $PV^{\infty} = constant$; while pressure changes with volume constant, the quantity PV^{∞} is constant, equal to infinity (Zucker & Bilbarz, 2002). This suggests that as the characteristic Peclet number decreases the polytropic exponent increases, without a limit imposed as the upper bound.

The data presented in Figure 4.19 suggests that at large characteristic Peclet numbers, the polytropic exponent is only weakly dependent on Pe^*, with little variation. However, at low characteristic Peclet numbers, the polytropic exponent is strongly dependent on Pe^*. It was found for the current data that the relationship between the normalized polytropic exponent and the characteristic Peclet number is best described by a power law expression:

$$\frac{n}{\gamma_0} = 2.5\left(\frac{Pe^*}{1000}\right)^{-1.5} + 1.05 \qquad (4.12)$$

The result of using the model presented in Eq. 4.12 is compared with the experimental data in Figure 4.20, revealing that the model describes the relationship between the polytropic exponent and the characteristic Peclet number accurately over the range of test conditions examined.

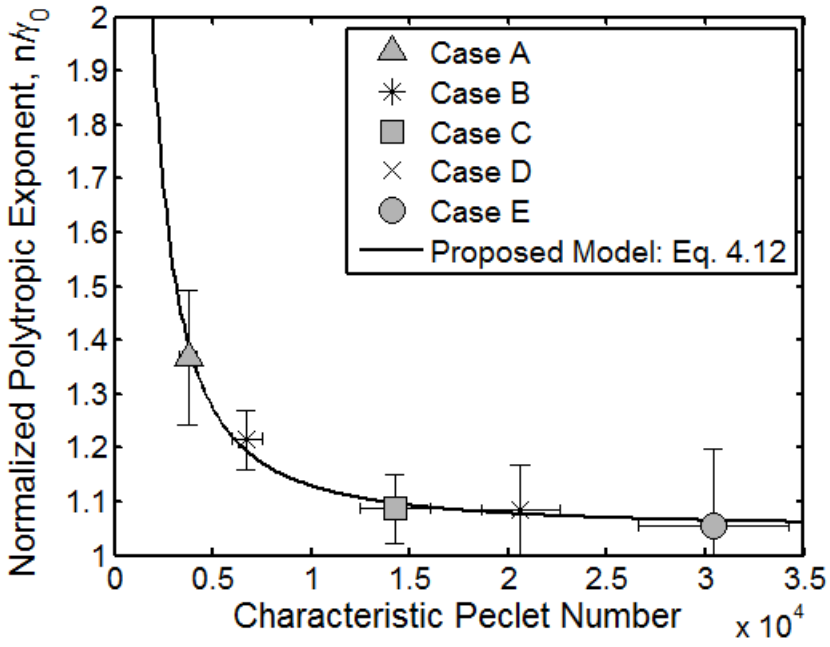

Figure 4.20 – Polytropic exponent normalized by the specific heat ratio at the beginning of expansion, versus the characteristic Peclet number calculated using Eq. 4.10-4.11.

The power law expression for the normalized polytropic exponent (Eq. 4.12) is in good agreement with the data collected in this study, as seen in Figure 4.20. The maximum difference between the data and the model is 2%, showing good agreement over the range of data collected. The power law relationship used reflects the strong dependence of *n* on the characteristic Peclet number at low Peclet numbers, and the weak dependence at large Peclet numbers. For $Pe^* \leq \sim 15{,}000$, it is seen in both the data and the proposed model that the normalized polytropic exponent varies significantly with the Peclet number, changing by approximately 25% between Test Case A and C. However, for expansions with characteristic Peclet numbers greater than 15,000, the normalized

polytropic exponent is nearly constant, varying by less than 3% between Test Case C and E.

An expansion characterized by a large characteristic Peclet number indicates that the time scale associated with the expansion process is much smaller than the time scale associated with the diffusion of heat. This implies a decrease in the amount of energy lost by the gas as heat, since the time required for heat diffusion is larger than the time present in the expansion process. This is consistent with the results shown in Figure 4.20, because the smaller polytropic exponent at large characteristic Peclet numbers indicates a decrease in heat transfer by Eq. 4.1.

Included in Figure 4.20 are error bars for both the normalized polytropic exponent and the characteristic Peclet number for the expansion. The values of these parameters obtained in this study and the associated uncertainties, are given in Table 4.2.

Table 4.2 - Polytropic Exponent for Each Test Case

Test Case	**Polytropic Exponent**	**Uncer-tainty**	**Normalized Polytropic Exponent**	**Uncer-tainty**	**Characteristic Peclet Number**	**Uncer-tainty**
Case A	1.71	7.26%	1.37	7.28%	3700	11.5%
Case B	1.52	3.59%	1.21	3.67%	6700	11.7%
Case C	1.36	4.72%	1.08	4.81%	14200	12.7%
Case D	1.36	6.27%	1.08	6.29%	20600	9.5%
Case E	1.32	10.84%	1.05	10.9%	30400	12.6%

The results seen in Figure 4.20 confirm the proposed relationship between the polytropic exponent and the characteristic Peclet number during the expansion, and Eq. 4.12 provides the functional form suggested by Eq. 2.24. The existence of this

relationship was proposed in Ch.2 by examining the time scales associated with the expansion process, and it was noted that other time scales could also be used to characterize the polytropic exponent. One such alternative is a time scale based on the mean piston speed and the acoustic velocity, and is discussed next.

4.5.2 Model Based on the Mean Piston Speed

It was proposed in Ch.2 that the time scale characterizing the expansion could be compared to a time scale representing the thermodynamic state of the gas, and that the polytropic exponent could be modeled using this ratio of time scales. The expansion rate can be characterized by the mean piston speed, and the state of the gas characterized by the acoustic velocity:

$$c = \sqrt{\gamma RT} \tag{4.13}$$

Since both γ and T vary during the expansion, the acoustic velocity, c, also varies during the expansion. In order to use this to characterize the polytropic exponent (which does not vary during the expansion for these tests), the value of c at the beginning of the expansion was used. As shown in Ch.2, comparing the expansion time scale with the acoustic time scale results in the following dimensionless quantity:

$$S_p^* = \frac{S_p}{\sqrt{\gamma_0 RT_0}} \tag{4.14}$$

Where S_p^* is a dimensionless form of the mean piston speed and represents the ratio between the acoustic time scale (characterizing the state of the gas) and the expansion time scale.

It was found that the polytropic exponent could be modeled using the dimensionless mean piston speed given by Eq. 4.14. Similar to the previously developed model for *n*, it was found that the polytropic exponent varied strongly at small values of the characteristic time scale, but varies only weakly at large values of this time scale. This could be modeled best by a piecewise model which describes these separate regimes independently, as shown in Eq. 4.15. For the development of this model, the polytropic exponent was normalized by the initial specific heat ratio, as previously discussed.

$$If\ S_p^* \leq 0.006: \qquad \frac{n}{\gamma_0} = 0.054 S_p^{*-1/2} + 0.4 \tag{4.15a}$$

$$If\ S_p^* > 0.006: \qquad \frac{n}{\gamma_0} = -13.5 S_p^* + 1.18 \tag{4.15b}$$

The comparison between this model for the normalized polytropic exponent and the experimental data is shown in Figure 4.21.

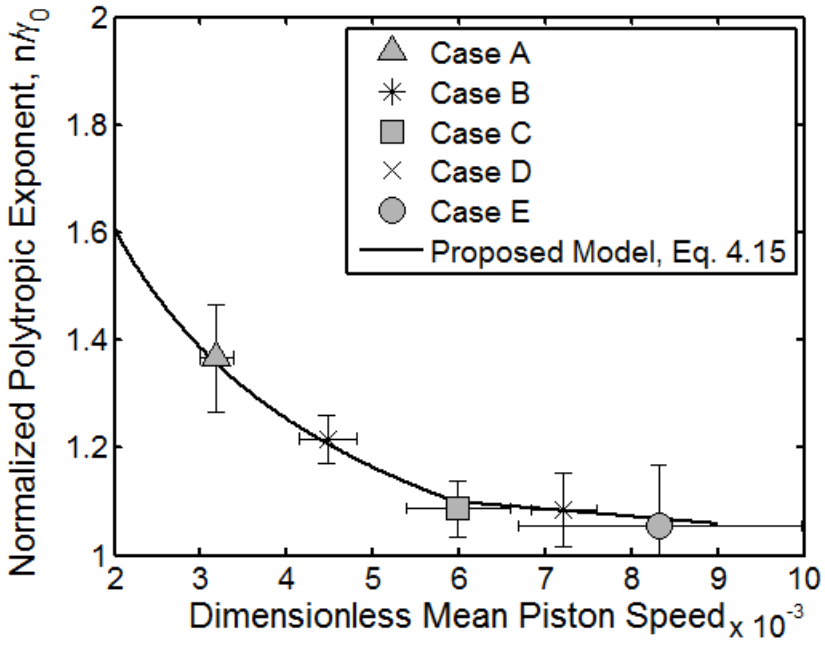

Figure 4.21 – Polytropic exponent normalized by the specific heat ratio at the beginning of expansion, versus the dimensionless mean piston speed defined by Eq. 4.14.

The results shown in Figure 4.21 show that the polytropic exponent can be modeled based on the dimensionless form of the mean piston speed proposed in Eq. 4.14. The use of a piecewise model to determine the polytropic exponent reflects the nature of the relationship between the polytropic exponent and the dimensionless mean piston speed. For low values of S_p^* it is seen that the polytropic exponent is strongly dependent on S_p^*, while at higher values the dependence is significantly reduced. This can be seen in Figure 4.21, and is a similar trend as seen in the model developed using the characteristic Peclet number, although in that scenario the model was more easily described by a single expression.

When the expansion time was characterized by the ratio between the heat diffusion and expansion time scales (resulting in the characteristic Peclet number, Eq. 4.10), it was found that the expansion rate was much larger than the rate of heat diffusion. This resulted in large Peclet numbers. Using the ratio between the acoustic time scale and the expansion time scale (resulting in the dimensionless mean piston speed, Eq. 4.14), it can be seen that the expansion rate is much smaller than the acoustic rate, resulting in small values of S_p^*. The acoustic velocity is a measure of how quickly the gas responds to a change in pressure, and for these tests it is seen that this value is always much larger than the mean piston speed.

As shown by Figures 4.20 and 4.21, the polytropic exponent can be modeled using a characteristic time scale for the expansion process. This can be done using either the characteristic Peclet number, representing the ratio between the heat diffusion and expansion time scales, or a dimensionless mean piston speed, representing a ratio between the acoustic and the expansion time scale. This shows that multiple functional forms are possible in developing a model for the polytropic exponent, but also reinforces the original proposition made in Ch.2 that the polytropic exponent is related to the time scale associated with the expansion process. Because of the importance of the polytropic exponent in the overall heat transfer model (Eq. 4.1), determining the most appropriate functional form for the polytropic exponent is a potential area of further future research. For the purposes of this study, the original model proposed via Eq. 4.12 is used as the

preferred model. This is because an instantaneous form of the Peclet number was also found to be significant to the heat transfer model given by Eq. 4.1.

The relationships given here for the polytropic exponent allow for the *a priori* determination of the polytropic exponent for the expansion process, because both the characteristic Peclet number and the dimensionless mean piston speed are calculable from geometric information concerning the expansion and the initial expansion conditions. This provides closure to the heat transfer model developed in Ch.2 and shown in Eq. 4.1, and allows for the heat transfer characteristics of the expansion process to be predicted. The heat transfer data collected during these experiments are next compared to the proposed heat transfer model.

4.6 Heat Transfer Model Validation

The experimentally determined Nusselt number was compared with that predicted by the proposed heat transfer model. The polytropic exponent was calculated using the model based on the characteristic Peclet number given by Eq. 4.12, and this polytropic exponent was then applied to the overall heat transfer model, Eq. 4.1. The results of this comparison for each test case conducted are given in Figures 4.22-4.26, and it is seen that the proposed model agrees very well with the experimental data.

As shown previously, the polytropic exponent could also be calculated using the model based on the dimensionless mean piston speed, described by Eq. 4.15. However, the model based on the characteristic Peclet number was selected as the preferred model

because the instantaneous Peclet number (see Eq. 4.4 and Figure 4.14) was also found to be very important in the overall heat transfer model, Eq. 4.1. The results from using the overall heat transfer model with the polytropic exponent calculated from the dimensionless mean piston speed (Eq. 4.15) are included in Appendix J, and are very similar to the results given below, where *n* was calculated using the characteristic Peclet number and Eq. 4.12.

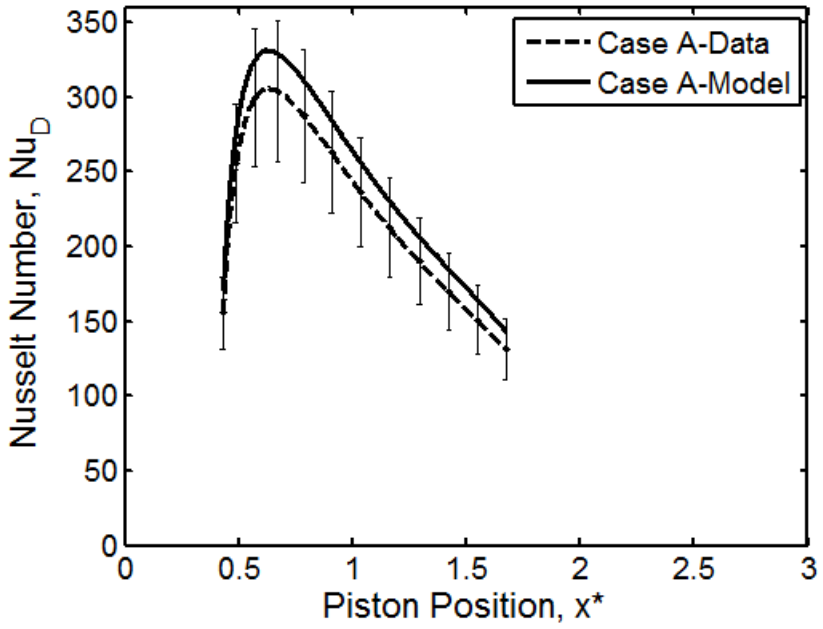

Figure 4.22 – Comparison of experimental results and the proposed heat transfer model (Eq. 4.1) for the Nusselt number during expansion, using Eq. 4.12 for *n* – Test Case A

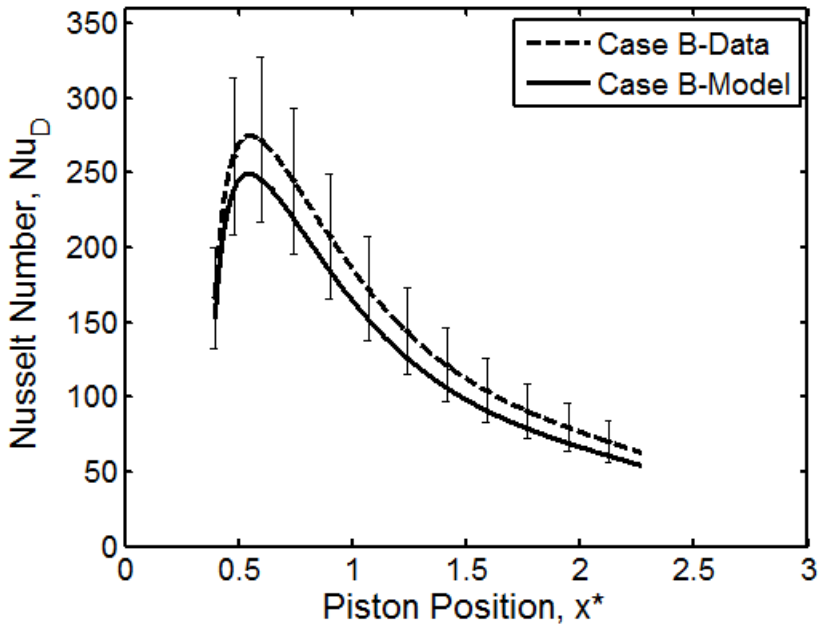

Figure 4.23 – Comparison of experimental results and the proposed heat transfer model (Eq. 4.1) for the Nusselt number during expansion, using Eq. 4.12 for *n* – Test Case B

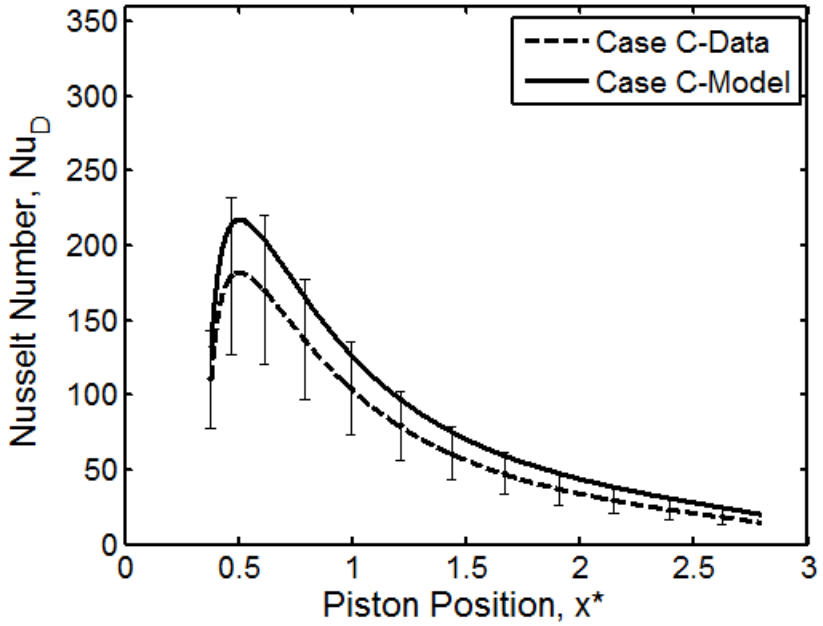

Figure 4.24 – Comparison of experimental results and the proposed heat transfer model (Eq. 4.1) for the Nusselt number during expansion, using Eq. 4.12 for *n* – Test Case C

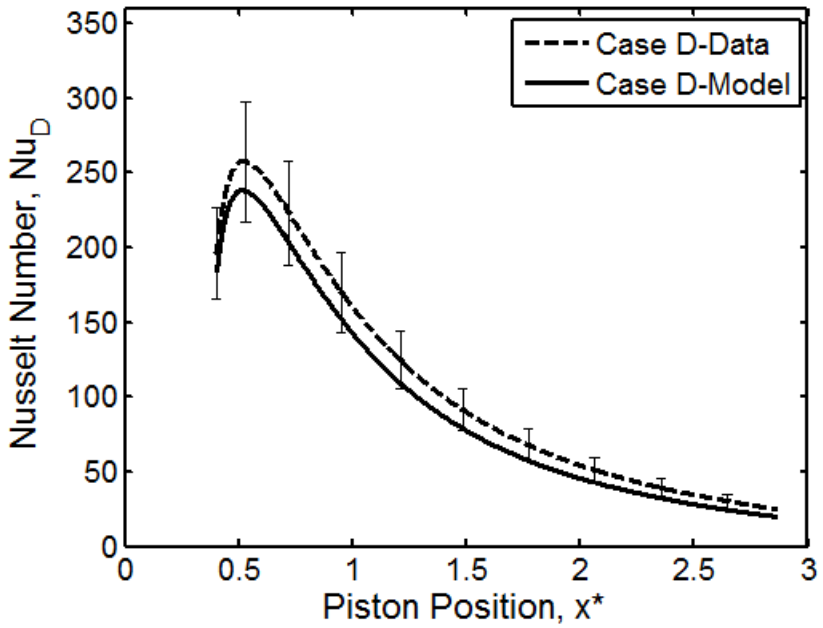

Figure 4.25 – Comparison of experimental results and the proposed heat transfer model (Eq. 4.1) for the Nusselt number during expansion, using Eq. 4.12 for *n* – Test Case D

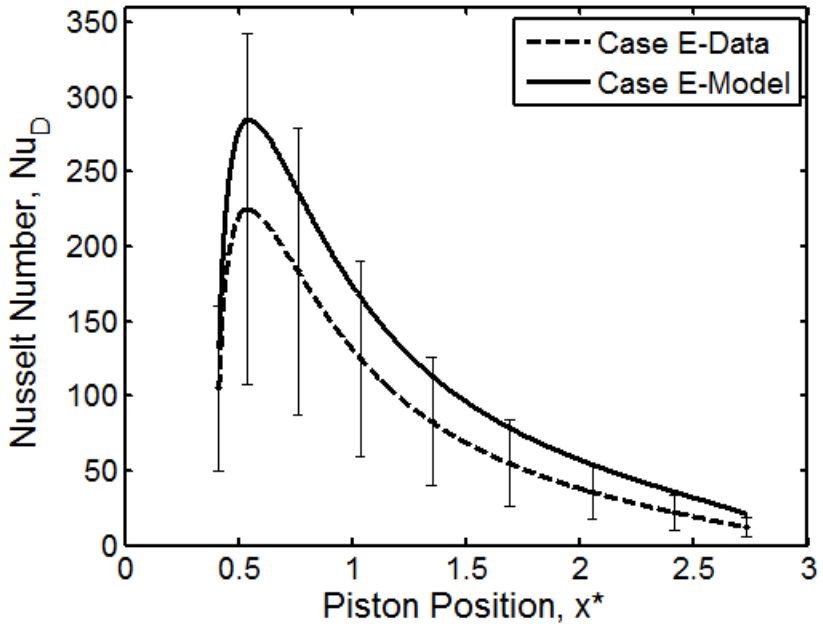

Figure 4.26 – Comparison of experimental results and the proposed heat transfer model (Eq. 4.1) for the Nusselt number during expansion, using Eq. 4.12 for *n* – Test Case E

The results reported in Figures 4.22-4.26 show that the proposed model for heat transfer during the piston-cylinder expansion of a gas matches well with the data. For all test cases, the Nusselt number calculated by the proposed model is within the margin of error for the experimental Nusselt number. Significantly, it is noted that the heat transfer model matches the trend of the data during the expansion, indicating a good transient response of the model to changing heat transfer characteristics. Differences between the model and the experimental data occur only by vertical shifts in Figures 4.22-4.26. These differences stem from the correlation of the polytropic exponent to the characteristic Peclet number shown by Eq. 4.12. Since the polytropic exponent term in Eq. 4.1 behaves as a multiplicative factor on the rest of the heat transfer model, errors in its calculation represent mainly vertical shifts in the Nusselt number versus position. In Cases B and D, the proposed model tends to under predict the heat transfer, while in Cases A, C and E the model over predicts. The characteristic peak in the Nusselt number in all the figures coincides with the peak in the instantaneous Peclet number during the expansion, as previously discussed. In the application of the heat transfer model, the temperature dependence of thermophysical properties has been included, evaluated at the bulk gas temperature, as discussed in Ch. 2.

In the comparison of the proposed model with the experimental data, it was found that the proposed model is sensitive to the value used for the polytropic exponent n. This is especially true when the value of n is small, such as for Cases C, D and E. For these cases, it was found that a change in n of 1% would cause a 13% change in the predicted

Nusselt number. For situations with larger values of *n*, such as Case A, a change in *n* of 1% would cause 6% change in the predicted Nusselt number. This sensitivity, especially for expansions with a small polytropic exponents (large characteristic Peclet numbers), indicates that future work could be done verifying the most accurate model for the polytropic exponent.

The proposed heat transfer model is seen to match all test cases satisfactorily well, within the margin of error for the experiments. It is also seen to capture the time evolution of the heat transfer characteristics accurately, which was of primary importance for this study. This time dependence was captured by using a Reynolds number that uses the instantaneous piston speed as the velocity scale and a Prandtl number based on temperature-dependent fluid properties, which were combined to form the instantaneous Peclet number shown in Eq. 4.1. The time dependence was also incorporating by the effects of the bulk gas temperature and piston position, as also shown in Eq. 4.1. The approach used to formulate this heat transfer model differs from many models proposed by other studies by focusing on capturing the time dependence of heat transfer. The differences between this proposed model and other models are discussed next, and compared with the heat transfer data collected.

4.7 Model Comparison

In Ch.1 several existing models for heat transfer during the expansion of a gas were examined. One of the common assumptions made in many previous heat transfer models has been the assumption that the process can be modeled in a pseudo-steady state fashion. Ultimately, this led to models of the form of Eq. 1.4, where the Nusselt number is related to the Reynolds number in a simple power law form. Commonly, the velocity scale used in the Reynolds number for the pseudo-steady state models was the mean piston speed, S_p (this is in contrast to the instantaneous piston speed, v_p, used in the present study) (Annand, 1963; Woschni, 1967; Hohenburg, 1980). To test this, a power law relationship with the Reynolds number based on mean piston speed and the Nusselt number determined from the experimental data are plotted in Figure 4.27.

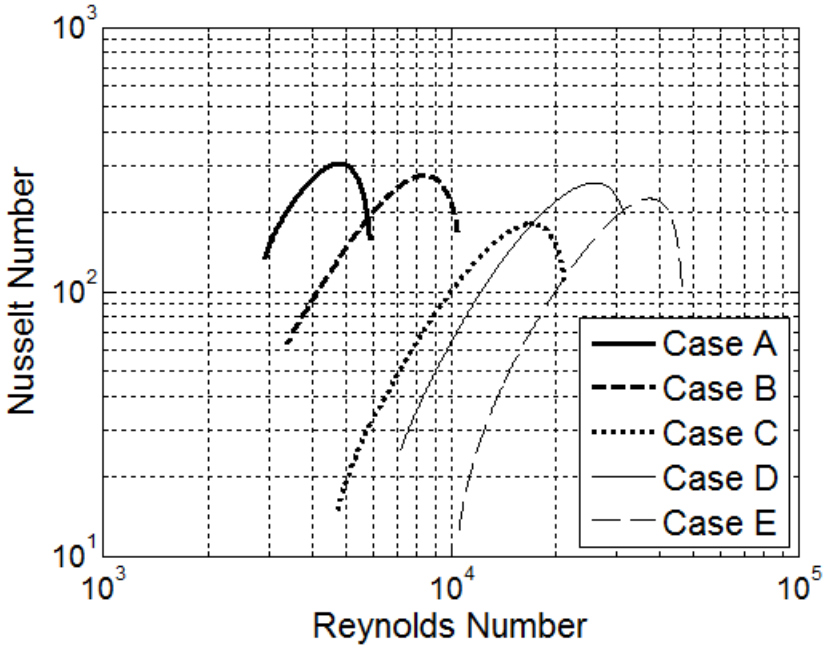

Figure 4.27 – Nusselt number during expansion versus the Reynolds number calculated using the mean piston speed (logarithmic scale)

It is seen from Figure 4.27 that the Nusselt and Reynolds numbers do not follow a purely linear relationship on a logarithmic scale during the expansion. This means that the pseudo-steady state model for heat transfer during the expansion of a gas is not accurate if the time-dependent heat transfer characteristics are important. This is amplified by the fact that the most non-linear portions of Figure 4.27 (at high Reynolds numbers) correspond to the portion of the expansion when the gas temperature is highest, when accurate knowledge of the heat transfer coefficient is most important. However, it is also seen from Figure 4.27 that a power law approximation may be justified if only cycle-averaged values are important and the transient behavior is not necessary, which was often the goal of these studies (Borman & Nishiwaki, 1987). This average power law

relationship between the Nusselt and Reynolds numbers appears to vary between test conditions, as the separate test cases do not collapse into a single curve. Accounting for this would require an additional method for describing the effect of different operating conditions beyond the power law relationship. Therefore, the power law relationship is shown not to perform well in predicting transient heat transfer behavior, or in adapting between operating conditions.

The necessity of including transient effects in a heat transfer model for the expansion of a gas can also be seen by comparing the Nusselt numbers predicted by existing models and the currently proposed model. The correlations published by Annand, Woschni, Lawton and Irimescu are compared with the existing experimental data, and with the proposed model (Annand, 1963; Woschni, 1967; Lawton, 1987; Irimescu, 2012). These models were selected for comparison because they are representative of much of the prior work in modeling the heat transfer during the expansion of a gas. The heat transfer models by Annand and Woschni assume a pseudo-steady state form of Eq. 1.4, and while they were developed in 1963 and 1967, respectively, they are still widely used to predict heat transfer, particularly in internal combustion engines (Soyhan et al., 2009; Demuynck, 2010). The models by Irimescu and Lawton represent some of the prior studies that incorporated transient effects in the heat transfer models. Irimescu did this by using a correlation for heat transfer in the turbulent entry length for pipe flow, while Lawton modified Annand's model to include the effect of expansion on the gas (see Ch.1 for more discussion of each correlation). The models of

Annand and Woschni required empirical constants to be selected to match observed conditions; in order to apply these models, these constants were chosen to match the data from Test Case D. The result is a value for C of 0.18 for Annand's model and $C = 0.013$ for Woschni's model. These values are approximately half the values suggested by Annand and Woschni, respectively, indicating that considerable flexibility must be exercised when determining these constants. Irimescu's model required that the velocity scale for the Reynolds number be from a simplified k-ϵ turbulence model, which increases the velocity from the piston speed; instead however, the piston speed was increased by a factor of two, selected to match the data from Test Case D. The comparison of each of these models, along with the data and proposed model from this study, is shown in Figure 4.28.

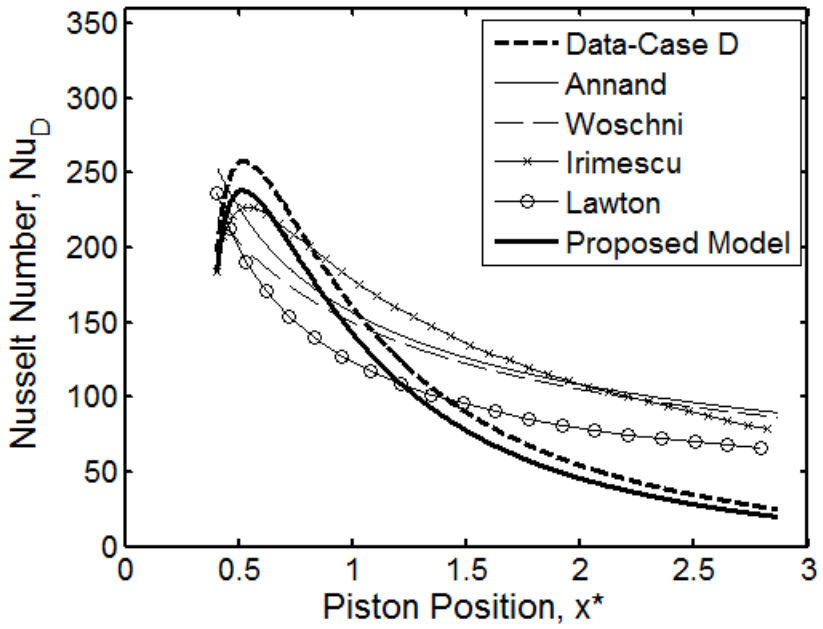

Figure 4.28 – Comparison of the proposed heat transfer model with models from other studies. Experimental data from Test Case D

Of the previously published studies, only the model proposed by Irimescu captures the initial increase in heat transfer properly; all the other studies show the Nusselt number decaying monotonically. This is because the velocity scale used by Irimescu varies with time/position, being based on the instantaneous piston velocity, while the velocity scales in the other previously published studies are based on the mean piston speed (constant for a given test case). None of the models are able to capture the decay of the Nusselt number during the expansion process accurately. Even the models by Irimescu and Lawton, which were developed including some transient effects, do not have the appropriate decay rate representing the decrease in heat transfer, although it is noted that Lawton's model appears to have the appropriate slope initially and tends to

over-predict in later stages of expansion. Therefore, if time-resolved heat transfer information is of interest, the currently proposed model is a significant improvement over the previous models.

The calculations made using the heat transfer models of Annand, Woschni, Irimescu, and Lawton in Figure 4.28 were made by modifying the empirical constants present in the models to fit the data from Test Case D. If the same constants are then applied to a different test condition, the results are in much worse agreement, as shown in Figure 4.29 for Test Case B.

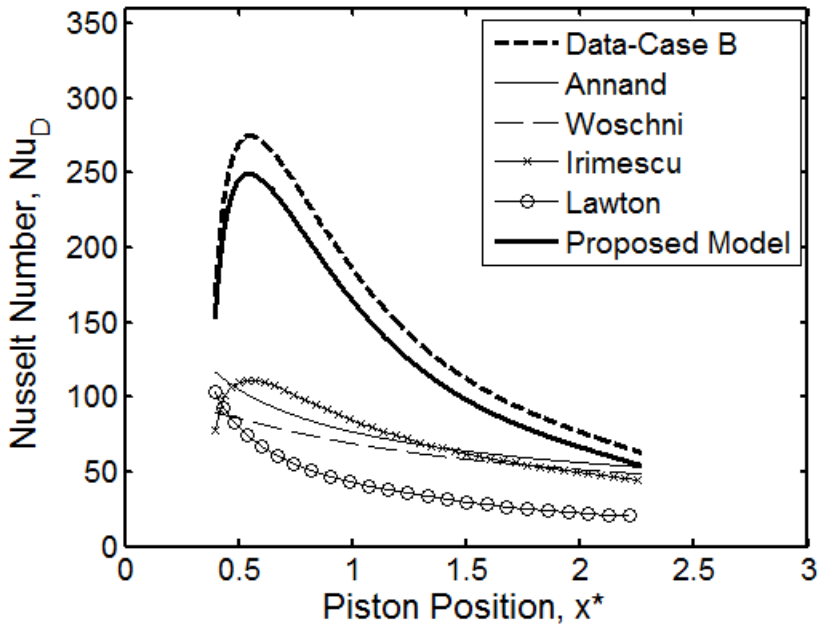

Figure 4.29 – Comparison of the proposed heat transfer model with models from other studies. Experimental data from Test Case B

Figure 4.29 illustrates the dependence of the previously mentioned heat transfer models on the empirically determined constants used to adjust the models to

observations. Using the same constants from the operating conditions of Test Case D for Test Case B resulted in severely under-predicted Nusselt numbers. These constants are difficult to predict, and relationships describing how one may predict them are not given. The proposed heat transfer model, however, appears to be much more able to adapt to changes in the operating conditions, according to the data collected in this study.

The results presented here show that the piston-cylinder expansion of a gas can be accurately modeled as a polytropic expansion, and that the polytropic exponent can be related to the characteristic time scales associated with the expansion process. The polytropic exponent was modeled with the characteristic Peclet number for the expansion process, representing the ratio between the expansion and heat diffusion rates, and resulting in a power law function relating the two parameters (Eq. 4.12). The polytropic exponent was also modeled with a dimensionless mean piston speed, representing the ratio between the acoustic and expansion time scales (Eq. 4.15). Both models were able to accurately reflect the data, showing that the polytropic exponent is related to the characteristic time scale of the expansion. The model for the polytropic exponent was then used in the overall model for heat transfer during the expansion of a gas developed in Ch.2 and given by Eq. 4.1. This model was found to predict the heat transfer accurately for all the test cases examined. Importantly, it accurately reflects the transient heat transfer characteristics exhibited during the expansion. When compared to pseudo-steady state models, it is found that the proposed model is more accurate at predicting transient heat transfer and is better at handling changes in operating conditions, for the test

conditions currently studied. The important findings of this study are summarized in the next chapter, and suggestions are given for areas of further research.

Chapter 5 – Conclusions

This study provides analytic and experimental evidence supporting a new expression for the time dependent heat transfer during the expansion of a gas in a piston cylinder assembly. While heat transfer during the expansion of a gas has been studied previously, many of the previously proposed models have left room for improvement. These models lack accurate time-dependent information concerning heat transfer during expansion, being based either on a pseudo-steady state assumption or by modifications to this assumption. Additionally, these models are not universal, but can require considerable adjustment by way of user-defined constants in order to match predicted heat transfer to experimental values. These empirically determined constants have been found to vary between experimental apparatuses and between operating conditions on the same test apparatus (Annand & Ma, 1970; Borman, 1987; Demuynck, 2010).

The model proposed by this study is based on a transient analysis of heat loss during piston cylinder expansion, arriving at the form of the heat transfer model presented by Eq. 4.1. The approach used to determine this model is a novel method based on a global thermodynamic analysis of the expansion process. Because it is grounded in a transient analysis, this model represents increased accuracy on the time dependent heat transfer over models based on a pseudo-steady state assumption. In order to complete the heat transfer model, a method for determining the polytropic exponent from other parameters is necessary. It is proposed that the polytropic exponent could be related to

the characteristic time scale associated with the expansion process; this was proven valid by the experiments conducted, and led to models being developed for the polytropic exponent. Using these models, the proposed heat transfer model is able to accurately predict the heat transfer characteristics of the expansion, both the transient aspects and the variations due to test conditions.

The form of the heat transfer model (Eq. 4.1) accounts for the transient predictive capabilities of the proposed model, and is proposed as a more accurate alternative to the pseudo-steady state form (Eq. 1.4). While the relationships developed between the polytropic exponent and the characteristic expansion time scales are seen to be valid by the results presented in Ch. 4, the universality of the exact relationships proposed need to be tested by performing further tests at different operating conditions and using different test apparatuses.

5.1 Transient Predictive Capability

One of the primary objectives of this study was to develop a heat transfer model that accurately reflects the transient aspects of the expansion process. These transient aspects include the developing nature of the velocity and temperature distributions within the cylinder, and the effect of expansion on the gas temperature in the boundary layer. The transient effects of the expansion process were incorporated by considering the entire expansion volume and performing a first law analysis. While this analysis excludes

spatial information (such as boundary layer information), it has been shown to encapsulate the necessary transient aspects of the process.

It was found that, among other things, the Nusselt number for the expansion process is dependent on the current expansion distance and the gas to wall temperature difference. These terms were commonly not included in pseudo-steady state models, but were found to be important in capturing the time dependence of the heat transfer in the expansion process. The term representing expansion distance, $1/(2 + 4x^*)$, is found to be especially important in modeling the transient heat transfer. This term arose from the ratio between the cross sectional and surface areas, which was simplified for the cylindrical expansion geometry used in this study. Neglecting this term causes the Nusselt number predicted by Eq.4.1 to be too low early in expansion, and too high later in expansion. While this may be suitable for average heat transfer values, it is not suitable for predicting time-dependent heat transfer characteristics, and therefore is essential for a transient model. While this term arose from characterizing the ratio between cross sectional area and surface area for the geometry under consideration, it is similar in nature to the modification commonly applied for heat transfer in the developing region of pipe flows (Eq. 1.9) and results in a similar effect, namely the enhancement of the heat transfer coefficient near the beginning of the cylinder.

While many pseudo-steady state models propose the use of a Reynolds number based on the mean piston speed, it is found that the instantaneous piston speed is the appropriate velocity scale to model the instantaneous heat transfer characteristics. This

has a profound importance on predicting the Nusselt number, and is responsible for the characteristic peak in both Reynolds and Nusselt numbers in Figures 4.11 and 4.15, respectively, as well as the peak in the Peclet number shown in Figure 4.13. This velocity scale was also justified by showing the importance of the piston speed for the instantaneous fluid velocity, as shown in Ch. 2.

Additionally, it is found that the Peclet number, rather than the Reynolds number, is best used to understand the heat transfer during the expansion process. This was seen from the original form of the heat transfer model, Eq. 2.13, which showed that the key non-dimensional parameter governing the process was not just the Reynolds number, but the product of the Reynolds and Prandtl numbers, which is the Peclet number. Since the Reynolds and Prandtl numbers change significantly during the expansion, modeling the process using the Peclet number incorporates the time dependence of the both the Reynolds and Prandtl numbers into the overall heat transfer model. The importance of using the Peclet number to characterize the expansion process is emphasized by the importance of the characteristic Peclet number on predicting the polytropic exponent.

5.2 Universality

One limitation with many current heat transfer models is their dependence on empirical constants, which may vary with both test apparatuses and test conditions. This lack of universality is a serious hindrance for one who wishes to predict heat transfer

without experimental data available. The universality of the proposed model is dependent on two factors which must be considered: the overall form of the proposed model, and the proposed relationship for the polytropic exponent.

The form of the heat transfer model (Eq. 4.1) was determined analytically for the expansion process; the key assumption involved was that the pressure and volume in the expansion followed a polytropic relationship, $PV^n = constant$, where *n* is constant. This is generally true for many processes, and the data collected here shows that assumption is valid for the current test conditions (Zucker & Bilbarz, 2002). The analysis behind this model was a straightforward application of the conservation of energy principle; because this is universally true, it is expected that the form of the heat transfer model is valid regardless of test conditions/apparatus, provided that the expansion behaves in a polytropic manner. If it were found for different tests that *n* was not constant but varied slightly, it is expected that the form of the heat transfer model could still be used; however the model for predicting *n* would have to be modified to account for variations during expansion.

It was proposed in Ch. 2 that a relationship exists between the polytropic exponent and the characteristic time scales associated with the expansion process. This characteristic time scale could be reported as a characteristic Peclet number, relating the expansion rate to the heat diffusion rate; or as a dimensionless mean piston speed, relating the expansion rate to an acoustic rate that describes the thermodynamic state of the gas. The models developed in Ch. 4 show that either characteristic time scale could be

used to describe the polytropic exponent, though the model based on the characteristic Peclet number was preferred due to the significance of the instantaneous Peclet number to the expansion process. While these relationships were validated by the data collected, the universality of these relationships cannot be judged without more extensive experiments conducted, both at different operating conditions and with other experimental apparatuses.

5.3 Recommendations

This study provides a new expression for heat transfer during the expansion of a gas based on an analytically derived heat transfer model, combined with experimental data. The experimental results are in very good agreement with the analytical results, supporting the proposed model. While it is expected that the overall form of the model could be applied to many situations, the proposed relationships for the polytropic exponent need further, independent tests to show how universally it could be applied. While the model for *n* responded well to changes in the operating conditions for these tests, the experiments conducted did not test variations with mixture composition or peak temperature at the beginning of expansion. Additionally, tests could be conducted with different geometries (such as a different cylinder diameter) than currently used. Testing the applicability of the proposed model for the polytropic exponent over different test conditions would provide further indication of the universality of the proposed model.

At several points during this study, it was found that some flexibility exists in the development and interpretation of the heat transfer model. In describing the polytropic exponent, it was found that a model could be developed using either the characteristic Peclet number or a dimensionless mean piston speed. While the model based on the characteristic Peclet number was proposed as the preferred model because of the significance of the instantaneous Peclet number to the heat transfer model, further research could be conducted to determine what characteristic time scale is the most appropriate to model the polytropic exponent. The length scale used in the Peclet, Reynolds and Nusselt numbers during for the majority of this study was the cylinder diameter. However, other length scales could be selected without invalidating the proposed heat transfer model, as discussed in Ch. 4. While the selection of this length scale does not affect the predictions for the heat transfer coefficient, it does affect how heat transfer in the expansion process is interpreted and understood. Therefore, future work could be done on determining whether a length scale other than the cylinder diameter is more appropriate in describing and modeling this process.

Finally, the model developed for heat transfer assumed that the expansion could be modeled as polytropic. While this was verified experimentally for the test conditions examined, it is possible that this assumption would not be valid for other test conditions. It is suggested that the overall heat transfer model, Eq. 4.1, could be used to model expansions that are not polytropic, provided that the exponent n does not change significantly during the expansion. However, the model for n would have to be altered to

reflect this deviation, indicating that the extension of the proposed heat transfer model to near-polytropic expansions is an area of possible further research.

BIBLIOGRAPHY

Annand, W.J.D. (1962). Heat transfer in the cylinders of reciprocating internal combustion engines. *Proceedings of the Institution of Mechanical Engineers*, 177, 973-996.

Annand, W. J. D., & Ma, T.H. (1970). Instantaneous heat transfer rates to the cylinder head surface of a small compression-ignition engine. *Proceedings of the Institution of Mechanical Engineers*, 185, 976-988.

Bhatti, M.S., & Shah, R.K. (1987). Turbulent and transition flow convective heat transfer in ducts. In S. Kakac, R. Shah, & W. Aung (Eds), *Handbook of Single-Phase Convective Heat Transfer* (pp. 243-409). Hoboken, NJ: Wiley

Borman, G., & Nishiwaki, K. (1987). Internal-combustion engine heat transfer. *Progress in Energy and Combustion Science*, 13, 1-46.

Carslaw, H.S. & Jaeger, J.C. (1959). *Conduction of Heat in Solids.* Oxford: Clarendon Press

Chang, J., Guralp, O., Filipi, Z., & Assanis, D. (2004). New heat transfer correlation for an HCCI engine derived from measurements of instantaneous surface heat flux. *SAE Paper 2004-01-2996*

Chen, K., & Karim, G.A. (1998). Evaluation of the instantaneous unsteady heat transfer in a rapid compression-expansion machine. *Proceedings of the Institution of Mechanical Engineers*, 212, 351-362.

Demuynck, J., Verhelst, S., & Paepe, M.D., Huisseune, H., Sierens, R. (2010). Evaluation of heat transfer models with measurements in a hydrogen-fuelled spark ignition engine. *Proceedings of the 14th International Heat Transfer Conference*, 3, 87-95.

Gnielinski, V. (1976). New equations for heat and mass transfer in turbulent pipe and channel flow. *International Chemical Engineering*, 16, 359-367.

Heywood, J. B. (1988). *Internal Combustion Engine Fundamentals*. Singapore: McGraw-Hill.

Hohenburg, G. (1980). Advanced approaches or heat transfer calculations. *SAE Paper 790825.*

Incropera, F. P., Dewitt, D. P., Bergman, T. L., Lavine, A. S. (2007). *Introduction to Heat Transfer, 5th ed.* Hoboken, NJ : Wiley

Irimescu, A. (2012). Convective heat transfer equation for turbulent flow in tubes applied to internal combustion engines operated under motored conditions. *Applied Thermal Engineering*, 50, 536-545.

Kakac, S. (1987). The effect of temperature-dependent fluid properties on convective heat transfer. In S. Kakac, R. Shah, & W. Aung (Eds), *Handbook of Single-Phase Convective Heat Transfer* (pp. 243-409). Hoboken, NJ: Wiley

Kakac, S. & Yener, Y. (1987). Basics of heat transfer. In S. Kakac, R. Shah, & W. Aung (Eds), *Handbook of Single-Phase Convective Heat Transfer* (pp. 243-409). Hoboken, NJ: Wiley

Kornhauser, A.A., & Smith, J.L. (1994). Application of a complex Nusselt number to heat transfer during compression and expansion. *Transactions of the ASME Journal of Heat Transfer,* 116, 536-542.

Lawton, B. (1987). Effect of compression and expansion on instantaneous heat transfer in reciprocating internal combustion engines. *Proceedings of the Institution of Mechanical Engineers*, 201, 175-186.

Molki, M. (1986). Empirical correlation for the average heat transfer coefficient in circular tubes. *Transactions of the ASME Journal of Heat Transfer*, 108, 482-484.

Moran, M., Shapiro, H. (2008). *Fundamentals of Engineering Thermodynamics, 6th ed.* Hoboken, NJ: Wiley

Ota, M. (2008). Heat transfer during compression and expansion of gas. *Journal of Heat Transfer*, 130, 1-6.

Rakapoulos, C. D., Kosmadakis, G.M., & Pariotis, E.G. (2010). Critical evaluation of current heat transfer models used in CFD in-cylinder engine simulations and establishment of a comprehensive wall-function formulation. *Applied Energy*, 87, 1612-1630.

Sitkei, G., & Ramanaiah, G.V. (1972). A rational approach for calculation of heat transfer in diesel engines. *SAE Paper 720027*.

Soyhan, H.S., Yasar, H., Walmsley, H., Head, B., Kalghatgi, G.T., & Sorusbay, C. (2009). Evaluation of heat transfer correlations for HCCI engine modeling. *Applied Thermal Engineering*, 29, 541-549.

Woschni, G. (1967). A universally applicable equation for the instantaneous heat transfer coefficient in the internal combustion engine. *SAE Paper 670931*.

Zucker, R., & Bilbarz, O. (2002). *Fundamentals of Gas Dynamics, 2nd ed.* Hoboken, NJ: Wiley

APPENDIX

Appendix A - Conservation Equations for Mass, Momentum, and Energy

The governing equations for many problems related to thermal-fluid sciences are the conservation of mass, conservation of momentum, and conservation of energy equations. This set of equations, together with the appropriate boundary conditions, describes the temperature, velocity, and density distributions within a fluid completely, provided that the flow is laminar. In their full form, these equations are all coupled and highly non-linear. However, they can be simplified significantly in many situations, such as when density, thermal conductivity, specific heat, and/or viscosity are constant, when time dependence is negligible, or when gradients are confined to a single direction. The problem of gas expansion involves large temperature ranges, therefore assuming constant properties is not realistic. The process is inherently unsteady, and indeed describing the transient heat transfer is the goal of this study, therefore the time dependence of the process cannot be neglected. Additionally, one can see that the flow must be at least two-dimensional simply by imposing the no-slip boundary condition on all walls. This forces a radial velocity gradient (since the velocity is non-zero at the centerline) and an axial gradient (since the velocity is zero at the end of the cylinder and non-zero at the piston face). Therefore, the set of conservation equations describing this process becomes very daunting, prompting the use of other analytic methods to investigate this problem.

The conservation equations can be written (using tensor notation) as follows (Kakac & Yener, 1987):

Conservation of Mass (continuity):

$$\frac{\partial \rho}{\partial t} + \frac{\partial}{\partial x_i}(\rho u_i) = 0 \tag{A.1}$$

Where ρ is the gas density and u_i is the velocity in the *i* direction.

Conservation of Momentum (Newton's 2nd law):

$$\rho \frac{Du_i}{Dt} = \rho g_i - \frac{\partial P}{\partial x_i} + \frac{\partial}{\partial x_j}\left[\mu\left(\frac{\partial u_i}{\partial x_j} + \frac{\partial u_j}{\partial x_i}\right) - \frac{2}{3}\delta_{ij}\frac{\partial u_m}{\partial x_m}\right] \tag{A.2}$$

Where *P* is the gas pressure and *g* is the body force per unit mass (such as gravity).

Conservation of Energy (1st law of thermodynamics):

$$\rho \frac{Dh}{Dt} = \nabla \cdot (\kappa \nabla T) + \frac{DP}{Dt} + \mu\Phi \tag{A.3}$$

Where *h* is the enthalpy per mass of the gas, and Φ is the viscous dissipation function:

$$\Phi = \frac{\partial u_i}{\partial x_j}\left(\frac{\partial u_i}{\partial x_j} + \frac{\partial u_j}{\partial x_i}\right) \tag{A.4}$$

These equations are non-linear because of the material derivative term, *D/Dt*. Additionally, they are each partial differential equations, and are highly coupled, meaning that they must be solved simultaneously. Because of these complexities, there is no known closed-form solution to these equations without considerable simplifications being made. The analysis conducted for this study was conducted on a spatially averaged consideration. This kept the essential time-dependence of the expansion process but simplified the problem greatly, as discussed in Chapter 2.

Appendix B - Characteristic Expansion Velocity

In order to better describe the characteristic fluid velocities seen within the cylinder during the expansion process, the axial velocity distribution was analyzed. This was done by applying the 1-D, differential form the continuity equation to this process. For the purposes of this analysis, a rigorous, detailed description of the velocity distribution is not necessary. Rather, it is desired to obtain a simple estimate of what the velocities within the cylinder are, which could be used to determine what velocity scale should be used to describe the overall process.

An estimate of the velocity distribution between the piston and the end of the cylinder can be made by using the differential form of the continuity equation, applied along the centerline as shown in Figure 2.2.

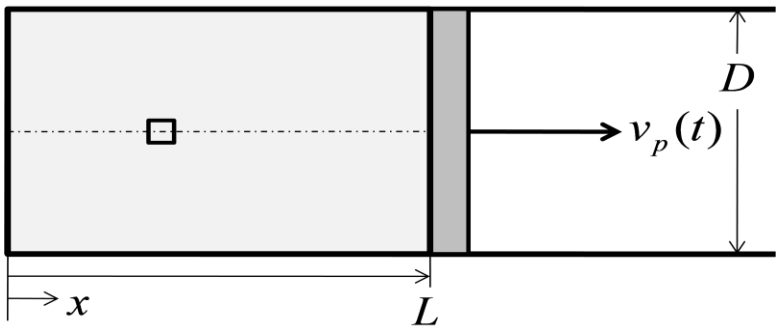

Figure B.1 – Geometry for use in determine the characteristic fluid velocity during expansion

The continuity equation in two dimensions can be written and expanded as:

$$\frac{D\rho}{Dt} + \rho\frac{\partial u}{\partial x} + \rho\frac{\partial v}{\partial y} = 0 \tag{B.1}$$

$$\frac{\partial \rho}{\partial t} + u\frac{\partial \rho}{\partial x} + v\frac{\partial \rho}{\partial y} + \rho\frac{\partial u}{\partial x} + \rho\frac{\partial v}{\partial y} = 0 \tag{B.2}$$

By confining this analysis to the 1-D velocity profile along the centerline (assuming symmetry), the derivatives with respect to *y* can be neglected.

$$\frac{\partial \rho}{\partial t} + u\frac{\partial \rho}{\partial x} + \rho\frac{\partial u}{\partial x} = 0 \tag{B.3}$$

To proceed with this analysis, some information concerning the spatial variation of density is required. In the prior analysis for heat transfer during an expansion, uniform pressure and temperature were assumed to simplify the analysis. Employing the same assumption implies that density is uniform within the cylinder via the ideal gas law (Eq. 2.3). Therefore, the continuity equation can be expressed as:

$$\frac{\partial \rho}{\partial t} + \rho\frac{\partial u}{\partial x} = 0 \tag{B.4}$$

Density can be re-written as $\rho = m/V$, and since the mass of the gas is constant this reduces Eq. B.4 to:

$$\frac{\partial u}{\partial x} = \frac{1}{V}\frac{\partial V}{\partial t} \tag{B.5}$$

The volume of the gas for the piston-cylinder geometry examined is $V(t) = A_c L(t)$, which is substituted into Eq. B.5 to form:

$$\frac{\partial u}{\partial x} = \frac{1}{L}\frac{\partial L}{\partial t} = \frac{v_p}{L} \tag{B.6}$$

Here the simplification has been made that $\partial L/\partial t$ is simply the piston speed, v_p. Integrating Eq. B.6 along *x* and using the boundary condition of $u(L) = v_p$ produces the velocity distribution given by Eq. B.7:

$$u = \frac{v_p}{L} x \tag{B.7}$$

This is a simple, linear velocity distribution for the fluid along the centerline of the piston-cylinder expansion. It varies from zero at the stationary end of the cylinder to the piston velocity, which changes over time. Since Eq. B.7 is linear, the average fluid velocity (found by integrating along *x* and dividing by *L*) is found to be half the piston speed:

$$u_m = \frac{v_p}{2} \tag{B.8}$$

This analysis represents a very simplified version of the expansion process. In particular, spatial gradients in density were ignored and the analysis was confined to the centerline assuming that non-axial gradients could then be ignored. While these assumptions may be too restrictive for a detailed model of the velocity distribution, that was not the intent of this analysis. Rather, the goal was to ascertain what would be an appropriate velocity scale for the fluid within the cylinder. This analysis suggests that the piston speed is the characteristic velocity of the expansion process. Since this was the velocity scale used in the Reynolds number for the heat transfer model, this analysis provides justification for that selection.

Appendix C – Experimental Apparatus

The experimental apparatus used for these tests was the single piston-cylinder assembly which undergoes a single combustion and an expansion event. It is located at the laboratory of Long Haul Power, Inc, and was built prior to this author's involvement. It is equipped with a piezo-resistant pressure sensor to measure initial fill pressure, two piezo-electric sensors for the rapid pressure rise and decay of combustion and expansion, and a cable-extension position transducer to determine piston position and therefore cylinder volume. As the gas expands, the work done on the piston is dissipated by raising a weight. While the schematic shown in Figure 3.1 illustrates the operating features of this experimental apparatus, photographs are included here in Figures C.1-C.2.

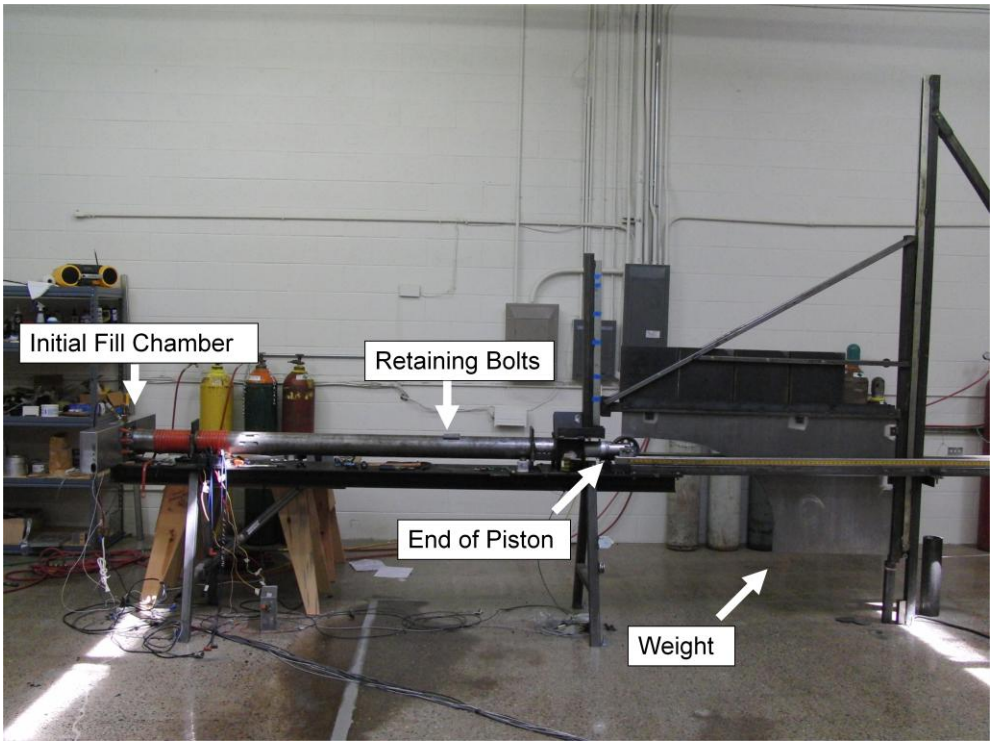

Figure C.1 – Image of test apparatus used for experiments

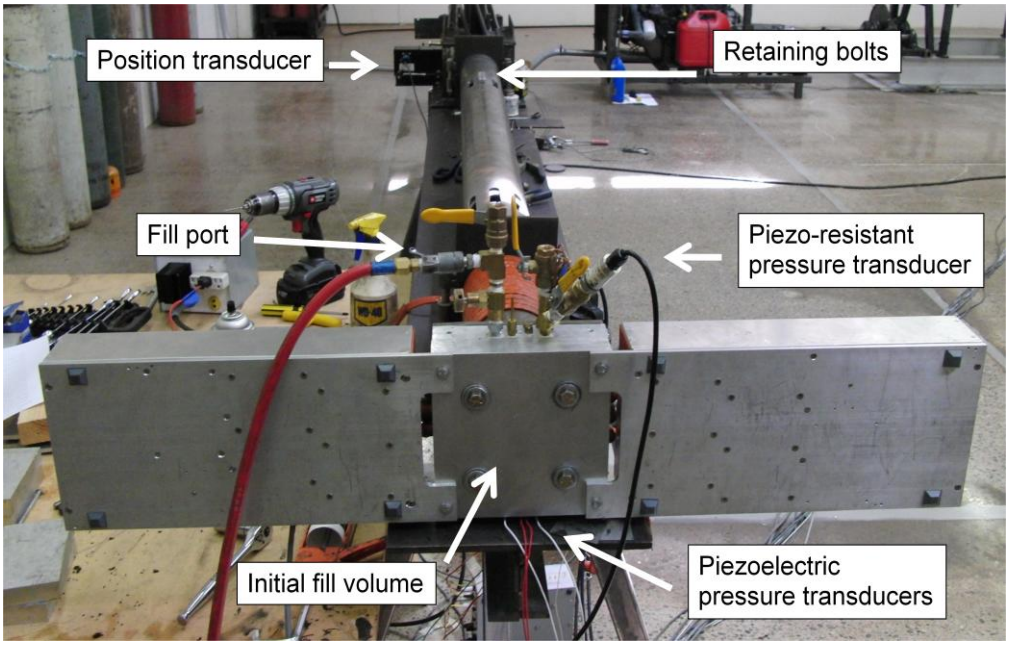

Figure C.2 – Image of test apparatus used for experiments, showing position of data acquisition instruments

The output from the sensors on the experimental apparatus were read and recorded by a LabVIEW controlled data acquisition system, which was also built by Long Haul Power prior to this author's involvement. This data acquisition system recorded samples at a rate of 25,000 Hz. The block diagram is given in Figures C.3-C.4, while a screenshot of the front panel is shown in Figures C.5-C.6. Both the block diagram and the front panel are split between two figures because of their size.

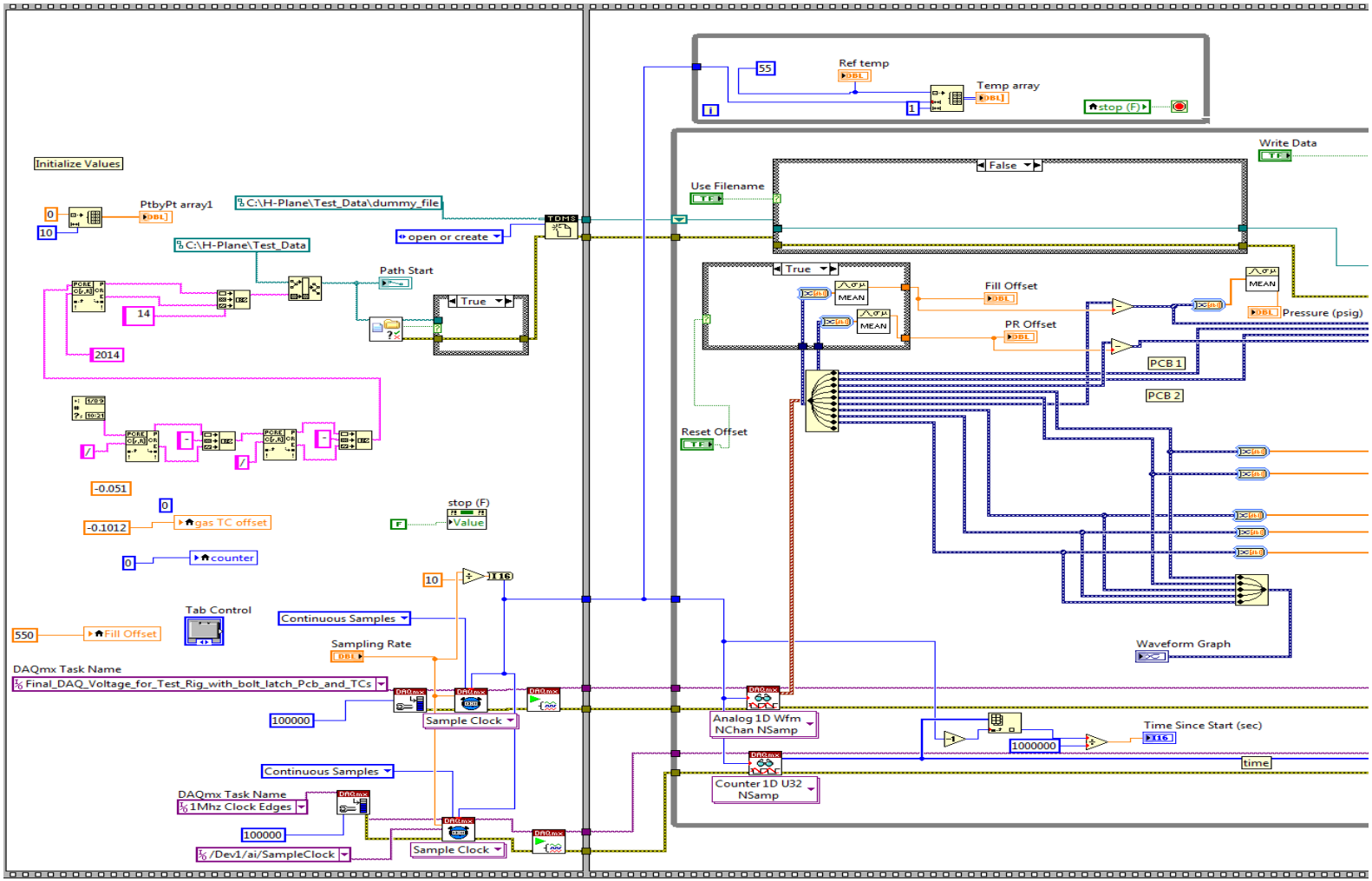

Figure C.3 – Screenshot of LabVIEW block diagram showing data collection system; Part 1 of 2

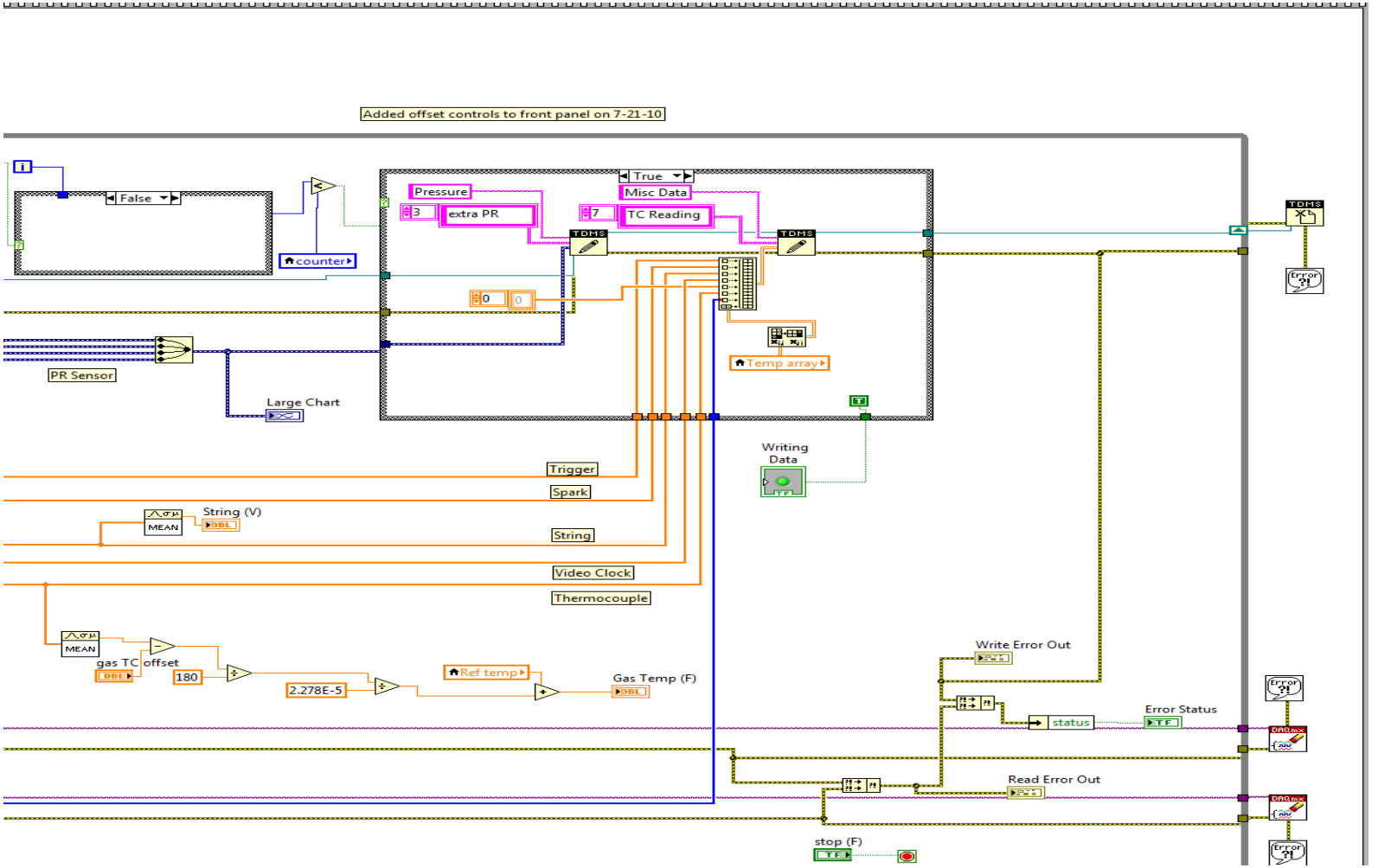

Figure C.4 – Screenshot of LabVIEW block diagram showing data collection system; Part 2 of 2

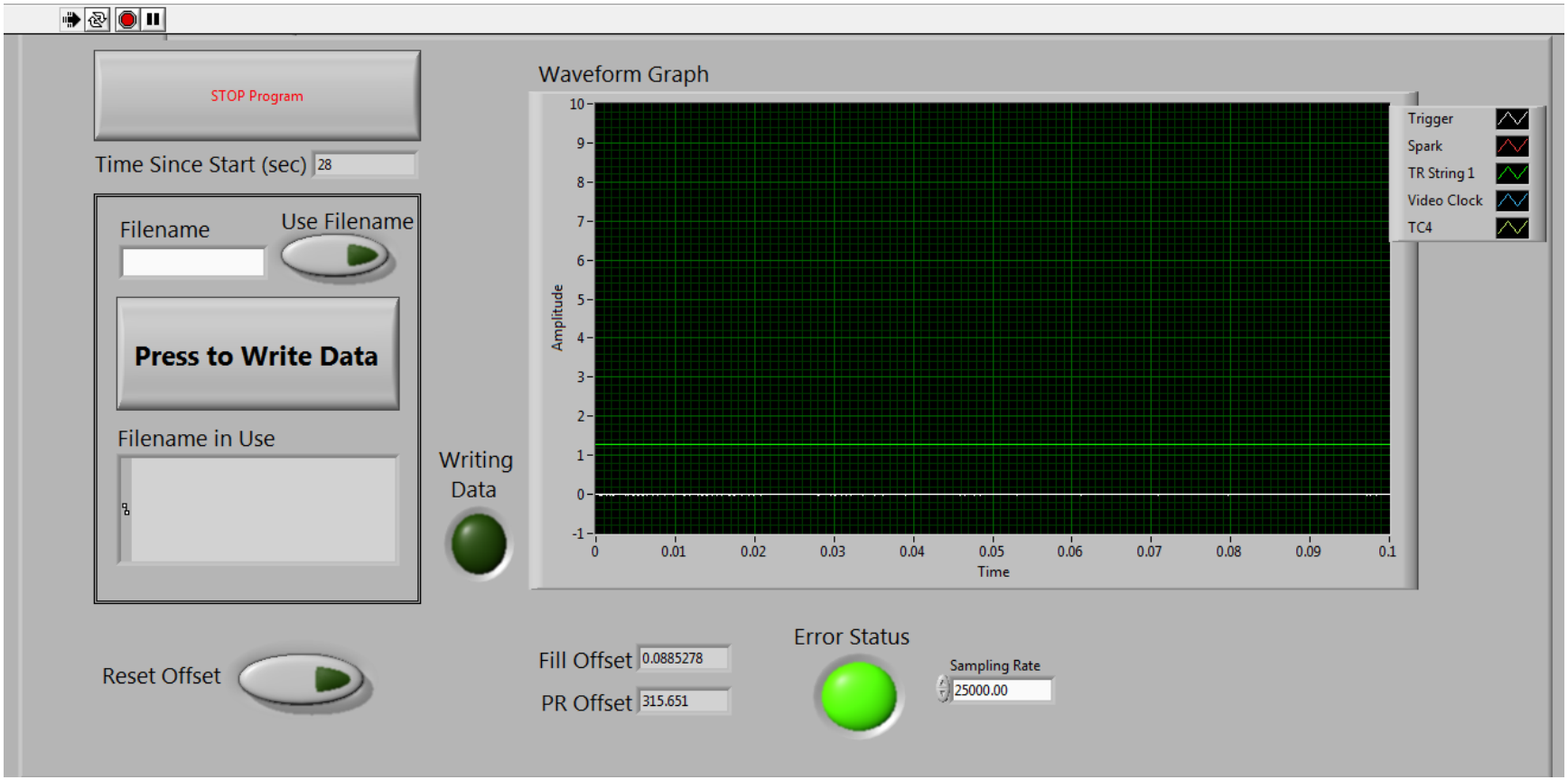

Figure C.5 – Screenshot of LabVIEW front panel showing data collection system; Part 1 of 2

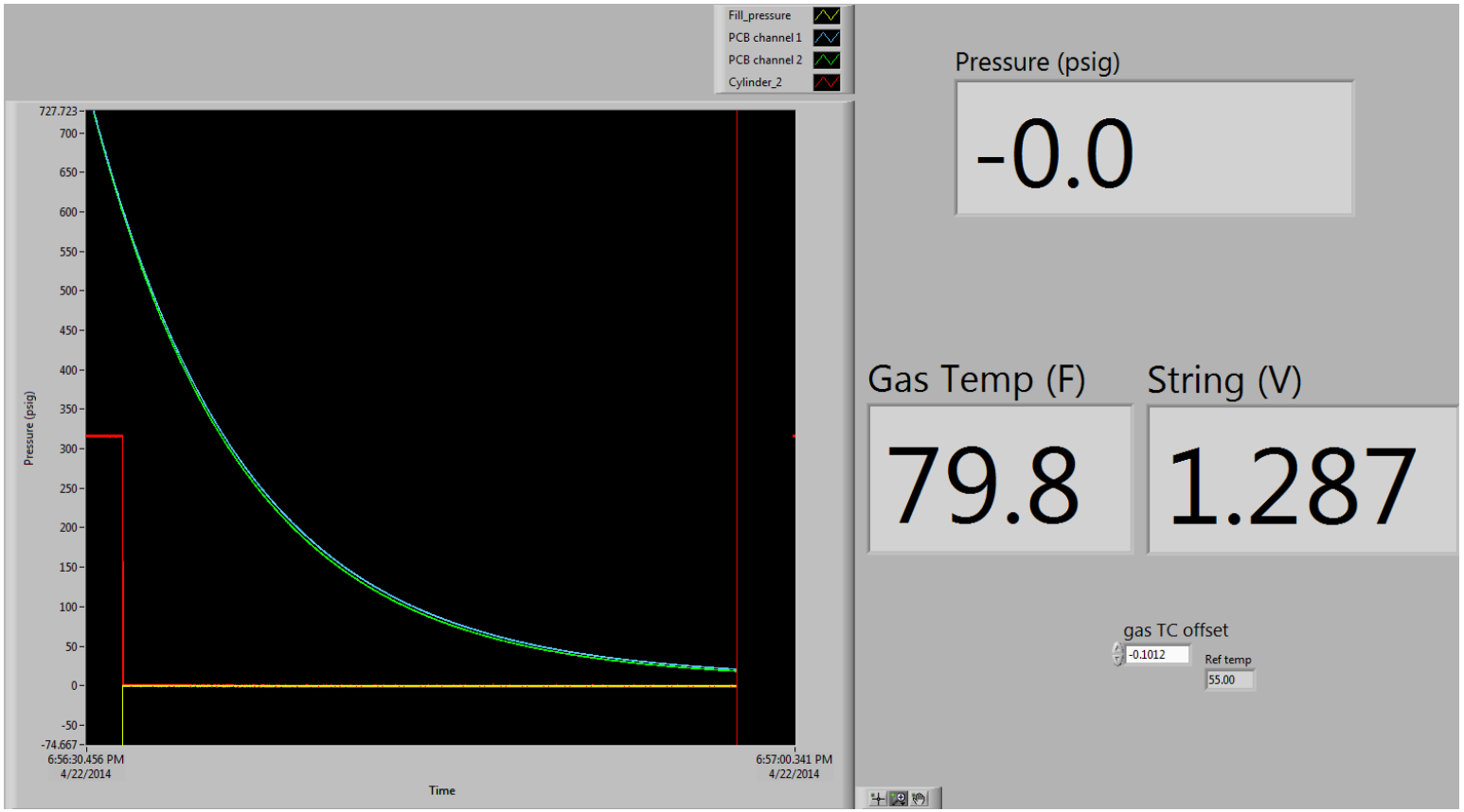

Figure C.6 – Screenshot of LabVIEW front panel showing data collection system; Part 2 of 2

Appendix D –Position Transducer Calibration

The test apparatus and instrumentation used for these tests were supplied by Long Haul Power, LLC, and had been installed prior to this author's involvement in the project. While calibration information was available for the pressure sensors used, it was not available for the position transducer. This position transducer was a cable-extension transducer by Celesco, model PT5A. It was mounted to a stationary frame, while the cable was attached to the free end of the piston (see Figure 3.1). To calibrate the position transducer, the piston position was determined by means of a measuring tape fixed to the side of the piston and compared to the voltage output for the position transducer. Piston position was referenced to zero when it was flush with the end of the cylinder. During expansion experiments the initial fill volume was attached to the end of the cylinder. Therefore, when applying the calibration curve to determine piston position and cylinder volume, the length of the initial fill volume was added to the position calculated from the calibration curve.

The calibration procedure consisted of first taking eight voltage readings with the piston flush to determine the zero readings. The piston was moved manually between tests to test the repeatability of the readings. Next readings were taken by moving the piston some random distance and recording the voltage output from the transducer. Piston distances were selected in no prescribed order to minimize any hysteresis effects. It was found that the voltage output varied linearly with position, as was expected. The equation of the line is given in Eq. D.1:

$$x = 8.884(V - 1.05) \qquad \text{(D.1)}$$

The curve fit error was calculated as the standard deviation between the position calculated from the curve fit and the measured position:

$$S = \sqrt{\sum_{i=1}^{N} \frac{(y_{meas} - y_{calc})^2}{N - 2}} \qquad \text{(D.2)}$$

Where *N* is the number of calibration points taken. The curve fit error was found to be 0.051 inches. This was combined with the uncertainties of the measurement standard used, which was 0.0313 inches (half the precision of the measuring tape used), in a root-sum-square fashion to give a final uncertainty of 0.060 inches.

The calibration curve data for piston position is shown in Figure D.1, and the calibration data is included in Table D.1.

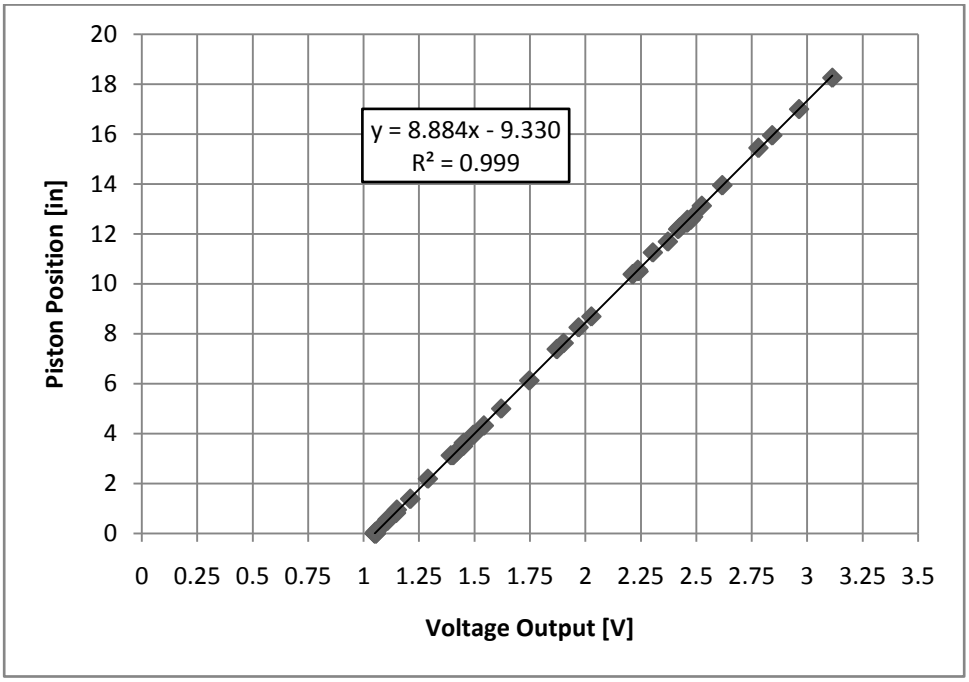

Figure D.1 – Calibration curve for the cable-extension position transducer

Table D.1 - Calibration Data for the Cable-Extension Position Transducer

Test #	Voltage Output (V)	Measured Piston Position (in)	Test #	Voltage Output (V)	Measured Piston Position (in)
1	1.050	0	24	2.474	12.5625
2	1.053	0	25	1.417	3.25
3	1.051	0	26	1.495	3.9375
4	1.054	0	27	1.290	2.1875
5	1.054	0	28	1.451	3.625
6	1.053	0	29	1.106	0.5
7	1.053	0	30	1.053	0.0625
8	1.053	0	31	1.069	0.1875
9	1.748	6.125	32	2.460	12.5625
10	2.459	12.4375	33	3.114	18.25
11	1.404	3.125	34	2.418	12.1875
12	1.620	5	35	2.425	12.25
13	2.240	10.5	36	1.872	7.375
14	1.150	0.9375	37	2.213	10.375
15	2.486	12.6875	38	1.394	3.125
16	2.027	8.6875	39	1.108	0.5625
17	2.372	11.6875	40	1.969	8.25
18	1.448	3.5	41	2.780	15.4375
19	1.146	0.8125	42	2.964	17
20	1.211	1.375	43	2.304	11.25
21	1.542	4.3125	44	2.525	13.125
22	1.902	7.625	45	2.618	13.9375
23	2.236	10.5625	46	2.843	15.9375

Appendix E – Wall Temperature Analysis

In the determining of the heat transfer coefficient from experimental data, it was assumed that the wall surface temperature was constant and uniform. To test this assumption, the surface area for heat loss (which includes the piston head, cylinder head, and cylinder wall) was modeled as a semi-infinite solid subjected to a step change in heat transfer coefficient.

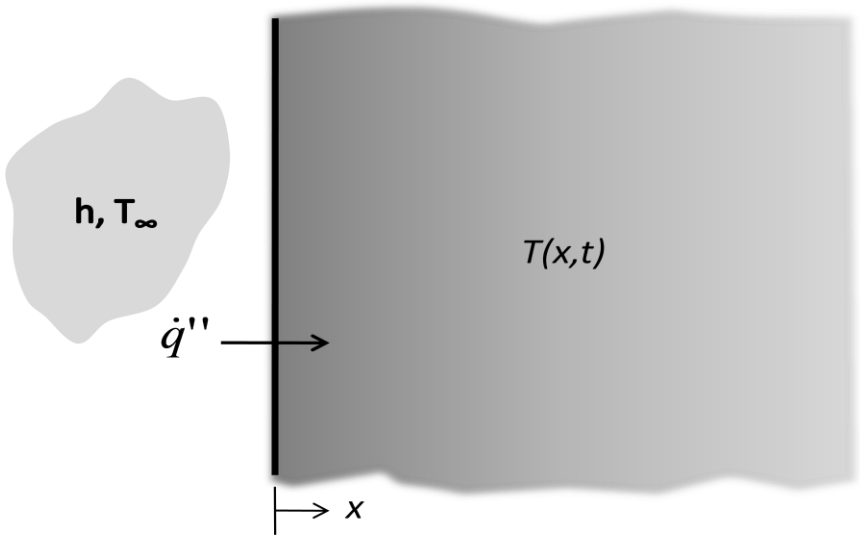

Figure E.1 – Schematic for wall temperature analysis

This is a 1-D transient conduction analysis; heat transfer through the solid is assumed to be only in the *x* direction. Assuming constant thermal conductivity and specific heat within the solid, the heat equation is:

$$\frac{1}{\alpha}\frac{\partial T}{\partial t} = \frac{\partial^2 T}{\partial x^2} \tag{E.1}$$

The boundary conditions for this problem are that the solid is initially at a uniform temperature, that the solid remains at this initial temperature as *x* approaches infinity, and that the surface (at $x = 0$) is exposed to a constant heat transfer coefficient, *h*, and a constant fluid temperature, T_∞. Since this analysis is meant to be for a worst-case scenario, the heat transfer coefficient and gas temperature applied in this analysis are peak values experienced in the experiments. The boundary conditions can be represented mathematically:

$$T(x, 0) = T_i \tag{E.2a}$$

$$T(x \to \infty, t) = T_i \tag{E.2b}$$

$$\kappa \frac{\partial T}{\partial x}\Big|_{x=0} = h(T(0, t) - T_\infty) \tag{E.2c}$$

This conduction problem has an analytic solution, which is given as (Carslaw & Jaeger, 1959):

$$\frac{T(x,t) - T_i}{T_\infty - T_i} = erfc\left(\frac{x}{2\sqrt{\alpha t}}\right) - \left[erfc\left(\frac{x}{2\sqrt{\alpha t}} + \frac{h\sqrt{\alpha t}}{\kappa}\right)\right]\left[e^{\frac{hx}{\kappa} + \frac{h^2 \alpha t}{\kappa^2}}\right] \tag{E.3}$$

Where α is the thermal diffusivity ($\alpha = \kappa/\rho c_p$), and *erfc* is the complementary error function and is related to the Gaussian error function, *erf* as: $erfc = 1 - erf$. The Gaussian error function is a well tabulated mathematical function.

The solution given by Eq. E.3 gives the temperature throughout the solid as a function of time and space, and is dependent on the material composition of the solid. The cylinder walls of the experimental apparatus are steel, while the cylinder head and piston face are aluminum. In order to make sure that the constant wall temperature

assumption is valid, the wall temperature distribution was calculated for both steel and aluminum walls. The thermal properties used for this analysis are given in Table E.1:

Table E.1 - Thermal Properties Used for Wall Conduction Analysis

Metal	**Thermal Conductivity**	**Thermal Diffusivity**
Steel	64 W/m-K	1.88E-05 m^2/s
Aluminum	177 W/m-K	7.30E-05 m^2/s

The wall temperature distribution was evaluated using Eq. E.3 and plotted as a function of distance into the wall and elapsed time. Distance was limited to 0.25 inches because that was the thickness of the cylinder wall. Time was limited to 50ms because that was the maximum expansion time during the tests conducted. The wall temperature used was $T_{wall} = 290\ K$, which is near the wall temperatures seen during the tests. The heat transfer coefficient was chosen as $h = 350\ W/m^2K$ and the gas temperature used was $T_\infty = 1800\ K$. These values were selected based on the maximum for each during the expansion (see Figures 4.10 and 4.15). In reality neither the heat transfer coefficient nor the gas temperature are constant, but instead they vary significantly with time. Since the maximum values are used here, this analysis is worst case and is expected to significantly over-predict the wall surface temperatures. Figure E.2 has the wall temperature distribution evaluated using the thermal properties of aluminum, while Figure E.3 has the wall temperature distribution evaluated using the thermal properties of steel.

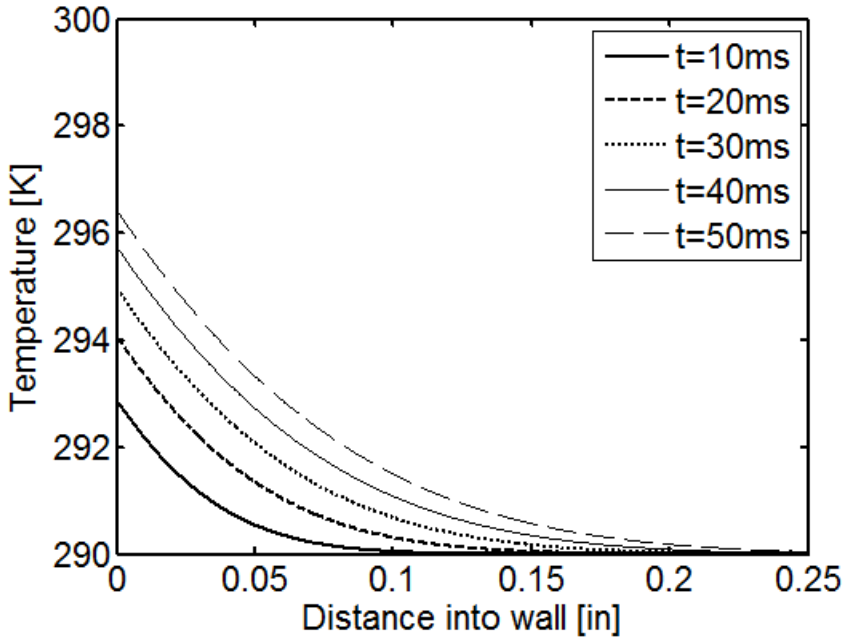

Figure E.2 – Temperature distribution for aluminum using a semi-infinite solid analysis

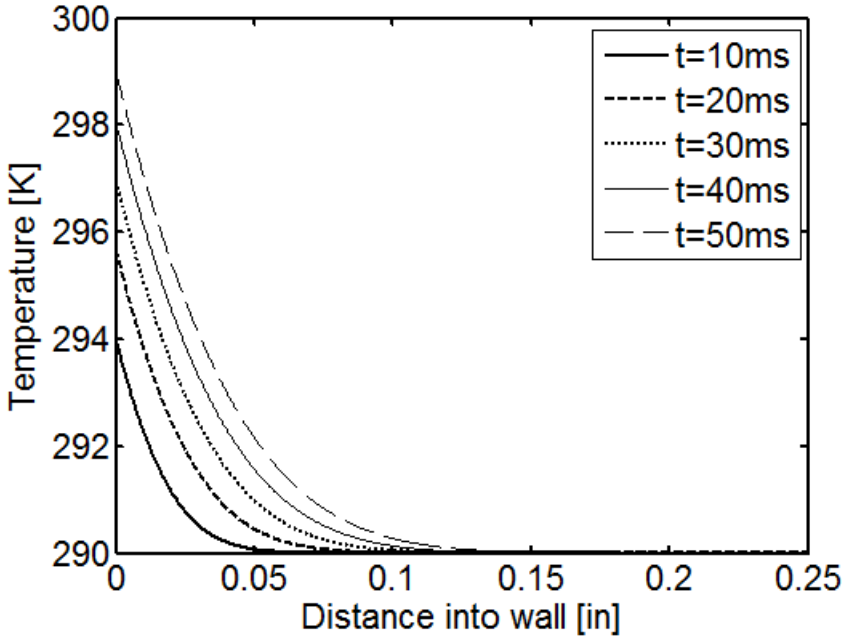

Figure E.3 – Temperature distribution for steel using a semi-infinite solid analysis

Figures E.2 and E.3 illustrate several key results. In both cases, the wall temperature at 0.25” is barely changed from the initial temperature, showing that the semi-infinite approximation is a valid model for the small expansion times of interest. The wall surface temperature is indicated by the temperature at a distance of $x = 0$. This is seen to rise approximately 6.5K for the aluminum case and 9.0K for the steel case. This difference reflects that aluminum allows heat to diffuse more easily than steel does.

In the case of either metal, the increase in surface temperature was small. The maximum increase in wall temperature was determined to be approximately 9K, or 3% of the wall temperature. The wall temperature was used to determine the gas to wall temperature difference, which was on the order of 400-1500K. This means that a wall temperature increase of 9K reflects a change in gas to wall temperature difference of 0.6%-2.3%. Since overall uncertainties in heat transfer coefficient during this study were 15%-25% (see §3.4), the effect of changing wall temperature was insignificant. Additionally, this represents the maximum change in wall temperature since the analysis was conducted for a worst-case scenario, while real values are expected to be lower. Therefore, the wall temperature during the expansion was assumed to be constant for the purposes of this study.

Appendix F – Data Processing

Data was taken in the form of pressure and volume measurements for the combustion and expansion process. The beginning of expansion was defined as the point when volume has increased by 1% of its original volume, as described in Ch. 2. Multiple tests were conducted at each operating condition in order to decrease uncertainties. These tests were then combined to form the representative data set for each operating condition.

Volume data was filtered by excluding outliers from the data set. These outliers were produced by vibrations/small oscillations present in the arm connecting the cable from the position transducer to the end of the piston. Because of the manner in which the arm was attached to the piston, these oscillations tended to produce outliers which were lower than the true signal. These were filtered by fitting a smooth polynomial to the raw data and computing a running five-point standard deviation based on the smooth curve. The cutoff value was chosen as five standard deviations (5σ); any values beyond this cutoff were removed and then replaced with the cutoff value, in order to keep the data set the same size. This filtering process is shown in Figure F.1.

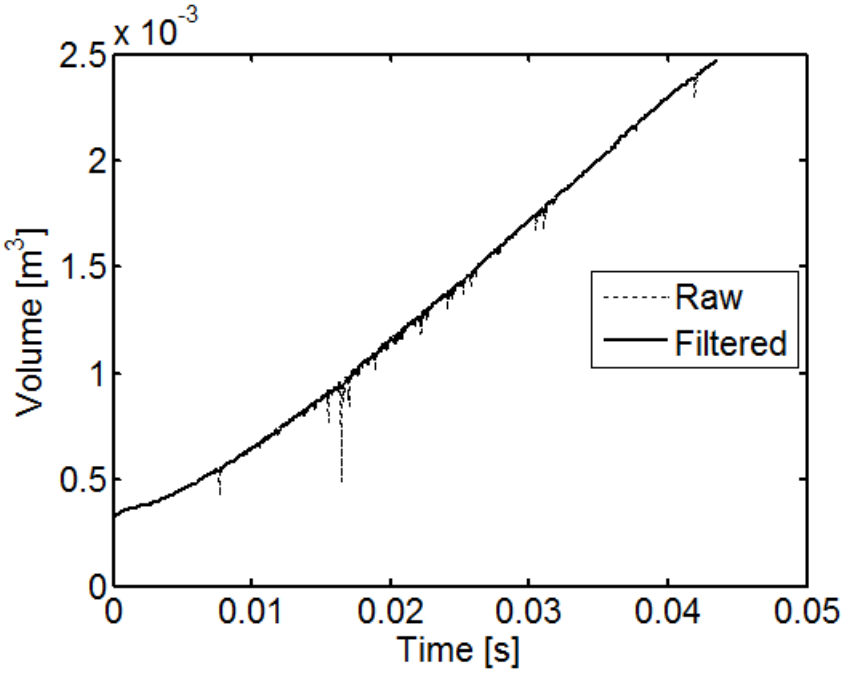

Figure F.1 – Volume versus time for a single expansion in Test Case D, showing raw and filtered data.

Multiple tests were conducted at each test condition and combined into a single curve representative of that test condition. It was found that the energy balance method used to extract heat transfer information required that the data be smooth; therefore these tests were combined by fitting a smooth curve through the combined tests. Volume data was fitted by a fifth order polynomial, which was determined by using the least squares regression function *polyfit* available in Matlab©. A fifth order polynomial was chosen because it was found to smoothly match the data well, both at the initial stage of expansion (when velocity is low but acceleration is high) and at the final stage of expansion (when velocity is high and acceleration is low). Pressure-volume data was found to match a power law curve very well, therefore this least

squares fit was done using a first order (linear) polynomial using the logarithms of pressure and volume (see Eq. 3.2). These curve fits can be seen in Figures F.2 and F.3.

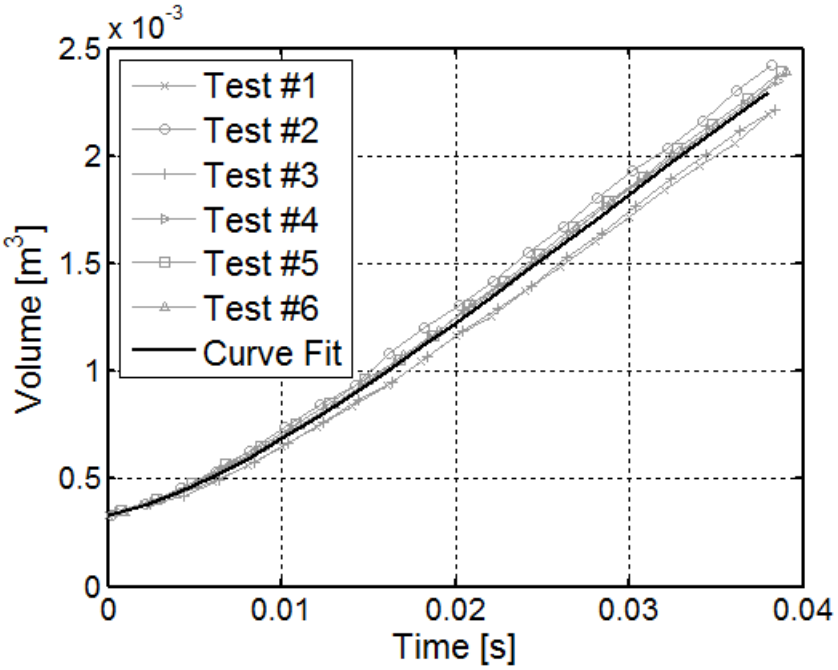

Figure F.2 – Volume versus time for Test Case D, showing individual runs and the polynomial curve fit.

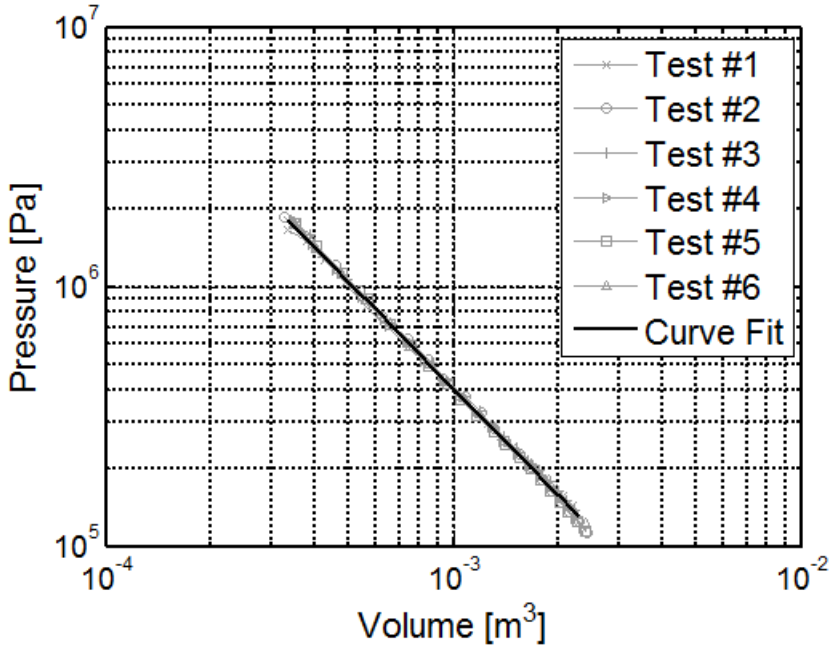

Figure F.3 – Pressure versus volume for Test Case D, showing individual runs and the power law curve fit.

Appendix G – Experimental Uncertainties

The uncertainties in calculated parameters, such as the heat transfer coefficient and Reynolds number, were determined by propagating the uncertainties from the measured variables. The uncertainty in a measured variable was determined by combining the instrument bias errors and the precision errors for the experiment, which were combined using the root-sum-square method. Bias errors were known from either the manufacturer's information or calibration. Precision errors were calculated from the sample standard deviation between test cases, assuming 95% confidence for the t-factor. For cylinder pressure and volume during expansion, the precision errors were evaluated at five points along the pressure-volume diagram and then averaged. It was found that the precision errors were significantly larger than the bias errors, however both contributed to the overall uncertainty in the experiments. Table G.1 reports the bias errors associated with each of the measured variables, and Table G.2 reports the precision errors associated with each of the measured variables. These were combined in a root-sum-square fashion to produce the total uncertainties reported in Table 3.3 and repeated here in Table G.3.

Table G.1 - Bias Uncertainties for Each Measured Variable

Test Case	**Diameter**	**Initial Volume**	**Fill Pressure**	**Ambient Temperature**	**Pressure**	**Volume**
Case A	0.01%	3.40%	2.63%	0.10%	1.30%	1.00%
Case B	0.01%	3.40%	1.94%	0.10%	1.30%	1.00%
Case C	0.01%	3.40%	1.41%	0.10%	1.30%	1.00%
Case D	0.01%	3.40%	1.12%	0.10%	1.30%	1.00%
Case E	0.01%	3.40%	0.87%	0.10%	1.30%	1.00%

Table G.2 - Precision Uncertainties for Each Measured Variable

Test Case	Diameter	Initial Volume	Fill Pressure	Ambient Temperature	Pressure	Volume
Case A	0.58%	5.05%	1.17%	1.39%	5.56%	3.71%
Case B	0.58%	5.02%	0.78%	0.24%	8.90%	6.63%
Case C	0.58%	5.42%	0.86%	0.00%	10.84%	8.79%
Case D	0.58%	4.13%	0.64%	1.09%	5.41%	4.48%
Case E	0.58%	1.30%	0.62%	0.53%	16.02%	13.28%

Table G.3 - Total Uncertainties for Each Measured Variable

Test Case	Diameter	Initial Volume	Fill Pressure	Ambient Temperature	Pressure	Volume
Case A	0.58%	6.09%	2.88%	1.39%	5.71%	3.84%
Case B	0.58%	6.06%	2.09%	0.26%	8.99%	6.70%
Case C	0.58%	6.40%	1.65%	0.10%	10.92%	8.85%
Case D	0.58%	5.35%	1.29%	1.09%	5.56%	4.59%
Case E	0.58%	3.64%	1.07%	0.54%	16.07%	13.32%

These uncertainties were propagated to calculated parameters using the Kline-McClintock method. This method calculates the uncertainty in a calculated parameter based on the gradient of the calculated parameter with respect to the measured parameter and the uncertainty in the measured parameter. If the calculated parameter is a function of multiple measured parameters, this method is repeated for each measured variable and the resulting uncertainties are combined in a root-sum-square manner. The Kline-McClintock method is represented mathematically by Eq. G.1:

$$u_R = \sqrt{\sum \left(\frac{\partial R}{\partial x_i} u_{x_i} \right)^2} \tag{G.1}$$

Where R is the calculated parameter, x_i are the measured variables, u_i are the uncertainties in the measured variables, and u_R is the uncertainty in the calculated

parameter. Using this procedure, the uncertainties in key calculated parameters were determined. For some parameters the uncertainty was fixed, while for others the uncertainty varied during the expansion. While the mean uncertainties were given in Tables 3.5 and 3.6 in the main body of the report, the minimum, maximum, and mean values are reported in Tables G.4-G.8 for each test case.

Table G.4 - Propagated Uncertainties for Test Case A

Parameter	**Minimum**	**Maximum**	**Mean**
Moles	7.10%	7.10%	7.10%
Density	8.10%	8.10%	8.10%
Bulk Gas Temperature	9.90%	9.90%	9.90%
Piston Velocity	0.00%	36.20%	3.60%
Heat Transfer Coefficient	8.60%	40.70%	13.40%
Reynolds Number	9.40%	35.40%	10.70%
Nusselt Number	11.40%	41.40%	15.40%
Prandtl Number	9.90%	9.90%	9.90%
Peclet Number	13.65%	36.76%	14.58%
Characteristic Peclet Number	11.49%	11.49%	11.49%

Table G.5 - Propagated Uncertainties for Test Case B

Parameter	**Minimum**	**Maximum**	**Mean**
Moles	6.60%	6.60%	6.60%
Density	9.40%	9.40%	9.40%
Bulk Gas Temperature	13.00%	13.00%	13.00%
Piston Velocity	0.00%	47.70%	3.80%
Heat Transfer Coefficient	7.90%	50.10%	17.40%
Reynolds Number	10.40%	44.50%	12.00%
Nusselt Number	12.50%	51.00%	20.10%
Prandtl Number	13.00%	13.00%	13.00%
Peclet Number	16.65%	46.36%	17.69%
Characteristic Peclet Number	11.66%	11.66%	11.66%

Table G.6 - Propagated Uncertainties for Test Case C

Parameter	Minimum	Maximum	Mean
Moles	6.70%	6.70%	6.70%
Density	11.10%	11.10%	11.10%
Bulk Gas Temperature	15.60%	15.60%	15.60%
Piston Velocity	0.00%	77.00%	6.40%
Heat Transfer Coefficient	8.10%	84.40%	26.70%
Reynolds Number	11.80%	71.20%	15.10%
Nusselt Number	14.20%	85.20%	29.40%
Prandtl Number	15.50%	15.50%	15.50%
Peclet Number	19.48%	72.87%	21.64%
Characteristic Peclet Number	12.66%	12.66%	12.66%

Table G.7 - Propagated Uncertainties for Test Case D

Parameter	Minimum	Maximum	Mean
Moles	5.67%	5.67%	5.67%
Density	7.30%	7.30%	7.30%
Bulk Gas Temperature	9.17%	9.17%	9.17%
Piston Velocity	0.00%	20.46%	2.42%
Heat Transfer Coefficient	6.80%	23.02%	13.91%
Reynolds Number	8.05%	18.78%	8.87%
Nusselt Number	9.69%	24.04%	15.62%
Prandtl Number	9.16%	9.16%	9.16%
Peclet Number	12.20%	20.90%	12.75%
Characteristic Peclet Number	9.48%	9.48%	9.48%

Table G.8 - Propagated Uncertainties for Test Case E

Parameter	Minimum	Maximum	Mean
Moles	3.90%	3.90%	3.90%
Density	13.90%	13.90%	13.90%
Bulk Gas Temperature	21.20%	21.20%	21.20%
Piston Velocity	0.00%	251.60%	16.60%
Heat Transfer Coefficient	4.70%	308.80%	48.70%
Reynolds Number	13.70%	241.50%	24.70%
Nusselt Number	16.60%	309.20%	52.20%
Prandtl Number	21.20%	21.20%	21.20%
Peclet Number	25.24%	242.43%	32.55%
Characteristic Peclet Number	12.56%	12.56%	12.56%

The propagation of uncertainty can also be represented graphically. This was done by linking the calculated parameter to the measured variables used to calculate it, along with the associated uncertainties. This is shown in Figures G.1-G.8, using values for the uncertainties from Test Case D.

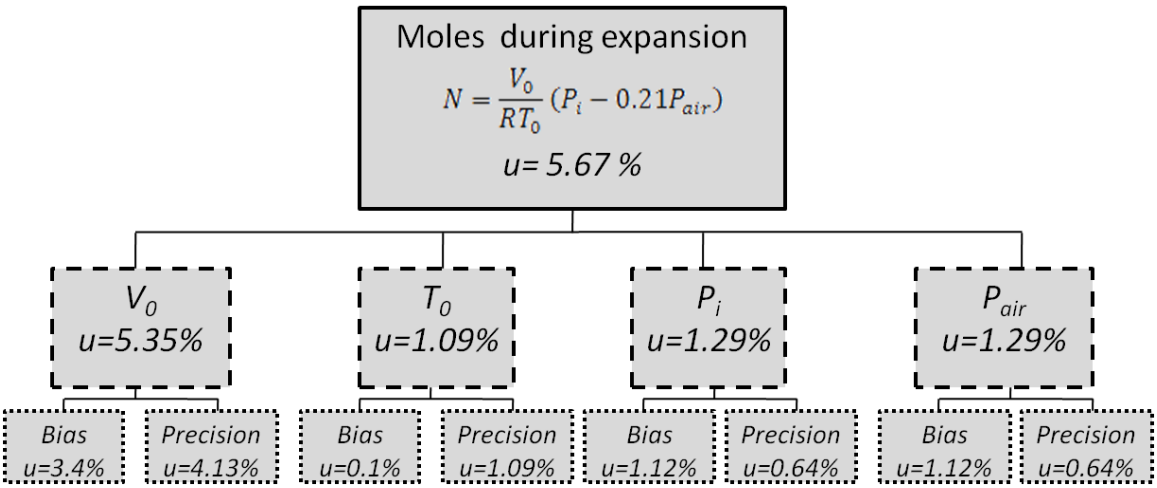

Figure G.1 – Propagation of uncertainty for the number of moles of gas in the cylinder during expansion

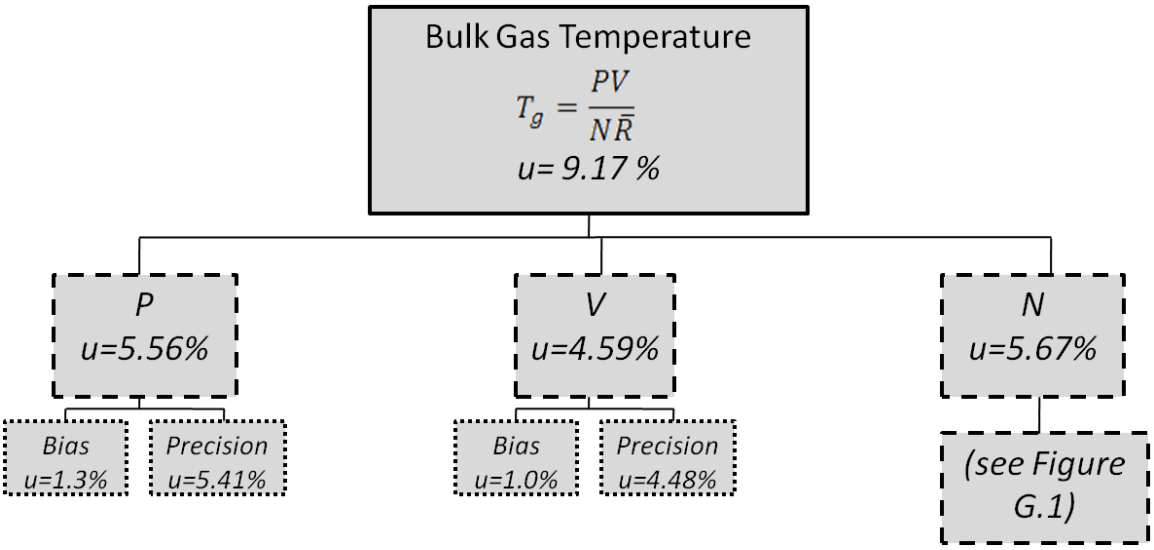

Figure G.2 – Propagation of uncertainty for the bulk gas temperature during expansion

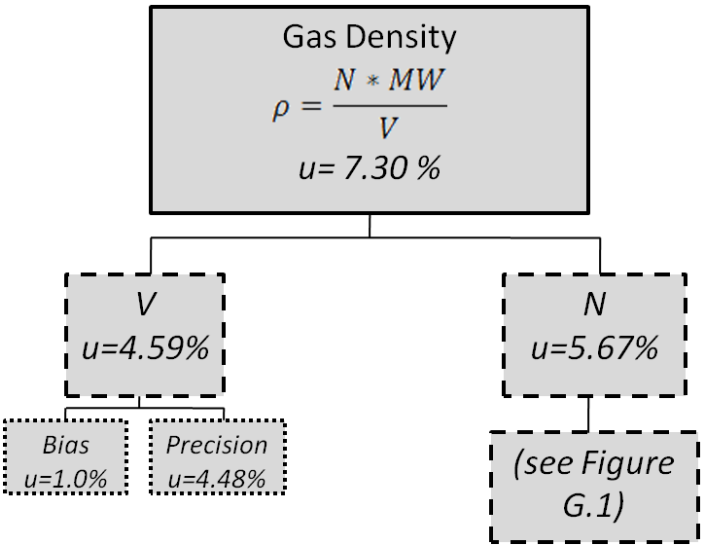

Figure G.3 – Propagation of uncertainty for the gas density during expansion

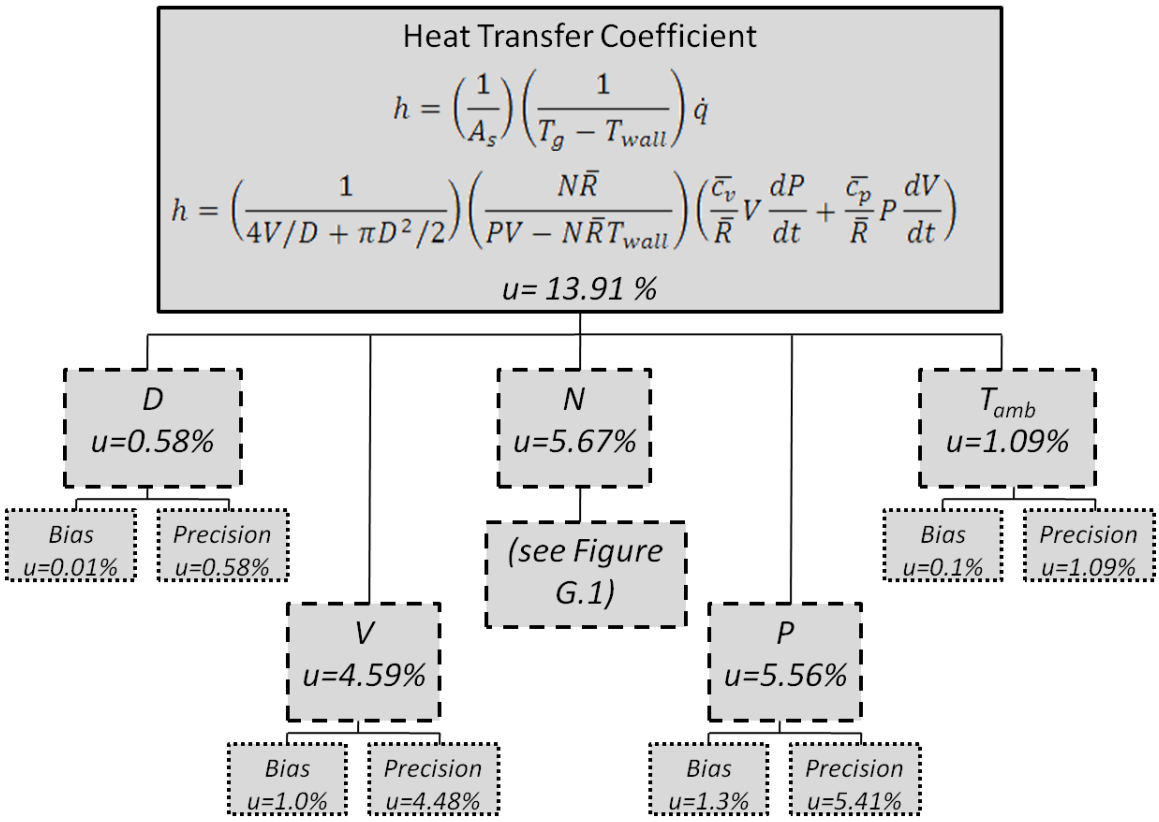

Figure G.4 – Propagation of uncertainty for the heat transfer coefficient during expansion

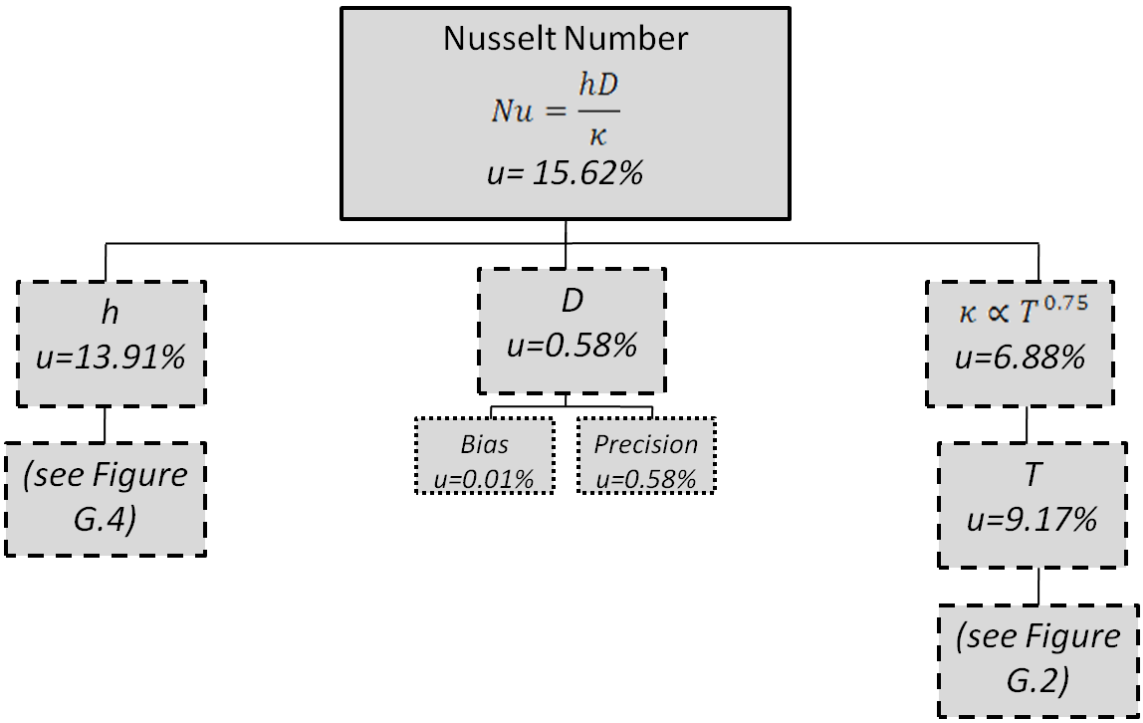

Figure G.5 – Propagation of uncertainty for the Nusselt number during expansion

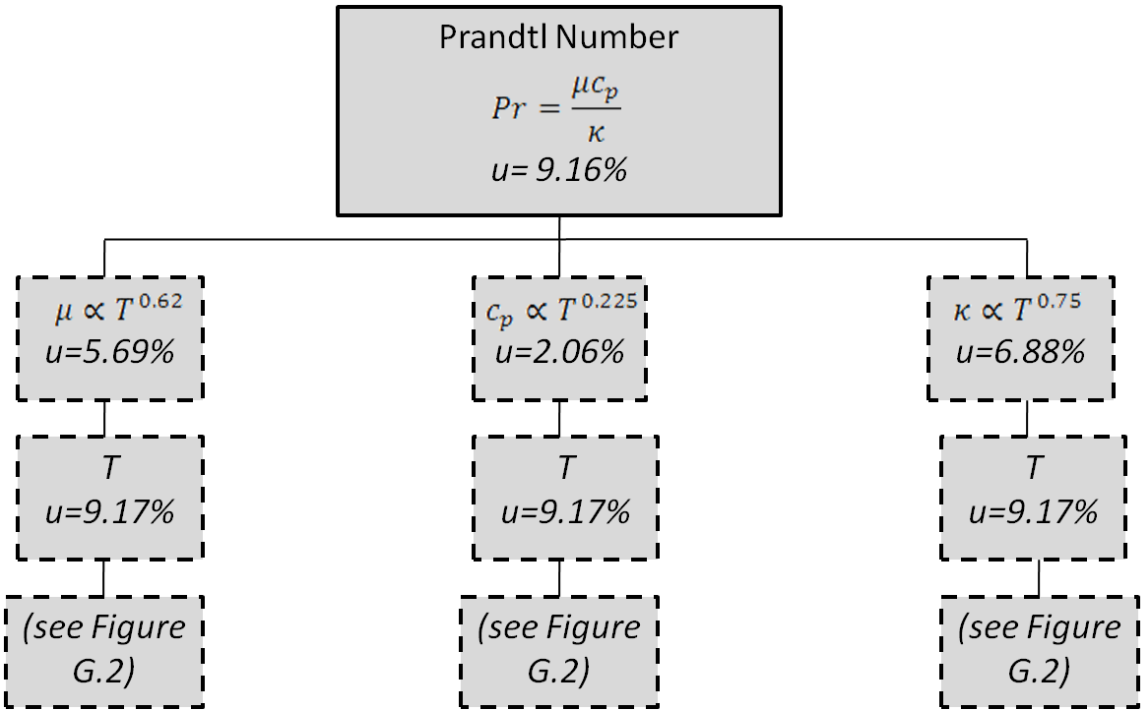

Figure G.6 – Propagation of uncertainty for the Prandtl number during expansion

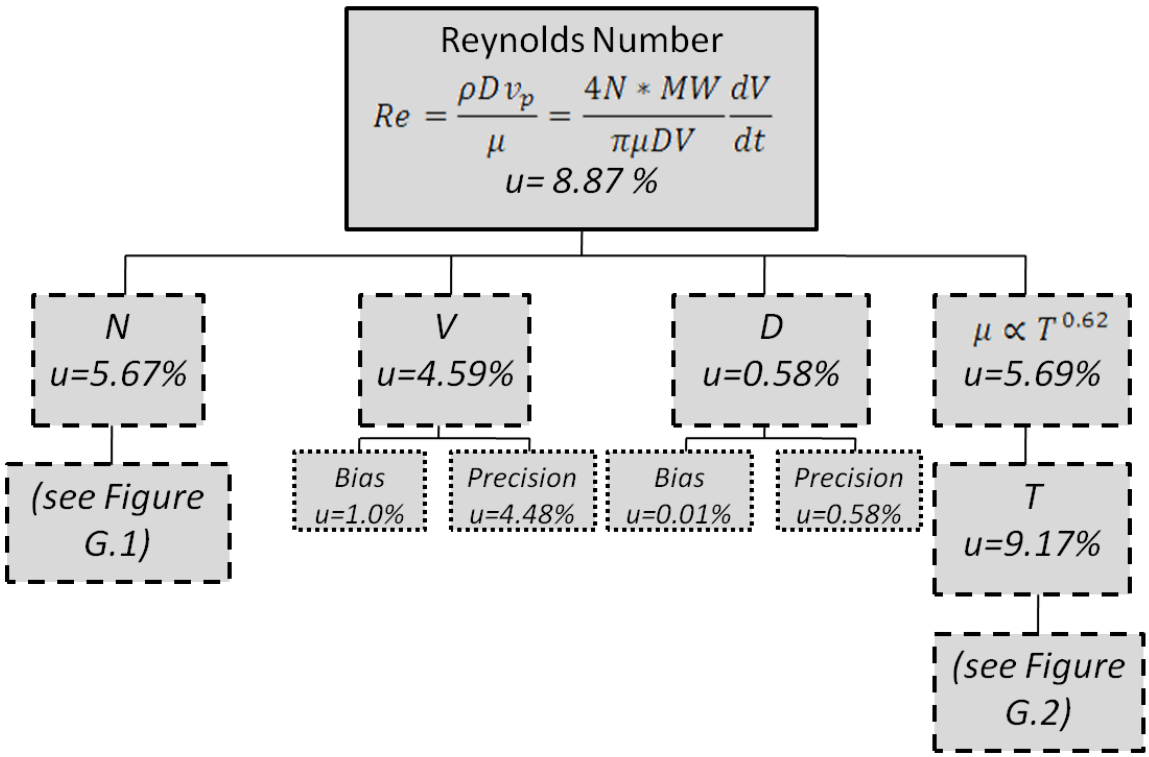

Figure G.7 – Propagation of uncertainty for the Reynolds number during expansion

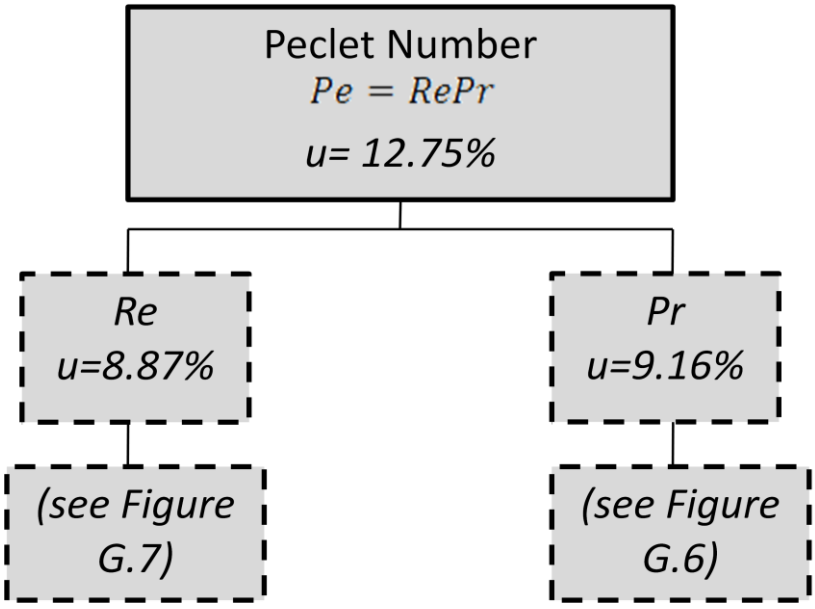

Figure G.8 – Propagation of uncertainty for the Peclet number during expansion

Appendix H - Experimental Data

Multiple tests were conducted for each test condition, and multiple test conditions were examined to determine overall trends. The results given in the main body of the report contain samples of the experimental data that represent the processes, but does not contain all the data for the sake of brevity. The figures included in this appendix represent the sum of the data collected for this study. Contained in Figures H.1 – H.5 are data from the constant volume combustion ("bomb") tests showing how combustion time was determined. Contained in Figures H.6 – H.10 are data showing the pressure and volume during a single combustion and expansion event. These figures illustrate how the combustion time information was used to justify that combustion was complete when expansion began. Contained in Figures H.11 – H.30 are the experimental data for gas expansion for each of the test cases conducted. These figures show the raw data and the curve fits applied to represent each test case.

Bomb Data

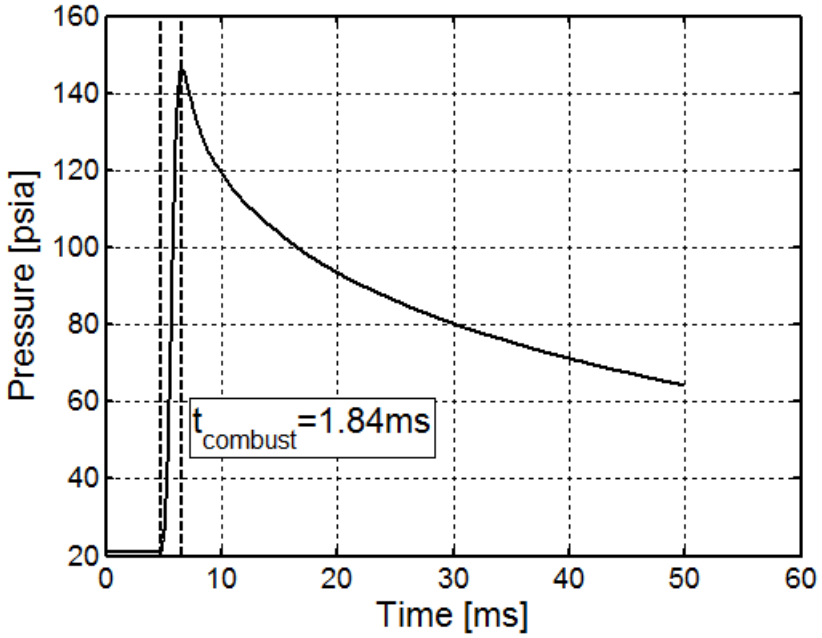

Figure H.1 – Bomb data for Test Case A

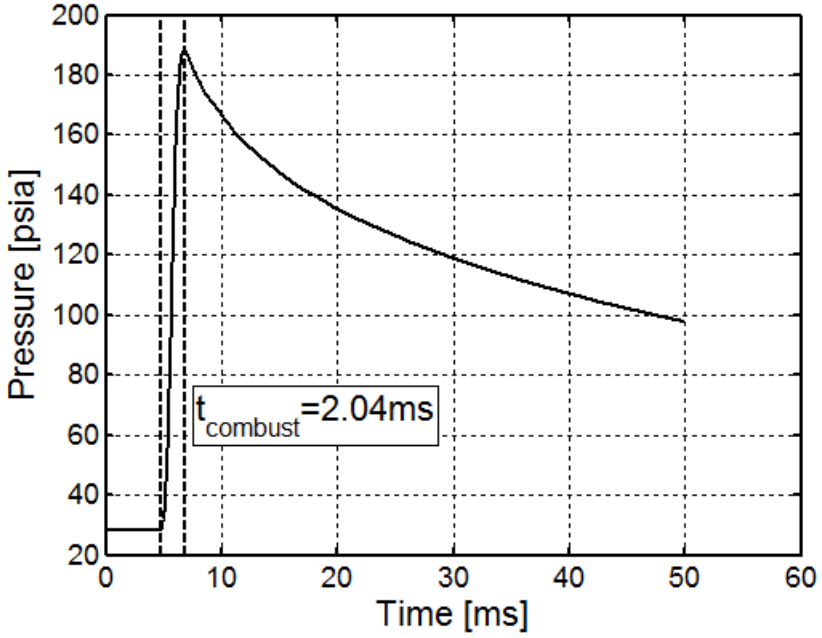

Figure H.2 – Bomb data for Test Case B

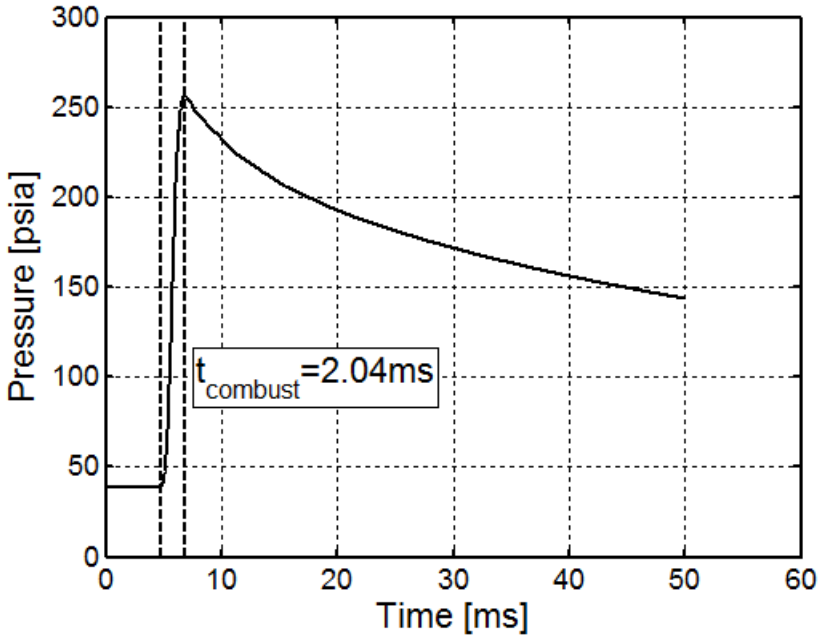

Figure H.3 – Bomb data for Test Case C

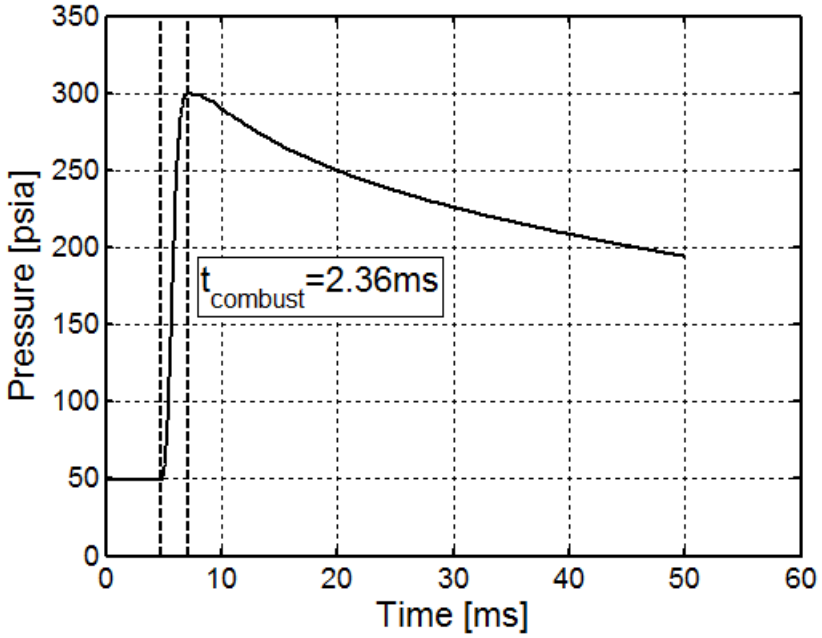

Figure H.4 – Bomb data for Test Case D

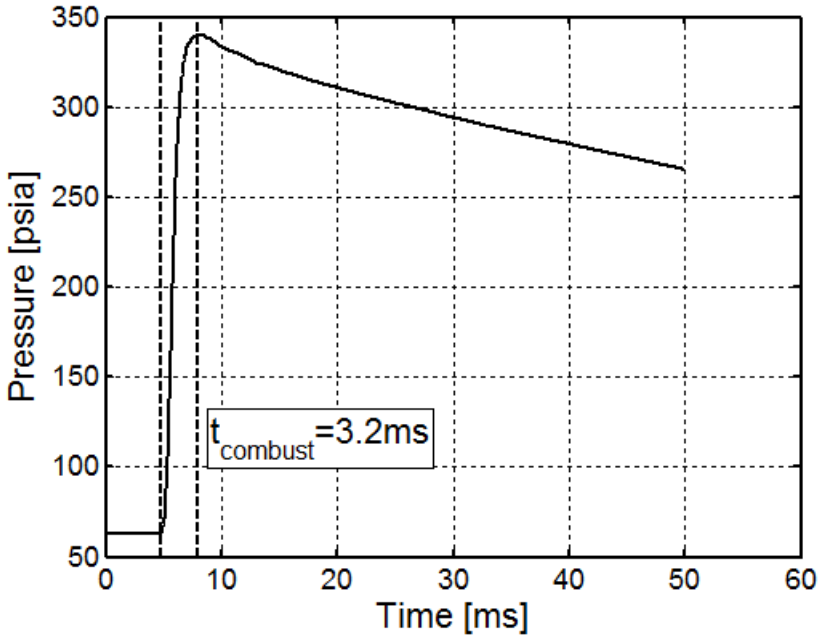

Figure H.5 – Bomb data for Test Case E

Combustion and Expansion Data

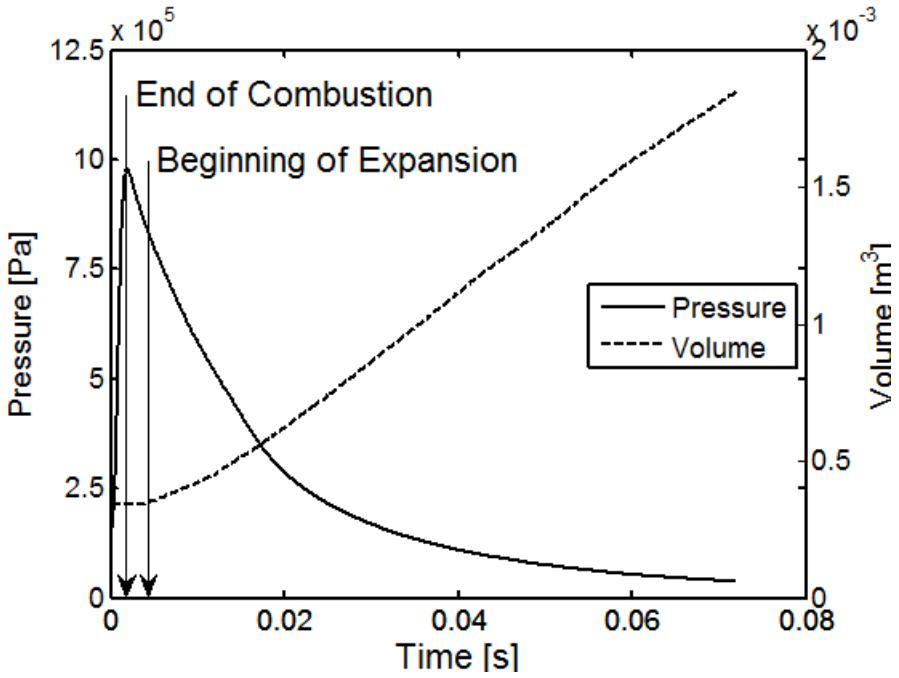

Figure H.6 – Combustion & expansion data for Test Case A, showing the end of combustion as obtained from bomb data and the beginning of expansion by 1% increase from initial volume.

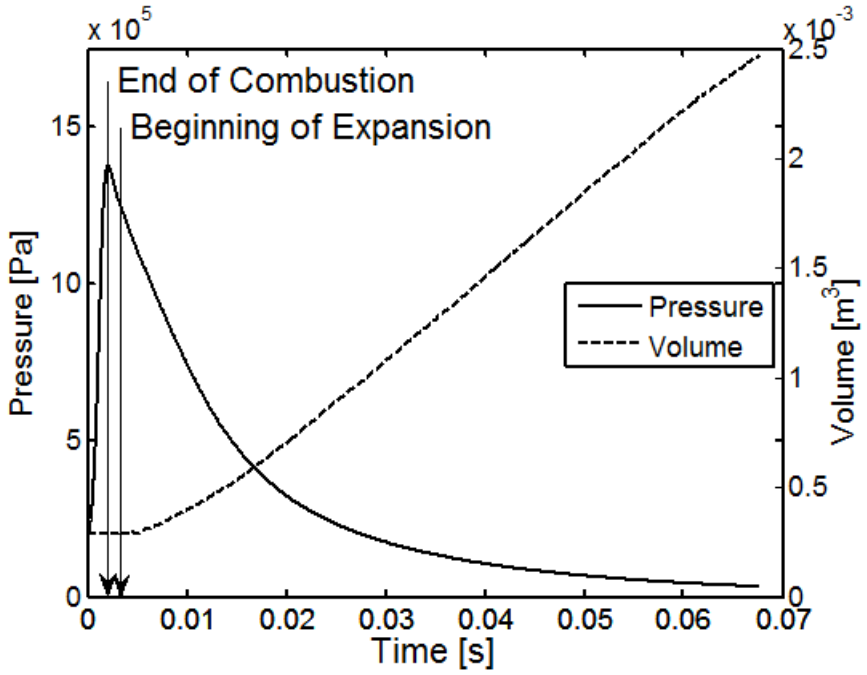

Figure H.7 – Combustion & expansion data for Test Case B, showing the end of combustion as obtained from bomb data and the beginning of expansion by 1% increase from initial volume.

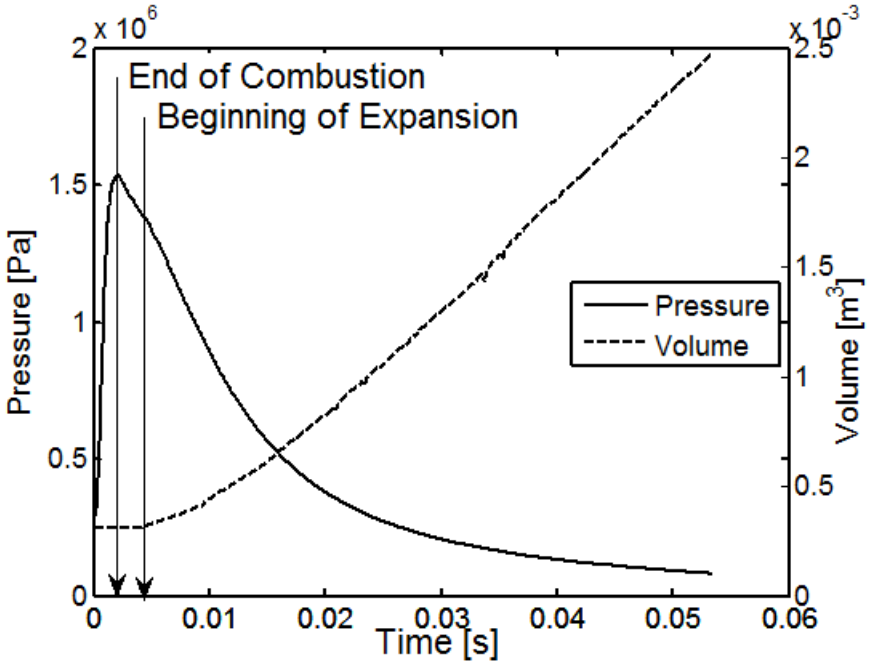

Figure H.8 – Combustion & expansion data for Test Case C, showing the end of combustion as obtained from bomb data and the beginning of expansion by 1% increase from initial volume.

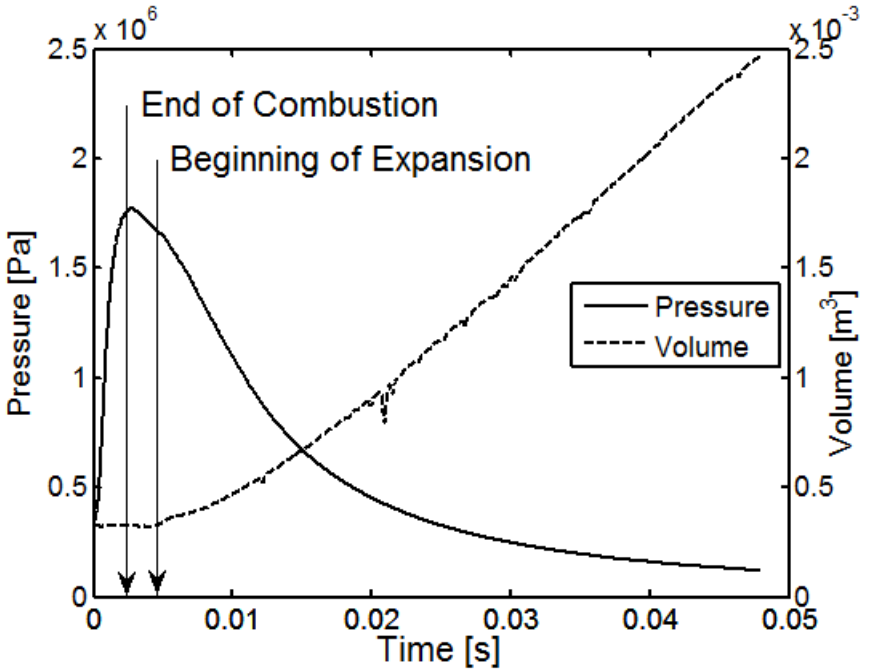

Figure H.9 – Combustion & expansion data for Test Case D, showing the end of combustion as obtained from bomb data and the beginning of expansion by 1% increase from initial volume.

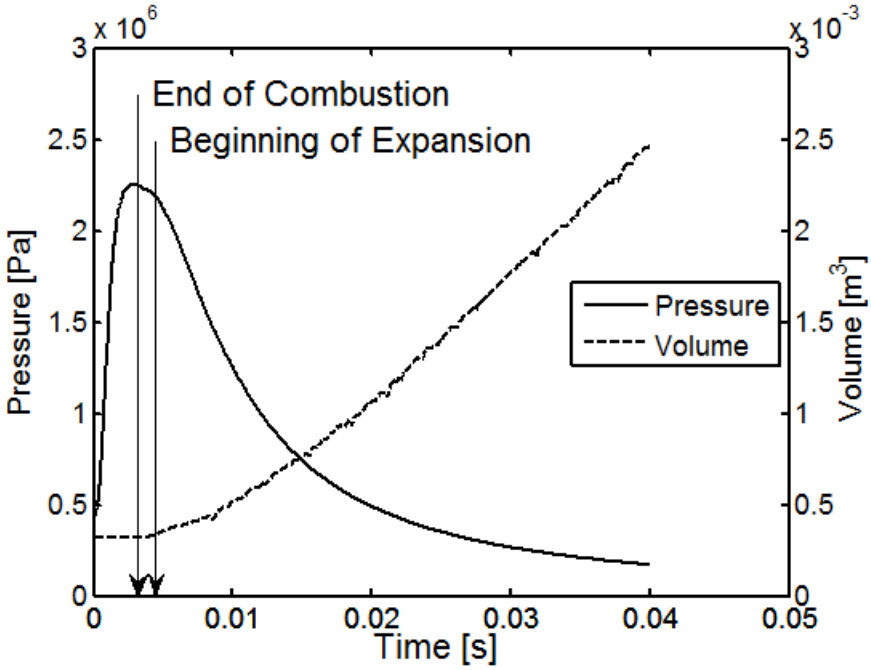

Figure H.10 – Combustion & expansion data for Test Case E, showing the end of combustion as obtained from bomb data and the beginning of expansion by 1% increase from initial volume.

Additional Experimental Data

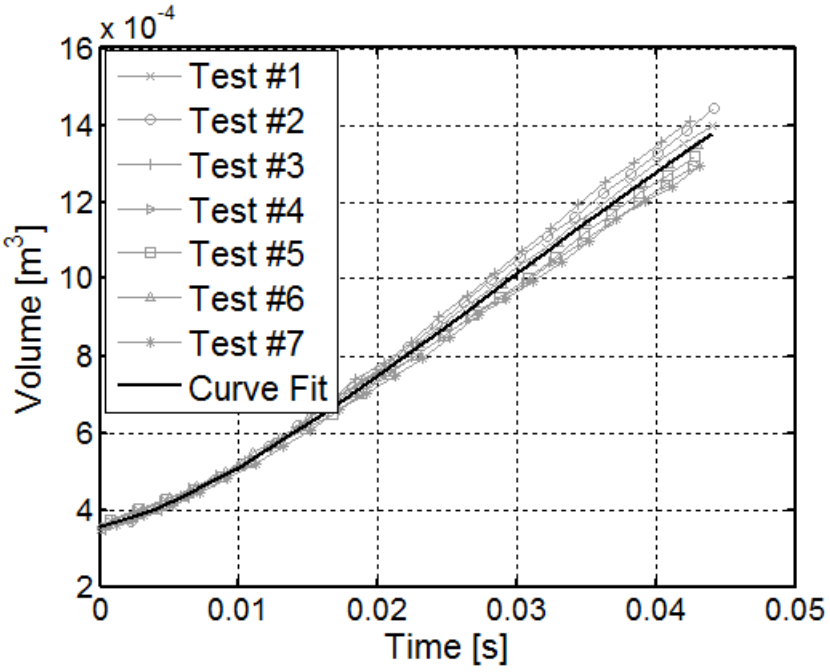

Figure H.11 – Measured cylinder volume versus time during expansion for Test Case A

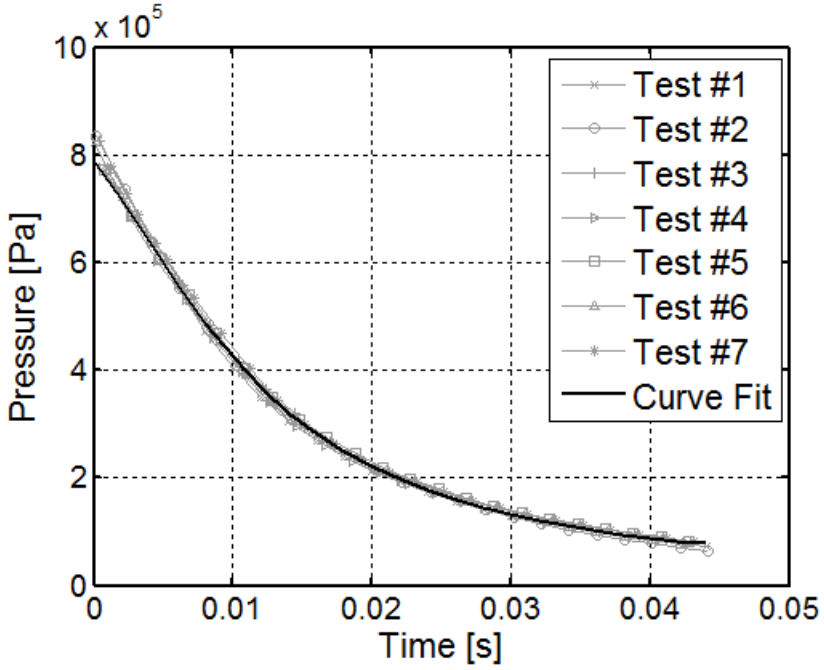

Figure H.12 – Measured cylinder pressure versus time during expansion for Test Case A

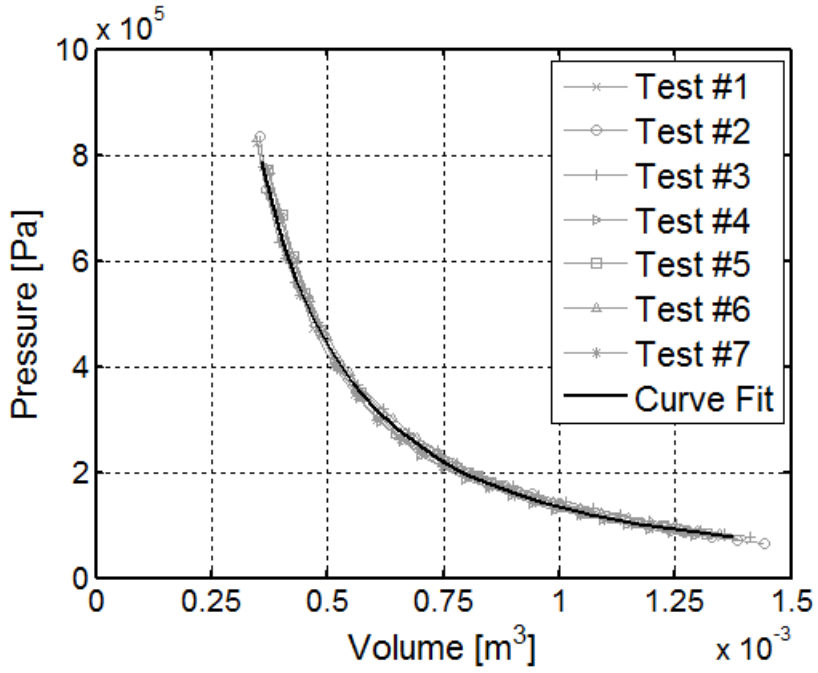

Figure H.13 – Measured pressure versus measured cylinder volume during expansion for Test Case A

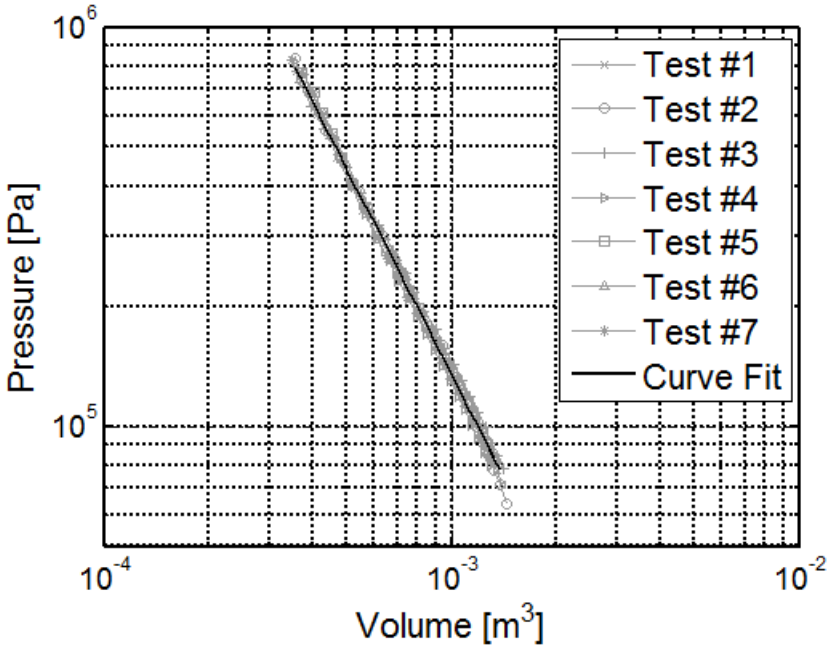

Figure H.14 – Measured cylinder volume versus time during expansion for Test Case A, logarithmic scale

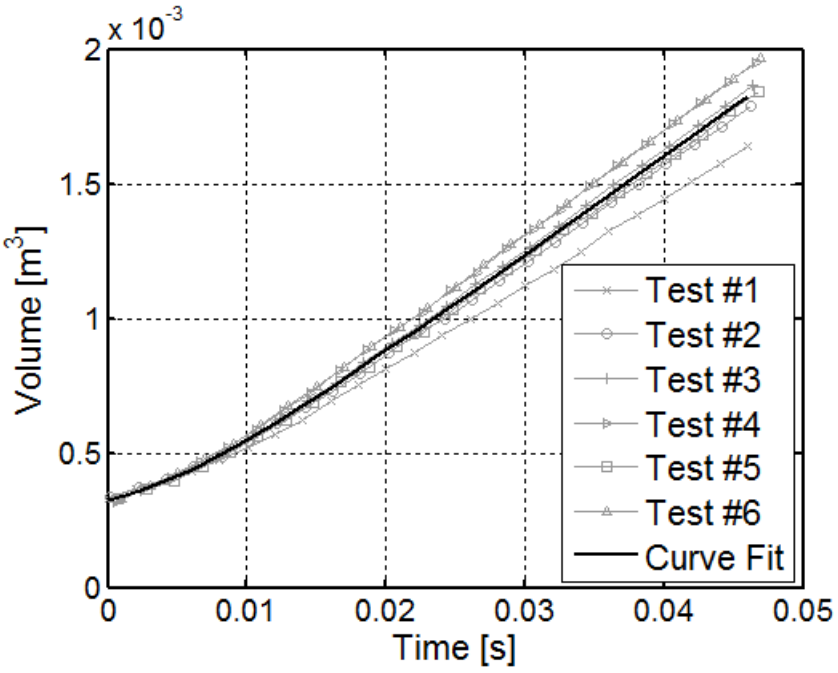

Figure H.15 – Measured cylinder volume versus time during expansion for Test Case B

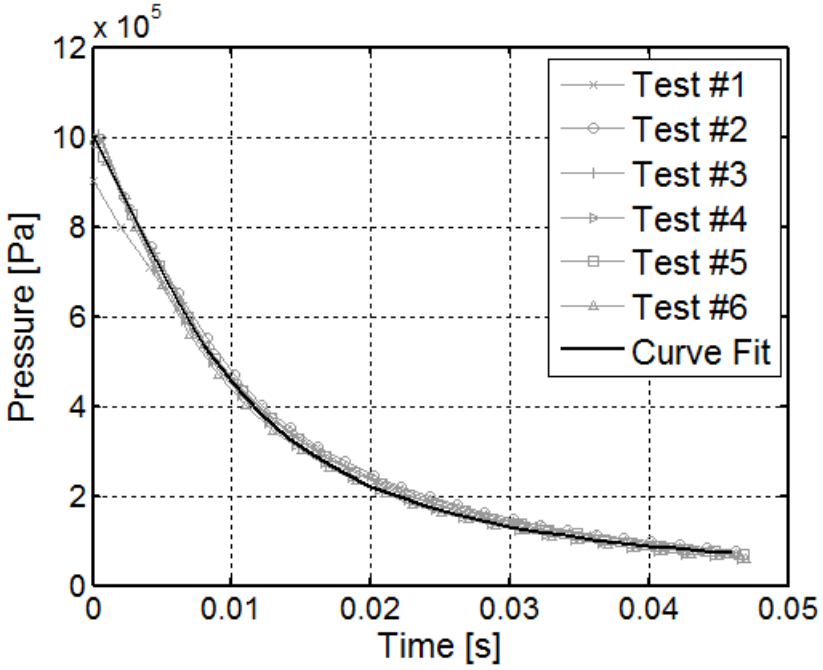

Figure H.16 – Measured cylinder pressure versus time during expansion for Test Case B

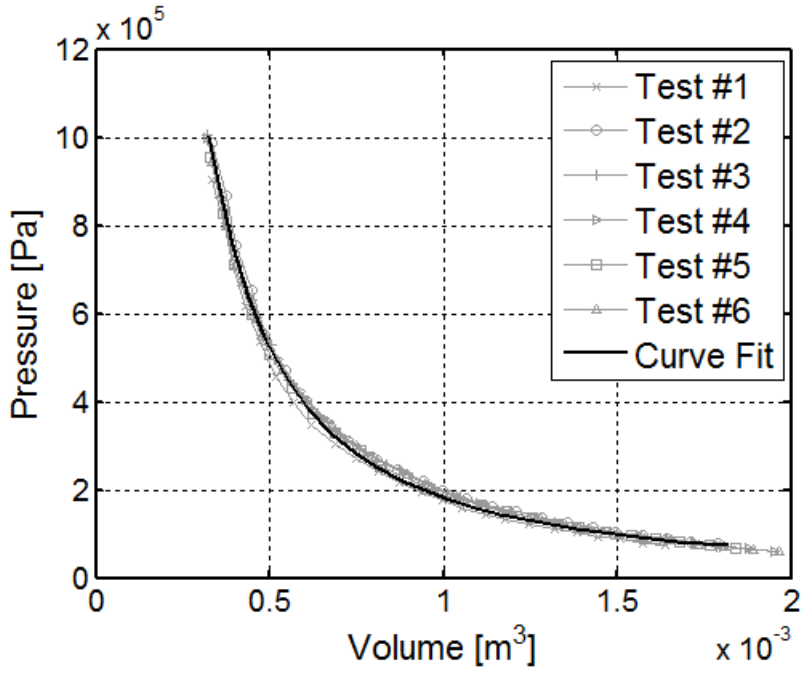

Figure H.17 – Measured cylinder pressure versus measured cylinder volume during expansion for Test Case B

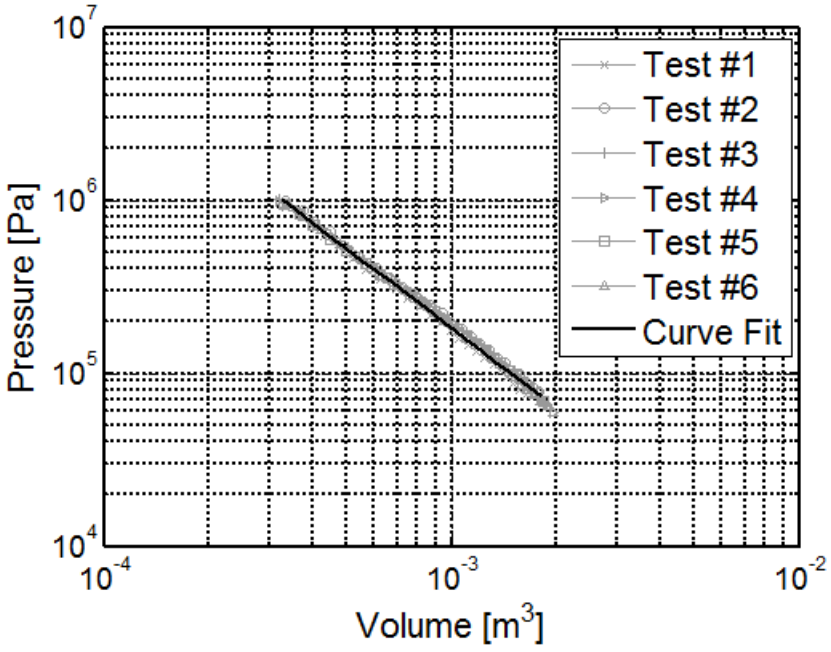

Figure H.18 – Measured cylinder pressure versus volume during expansion for Test Case B, logarithmic scale

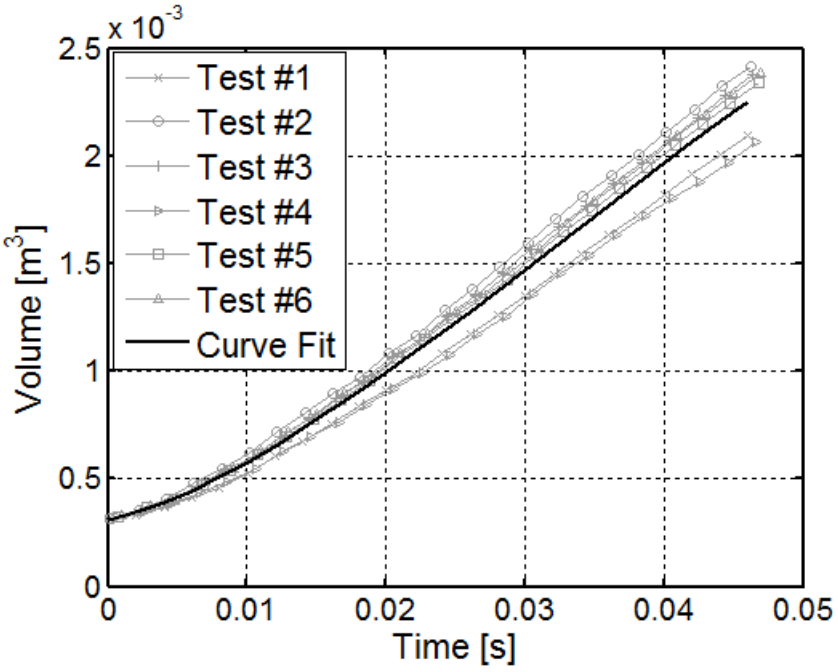

Figure H.19 – Measured cylinder volume versus time during expansion for Test Case C

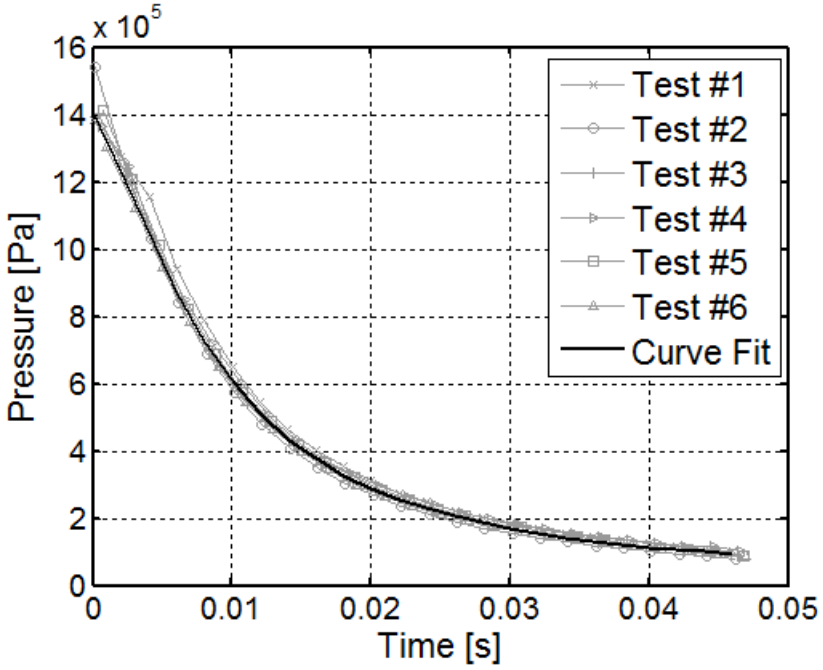

Figure H.20 – Measured cylinder pressure versus time during expansion for Test Case C

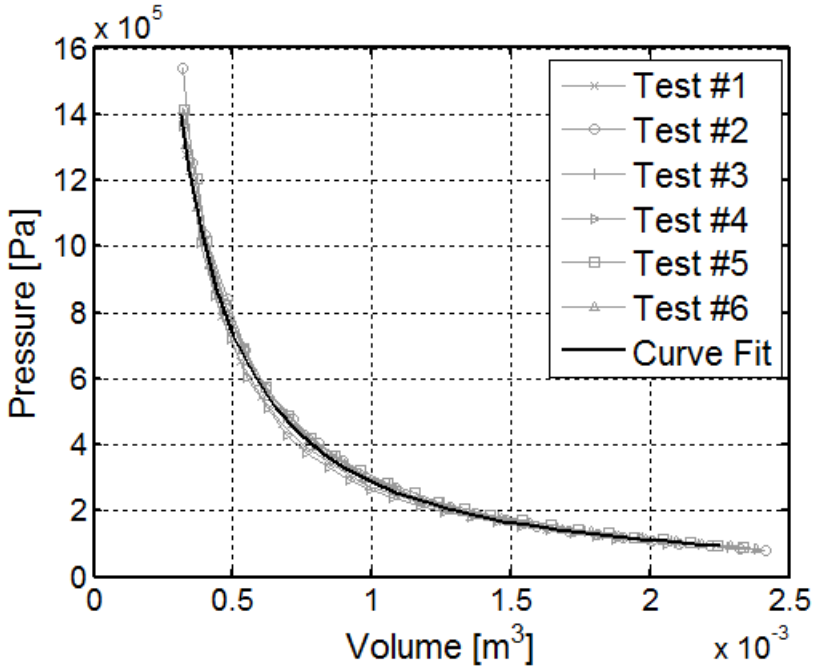

Figure H.21 – Measured cylinder pressure versus measured cylinder volume during expansion for Test Case C

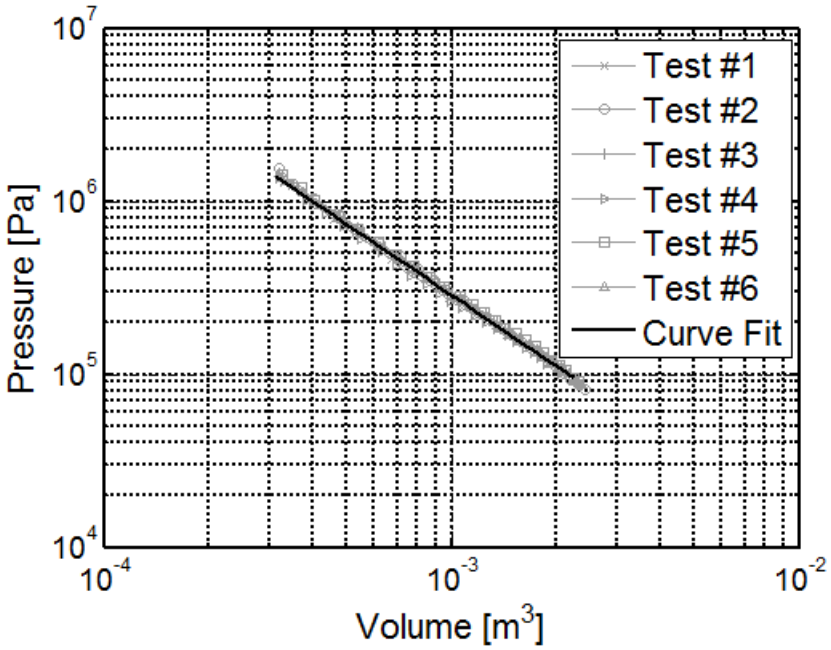

Figure H.22 – Measured cylinder pressure versus volume during expansion for Test Case C, logarithmic scale

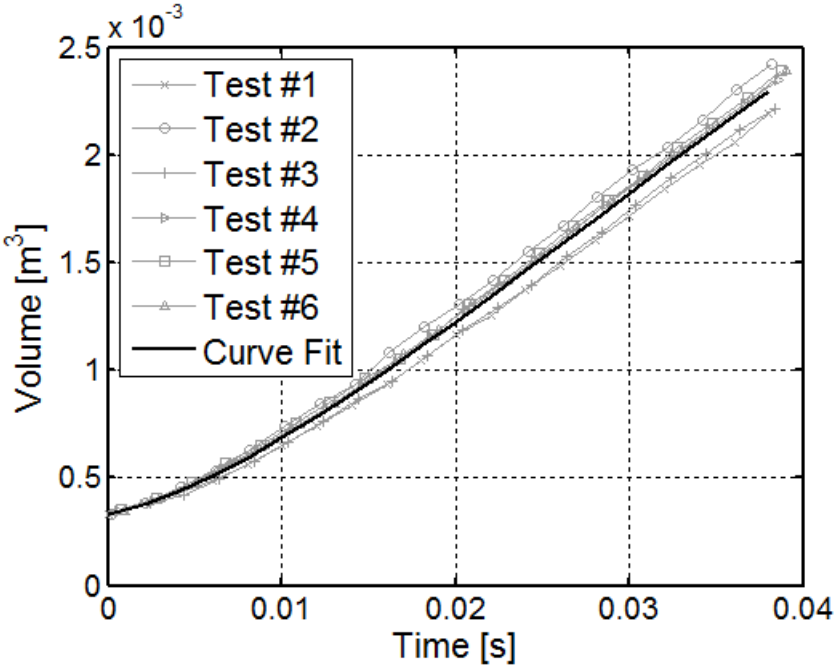

Figure H.23 – Measured cylinder volume versus time during expansion for Test Case D

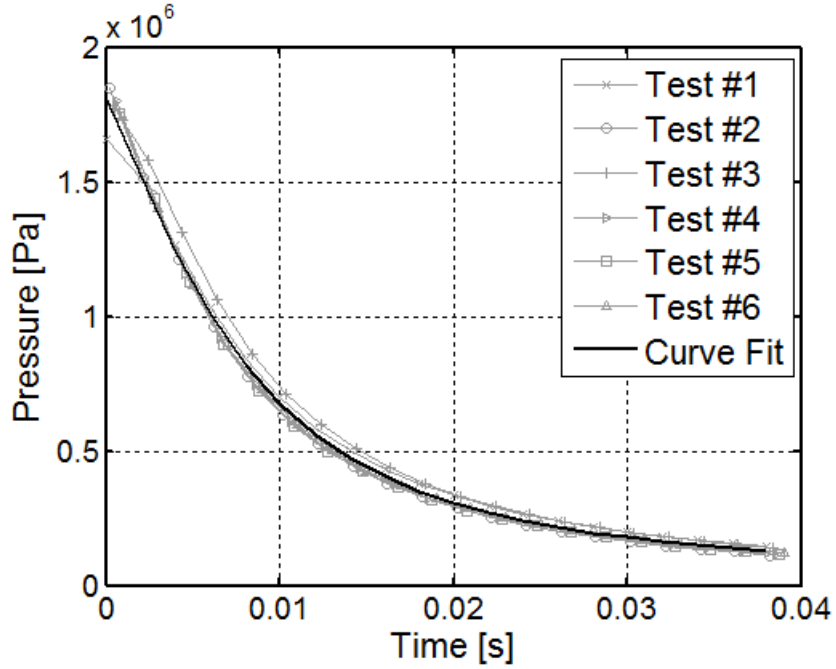

Figure H.24 – Measured cylinder pressure versus time during expansion for Test Case D

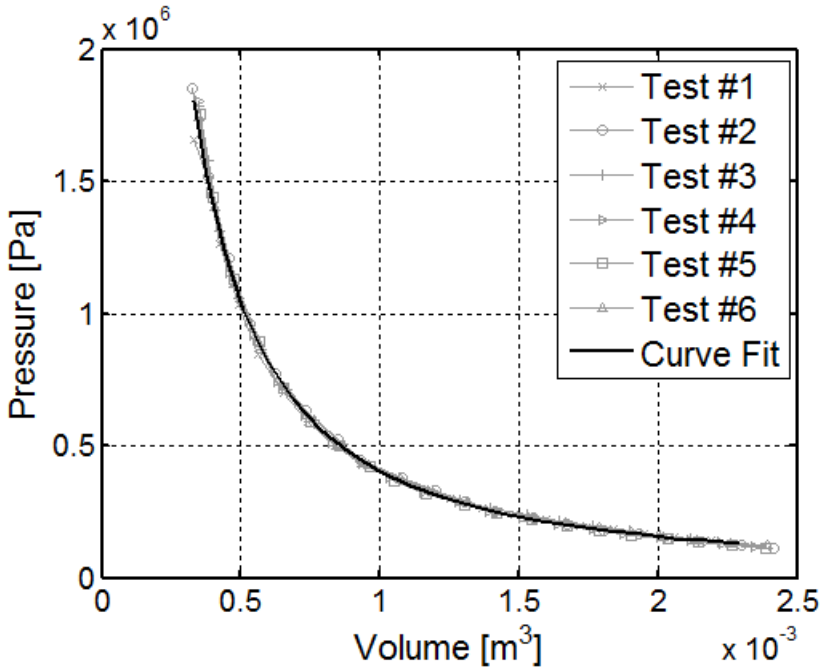

Figure H.25 – Measured cylinder pressure versus measured cylinder volume during expansion for Test Case D

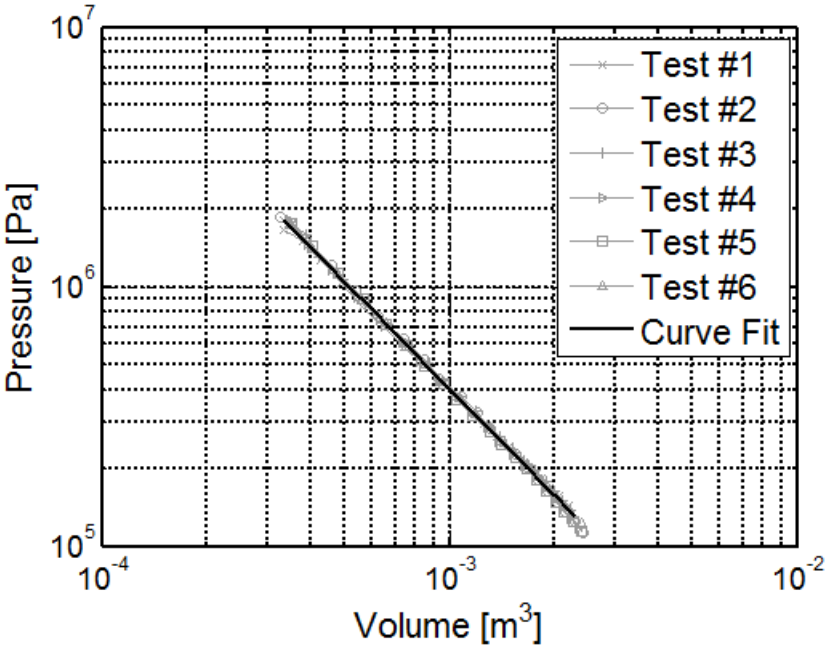

Figure H.26 – Measured cylinder pressure versus volume during expansion for Test Case D, logarithmic scale

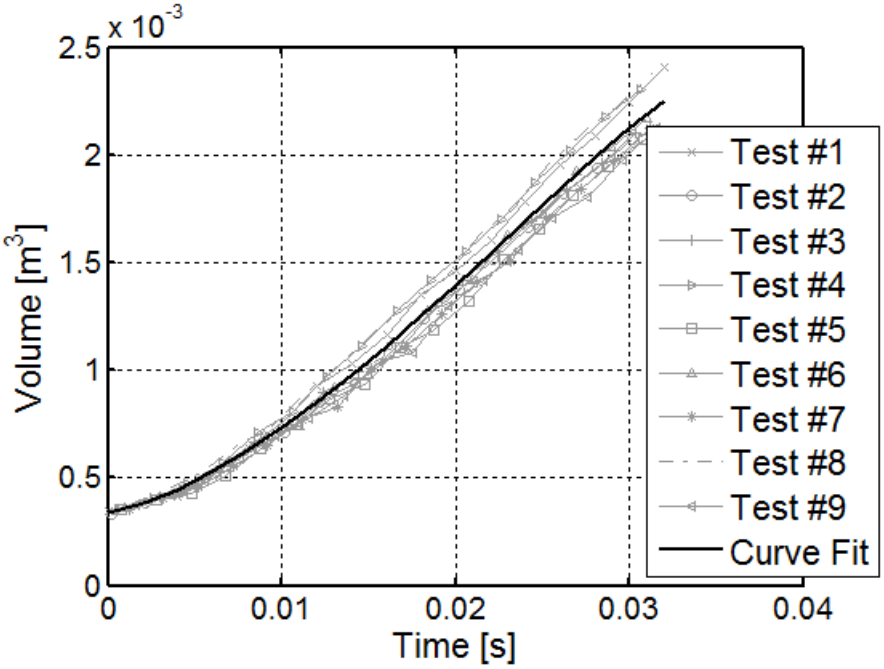

Figure H.27 – Measured cylinder volume versus time during expansion for Test Case E

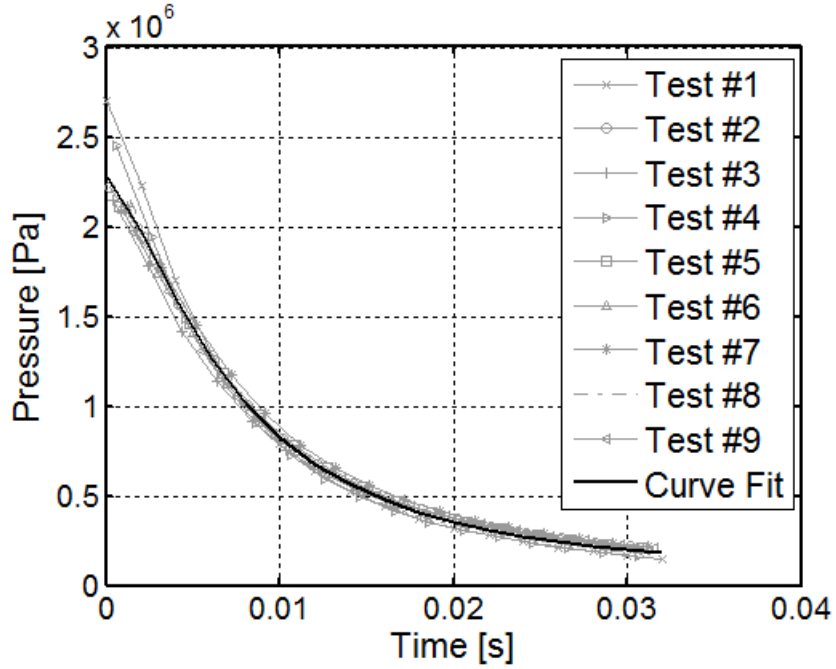

Figure H.28 – Measured cylinder pressure versus time during expansion for Test Case E

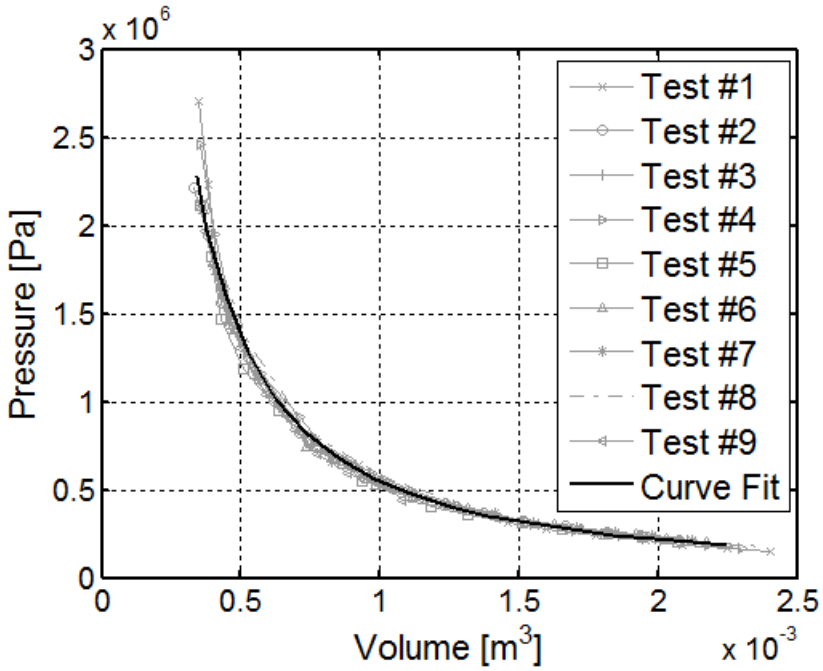

Figure H.29 – Measured cylinder pressure versus measured cylinder volume during expansion for Test Case E

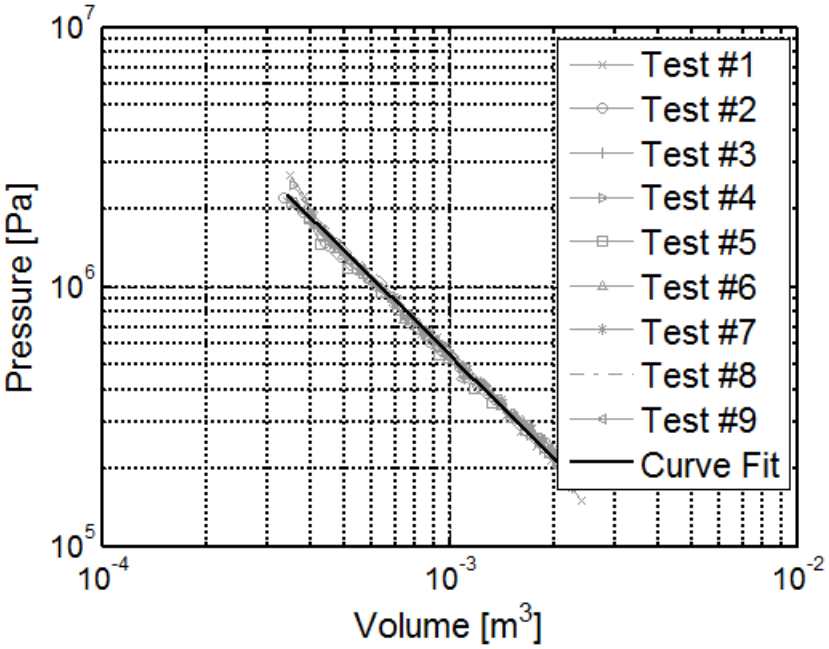

Figure H.30 – Measured cylinder pressure versus volume during expansion for Test Case E, logarithmic scale

Appendix I – Thermophysical Fluid Properties

In order to analyze the gas expansion process and calculate key non-dimensional parameters, several thermophysical properties were necessary. The necessary quantities were the dynamic viscosity, μ, the thermal conductivity, κ, and the specific heat at constant pressure, c_p. These quantities were taken from the computer program *Engineering Equation Solver*, also known as *EES*. This program has the desired thermophysical properties available as built in functions, determined assuming ideal gas behavior so that they are functions of temperature only. These functions were used to generate tables of μ, κ, and c_p for a range of temperatures for the gas species present during expansion (N_2 and H_2O). Since the data processing was done using Matlab©, these tables generated from *EES* were imported into Matlab© and turned into functions, which returned the desired thermophysical property given the gas temperature. Mixture properties of μ, κ, and c_p were determined by a mass average of N_2 and H_2O. Figure I.1 shows the viscosity of the gas mixture during expansion, Figure I.2 shows the thermal conductivity of the gas mixture during expansion, and Figure I.3 shows the specific heat at constant pressure of the gas mixture during expansion. Figure I.4 shows the thermal diffusivity, $\alpha = \kappa/\rho c_p$. Because this property varies with pressure as well as temperature, it generally varies more than the other thermal properties. Shown in each figure are the properties for each test case. Since all tests were conducted at the same gas composition, differences

between test cases primarily reflect different temperatures at that point in the expansion. For Test Case D, thermal diffusivity changed by approximately a factor of three between the start and end of expansion, thermal conductivity changed by approximately a factor of two, viscosity changed by a factor of ~1.5, and specific heat changed by a factor of 1.2.

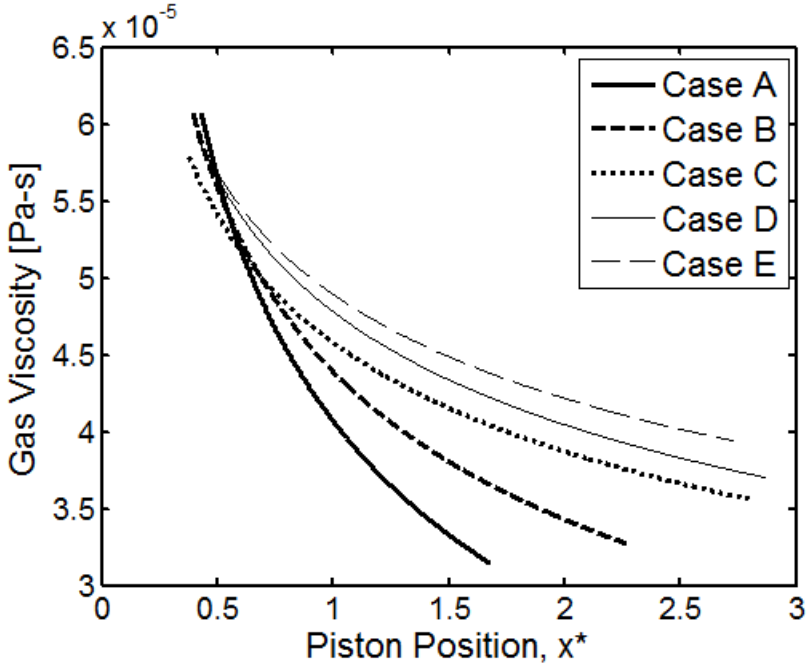

Figure I.1 – Viscosity of the gas mixture for each test case during expansion

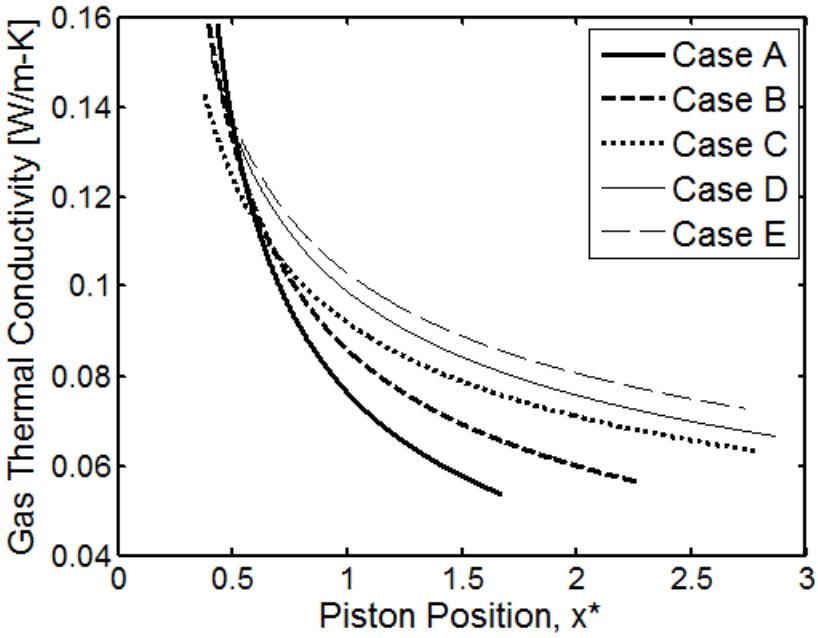

Figure I.2 – Thermal conductivity of the gas mixture for each test case during expansion

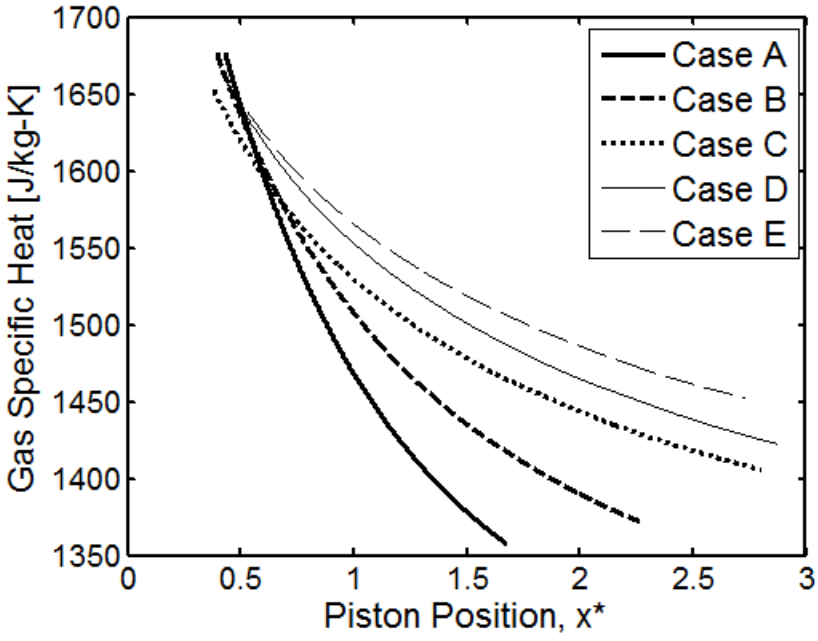

Figure I.3 – Specific heat at constant pressure of the gas mixture for each test case during expansion

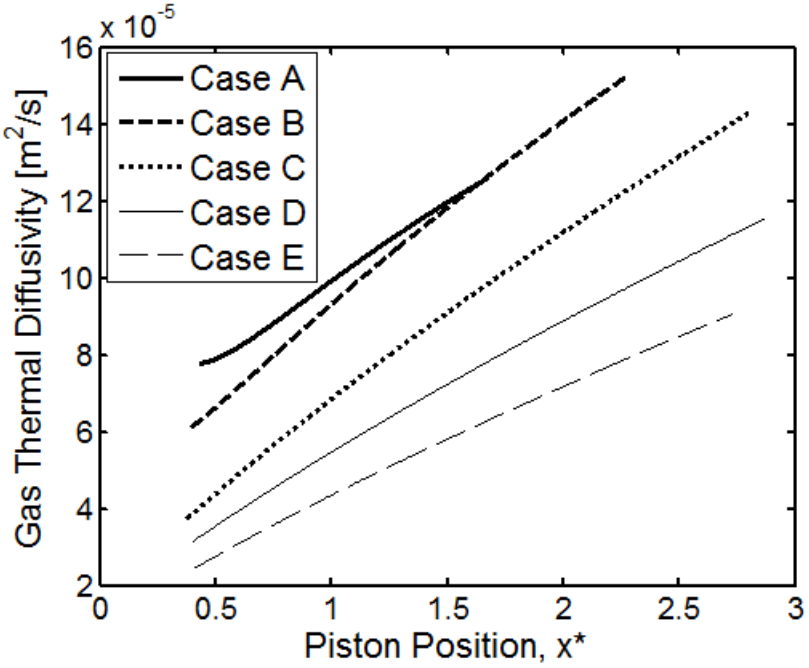

Figure I.4 – Thermal diffusivity of the gas mixture for each test case during expansion

Appendix J – Results of Applying the Alternate Model for the Polytropic Exponent

In Chapter 4, it was shown that the polytropic exponent, *n*, can be modeled using a characteristic time scale for the expansion process. Two models for *n* were proposed; a model based on the ratio between the heat diffusion time scale and the expansion time scale (this was simplified into the characteristic Peclet number), and a model based on the ratio between the acoustic time scale and the expansion time scale (this was termed the dimensionless mean piston speed). Both models were shown to be viable methods of describing the polytropic exponent.

The model based on the characteristic Peclet number is given by Eq. 4.12, and was used as the preferred model in this study because the instantaneous Peclet number was also found to be important to the heat transfer. When assessing the overall heat transfer model in Figure 4.22-4.26, the polytropic exponent was calculated using the model based on the characteristic Peclet number. However, calculating the polytropic exponent based on the dimensionless mean piston speed from Eq. 4.15 is a viable method of determining *n*, and when applied to the overall heat transfer model good agreement between the data and the model is achieved. The results of calculating *n* using Eq. 4.15 (reproduced below as Eq. J.1) and using this for the overall heat transfer model are shown in Figures J.1-J.4.

Alternate Model:

$$If\ S_p^* \leq 0.006: \qquad \frac{n}{\gamma_0} = 0.054 S_p^{*-1/2} + 0.4 \tag{J.1a}$$

$$If\ S_p^* > 0.006: \qquad \frac{n}{\gamma_0} = -13.5 S_p^* + 1.18 \tag{J.1b}$$

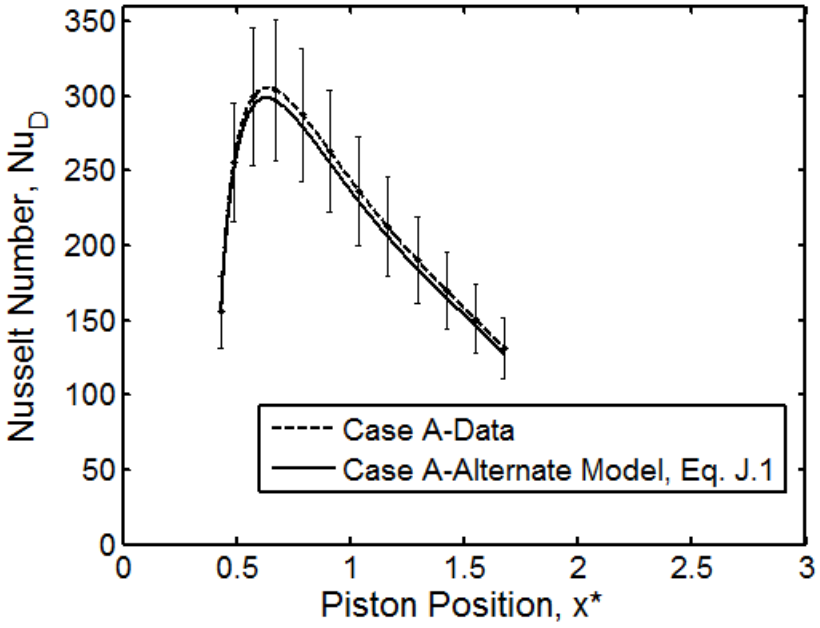

Figure J.1 – Comparison of experimental results and the alternate heat transfer model for the polytropic exponent – Test Case A

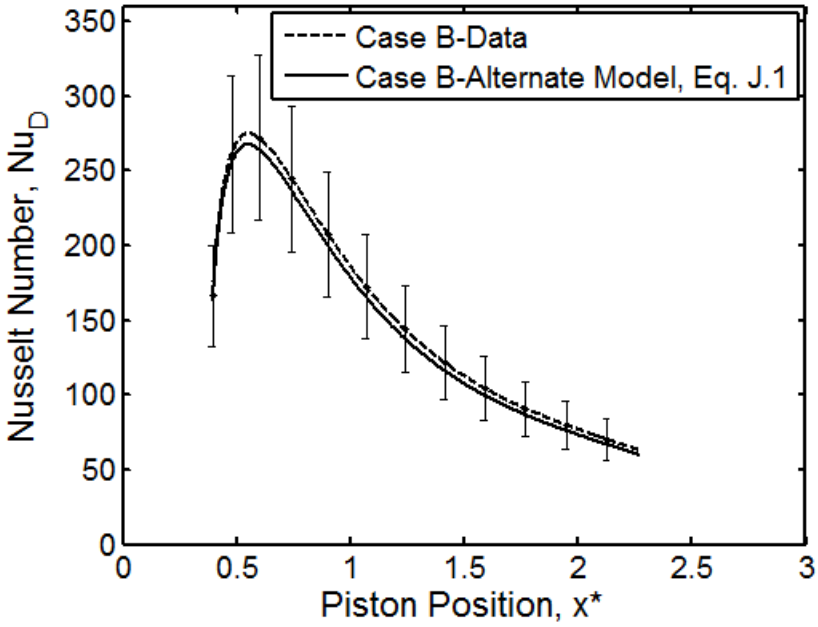

Figure J.2 – Comparison of experimental results and the alternate heat transfer model for the polytropic exponent – Test Case B

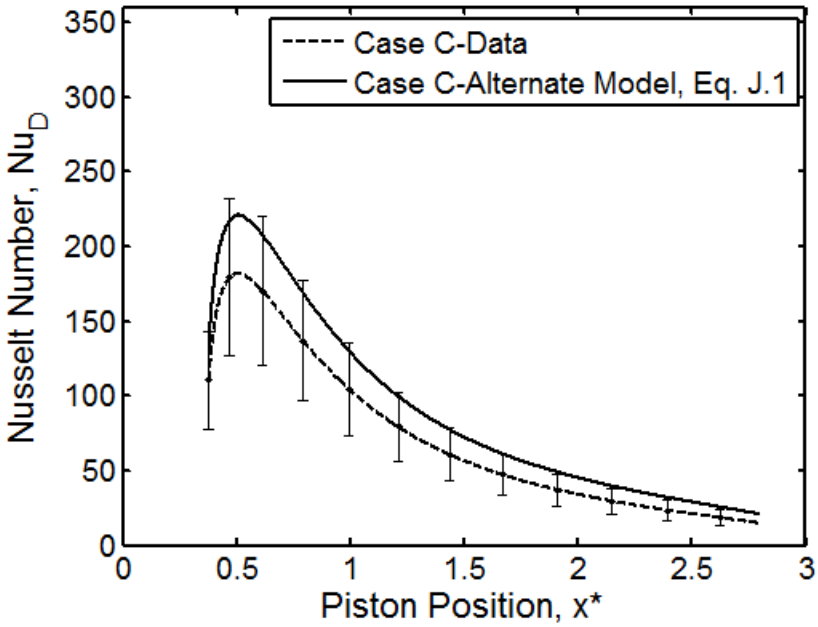

Figure J.3 – Comparison of experimental results and the alternate heat transfer model for the polytropic exponent – Test Case C

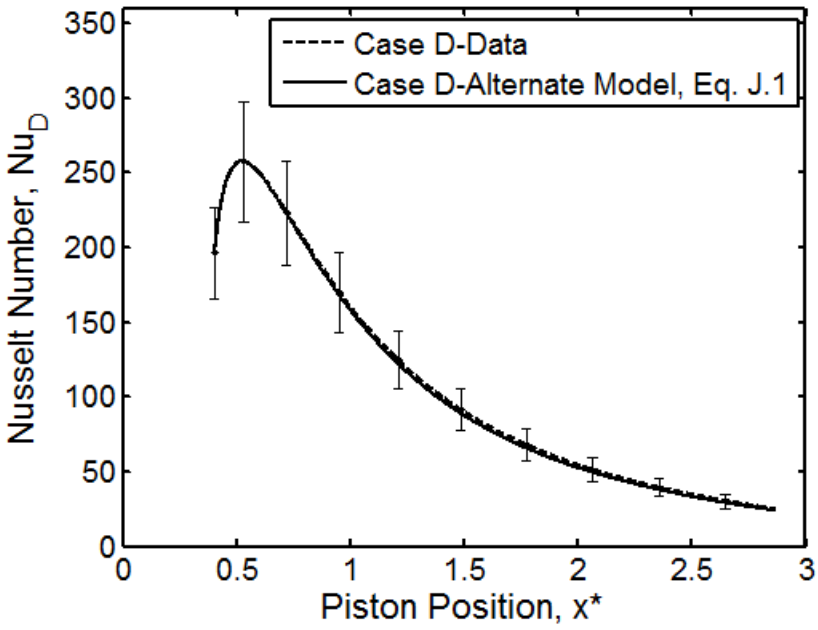

Figure J.4 – Comparison of experimental results and the alternate heat transfer model for the polytropic exponent – Test Case D

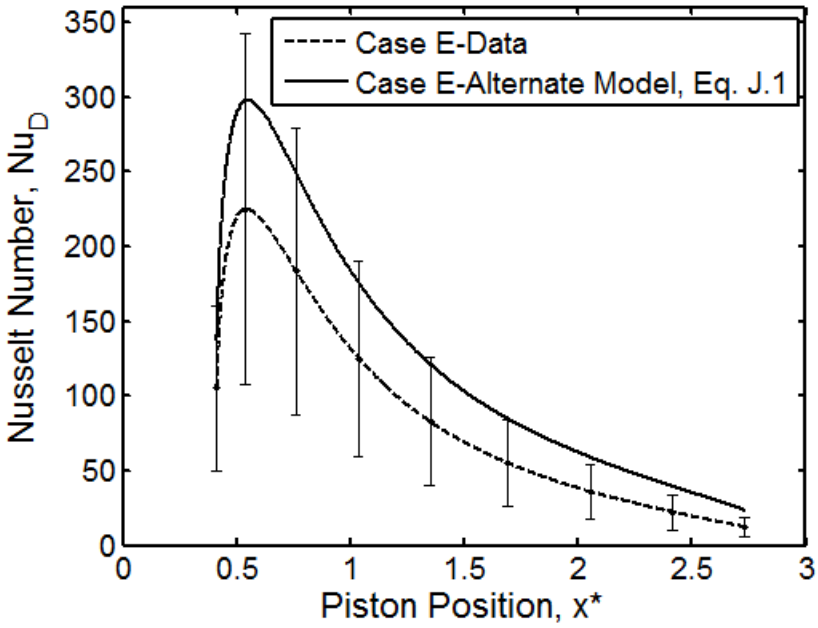

Figure J.5 – Comparison of experimental results and the alternate heat transfer model for the polytropic exponent – Test Case E